Sapienza Università di Roma

Dipartimento Ingegneria Chimica Materiali ed Ambiente

OPTIMIZATION OF DRYING FOOD PRODUCTS: APPLICATION TO FRUITS

PhD in Chemical Engineering
XXX cycle

Tutor
Prof.ssa Paola Russo

Candidate
Renato Buonocore

A.A. 2016/2017

Acknowledgements

I would like to express my acknowledgements for the support in the experimental work to the team of the Laboratorio di Tecnologie Alimentari, Dipartimento Ingegneria Industriale, Università di Salerno and the Laboratorio di Risonanza magnetica “Annalaura Segre”, Istituto di Metodologie Chimiche, CNR.

Abstract

Air drying is one of the most used unit operation in food processing. Simulation or designing the air-drying operation requires the mathematical description of food moisture evolution during the process, known as drying kinetics. The structure of the food materials goes through deformations due to the simultaneous effect of heat and mass transfer during the drying process. These deformations lead to changes in many quality attributes and directly affect physical properties (i.e. the mass diffusion coefficient). Changes in volume, "shrinkage", negatively impact the quality perception of dried products by consumer. The knowledge of the changes in the properties of foods that occur during drying is hence needed for better designing the process.

The aim of this study is to understand the effect of drying on quality of fruit which typically has high moisture content (i.e. pear and grape) and to develop a mathematical model which quantify the drying of this food matrix. To this purpose the drying kinetics, shrinkage and structure modifications (through SEM analysis) were experimentally evaluated.

During drying, the macroscopic transport of water through the cellular tissue constituting the fruit is largely controlled by the microscopic distribution of water and air on a cellular and subcellular distance scale and by membranes permeability. ^{1}H pulsed low resolution NMR allows to obtain quantitative information on water distribution and diffusion by detecting the proton signal predominantly due to H_2O contained in vegetable tissue. Therefore, portable-NMR was used to determine the drying moisture profile and thickness reduction of pears. Portable-NMR also allowed to investigate water mobility in fresh and dried pears by measuring the longitudinal and transverse relaxation times, and the self-diffusion coefficient.

For fruit, such as grape, drying is a slow and very energy intensive process because the waxy peel has low permeability to moisture. In order to enhance the drying rate, pretreatments are used. In this thesis, both chemical (by dipping in an ethyl oleate solution) and physical (by abrasion) pretreatments were analysed. It was found that ethyl oleate and abrasion pretreatments have the same effect in reducing the drying time, but the second one is to be preferred because it avoids the use of chemical additives and permits safer raisin to be produced. Moreover, the samples pretreated by peel abrasion showed less shrinkage and no cracks on the peel surface with respect to those pretreated with ethyl oleate solution.

To obtain a detailed prediction of moisture distribution during drying, in the thesis, a diffusion model with Fickian moisture transfer was coupled with an empirical law which considers the effect of shrinkage. A numerical solution technique, based on the method of finite elements,

is used with an adaptive mesh. The results match well with the experimental results. In particular, a good agreement between experimental and theoretical data of moisture ratio during drying was found for both fruits. The model also well predicted the moisture profile along the pear thickness obtained by NMR.

Contents

CHAPTER 3

Modelling of pear drying

CHAPTER 4

Drying of grapes

List of Figures

CHAPTER 1

CHAPTER 2

CHAPTER 3

CHAPTER 4

List of Tables

CHAPTER 1

CHAPTER 2

CHAPTER 3

CHAPTER 3

CHAPTER 1

Drying of fruits and vegetables

1 Introduction

Drying of fruit and vegetables is a common process to improve their stability. Drying is a process involving heat and mass (moisture) transfer between a hygroscopic product and drying air. In the drying process of a wet porous solid, the air supplies heat to the solid and absorbs water of it in vapour phase. In general, drying is conducted with higher air temperatures than the boiling point of the liquid to be eliminated. The heating of the drying air, in order, to reduce the relative humidity and increase its enthalpy and evaporative capacity, must be properly controlled to avoid physical, chemical and biological damage that can cause to the product.

The convective hot air drying is the simplest and economical way to dry fruits with respect to other techniques, such as osmotic dehydration (Rastogi et al., 1996, 1998, 2004), freeze drying, superheated steam etc.

Dehydration decreases water activity, reduces microbiological and enzymatic activity and minimizes physical and chemical reaction during storage. Drying technology has the effect to prolong shelf-life of the product. Further advantages of drying are reduction in weight and volume, minimizing packing, storage and transport cost, allowing the product storage at room temperature and facilitation in grinding (Sagar and Kumar, 2010).

In the present economic context, trade and consumer impose their demand for supply chain, availability, habits, nutritional value, and so on. Dried foods must be processed with the goal of maintaining their quality, such as flavour, texture, convenience, and functionality, increasing their nutritional content, and reducing anti-nutritional factors or toxins.

The quality of foods refers first to safety, and then to sensory and nutritional properties. But in many cases, the severity of processing is differently related to safety and to sensory or nutritional quality. Severe processing generally results in higher nutritional loss and in poorer quality, whereas it increases food safety. An optimal drying time and the right level of severity of processing must, therefore, be designed in order to obtain the desired food characteristics. Today, different types of sophisticated dryers are used to dry different varieties of products (Guiné et al., 2008), so operating parameters as drying temperature, ventilation velocity, amount of moisture present, drying time are important to be optimized (Silva et al. 2014).

The control of the mentioned properties relies, often in a complex way, on all the chemical and physical phenomena occurring during drying and subsequent storage. The chemical composition of foodstuff is variable and complex, including carbohydrates, proteins, lipids, minerals, vitamins, aromas, and so on. This complexity induces properties that change throughout drying and storage, and that must be controlled. Besides water content and water activity, many factors with positive and negative effects must be considered, such as:

-the temperature and humidity conditions during processing;

-the changes in shape, structure, porosity, and mechanical properties;

-the sticking and crystallization phenomena linked with glass transition;

-the chemical reactions, specifically their nature and rate in relation to pH and temperature;

-the transfer conditions of heat and water related to diffusivity and conductivity.

One of the most important physical changes is the reduction of the fruit external volume and changes in porosity (Pavon-Melendez et al., 2002; Guinè et al., 2007a,c).

As an example, Russo et al. (2013) analysed the effect of the drying conditions on parameters such as colour, shape, roughness and water content of eggplant. In particular, they found that the drying temperature influences strongly the microstructure of dried samples: the porosity increases with the air temperature, but the structure is better preserved at intermediate temperature (60 °C) as confirmed by the lower firmness values with respect to the other dehydrated samples (40, 50 and 70 °C). In these latter, the longer drying time and the higher temperature, respectively, causes the development of a wrinkled structure. At 70°C the structure of dehydrated samples appears totally broken with a consequent faster water uptake during rehydration.

During convective hot air drying, if water migrates in the liquid state from the centre of a solid product towards the surface, some shrinkage will be observed as a function of evaporated water volume. The consequences will appear as mechanical effects, and changes in shape and structure, especially if the product is malleable (e.g., fruits, vegetables). These changes will only partially disappear during rehydration, because most of the physico-chemical changes that occur during drying, like disruption of cellular integrity, starch gelatinization or protein denaturation, are not reversible. Another important consequence of shrinkage is the decrease in the rehydration capability of the dried products.

The theoretical basis for predicting shrinkage should involve mechanical laws which take into account material stresses and deformations during dehydration. However, such an analysis is extremely complicated for foods because of the multiphase and cellular nature of the materials and because the variation of the mechanical properties with water content and temperature is generally not available. Therefore, most studies of food shrinkage are

experimentally based. Many authors have evaluated the shrinkage on the basis of a bulk shrinkage coefficient, defined as the ratio of sample volume at time t to the initial volume.
In the recent years, researchers have done many experiments on various fruits such as, pear (Guine et al., 2006, 2007b), grape (Adiletta et al., 2016), banana (Rastogi et al., 1996), pineapple (Rastogi et al., 2004), prune (Sabarez, 2012) etc. Their aim was to understand the effect of drying on fruit properties changing the operation conditions, and to represent the experimental drying kinetics with mathematical models (Kiranoudis et at., 2007).
To optimize the quality of the final dried product, modelling tools are often used. Models are created to describe the history of the product during the drying process, using parameters such as time, temperature, water content and quality index.
Mathematical models developed for food drying, their application and their results are reported in the following paragraph. Then the application of novel technique i.e. NMR relaxometry and MRI for the characterization of internal properties of food is discussed.

1.1 Major approaches in drying modelling of fruit and vegetables

The development of suitable mathematical models, providing temporal evolution of state variable is a matter of practical interest to achieve the optimal process conditions for extending shelf-life of the product.
Various theories and consequent mathematical models are reported in the literature.
These models are based on two approaches. They are theoretical or empirical (Datta, 2007a,b). Then, the mathematical model to describe the process involves the diffusion equation. The diffusion equation has analytical solutions for several simple geometries, such as slab, infinite cylinder and a sphere, among others (Crank, 1975). In these solutions, it's is normally supposed that the medium has constant volume and thermo-physical properties.
In general, all the theoretical models are based on Fick's second law of diffusion and were usefully applied for drying processes of many food products. They provide useful information about physical mechanisms involved in drying process and assure good prediction of temporal evolution of state variables when the process conditions changes.
Moreover, they are often exploitable in a wide class of different fruits.
In contrast, empirical models are either derived by series expansion of theoretical model's general solutions or, often, are pure kinetics formulas depending on process conditions. They are easy to deal with, but they do not provide any physical information and their use is restricted to specific process conditions.

One the most important consequences of air-drying of fruit is shrinkage: a volume reduction, coupled with shape and porosity changes and hardness increase. Shrinkage has to be avoided because such physical changes contribute in general to reduce the quality perceived by the end consumer of dehydrated food, traditionally consumed fresh.

Since shrinkage influences drying, it has to be taken into account in mathematical modelling of such processes.

In literature are available several models for the prediction of volume changes, as will be discussed in the following paragraph 1.2.3.

Hence today, always more often, technique as finite volume method and finite element method are used to predict heat and mass diffusion in porous material. Because with them it is possible to consider that the medium has not constant thermo-physical properties, has a complex geometry and it's possible to introduce the shrinkage effect.

1.2 Drying models

In this section some of the mathematical models available in literature for drying of fruit and vegetables are presented.

Mathematical models of drying are identified as experimental models (empirical drying rate models), model based on analytical solution of Fick second law of diffusion in regular geometries, model based on heat and mass transfer, and models that add the shrinkage effect.

1.2.1 Empirical models

Generally, it's easy to develop an experimental based model. A simple empirical process model involves the variation of specific input setup parameters, such as temperature, relative humidity, air velocity, that provided to the experiment apparatus and then measuring of output quantities by a data logging system. The use of correlations to approximate experimental data are used to develop an empirical model. Empirical models only consider average conditions of moisture content and temperature, which restrict their use for the specific case.

Experimental observations are important for drying models. In this kind of approach experiments are done in the laboratory to find a mathematical function to represent the data observed, based on different temperature and air velocity conditions. In this case it's difficult to obtain accurate measurements. Different experiments may derive different equations.

Experimental studies have been conducted on various fruits and vegetables such as potato, carrot (Doymaz, 20034), avocado (Ceylan et al., 2007), banana (Ceylan et al., 2007), apple (Veliè et al., 2004), kiwi (Simal et al., 2005) etc. A large amount of empirical and semi-empirical models have been introduced.

On measuring the drying moisture content M(t) with time t, the drying curve of each experiment is obtained plotting the decay of dimensionless moisture in the sample with the drying time. The empirical constants for the drying models were determined experimentally from normalized drying curves (moisture ratio $M_R = M_t / M_0$) at each drying temperature.

The most common models adopted are reported in Table 1:

Model name	**Equation**	**References**
Handerson and Pabis	$M_R = a\exp(-kt)$	Handerson and Pabis (1961) and Park et al. (2002)
Page	$M_R = \exp(-kt^n)$	Doymaz (2005) and Kashaninejad and Tabil (2004)
Logarithmic	$M_R = a\exp(-kt^n) + c$	Yagcioglu et al. (2009)
Two term	$M_R = a_1\exp(-k_1 t) + a_2\exp(-k_2 t)$	Henderson (1974)

Table 1 *Empirical models applied to drying curves.*

These models fail to identify the general complexity of the drying processes. Robust mathematical models for drying kinetics is normally based on physical mechanism such as the effect of air temperature, air humidity and air velocity and characteristics of sample size. Moisture content and temperature are function of both space and time, but this is not included in empirical models. The distribution of moisture and temperature characterize the quality indicator during drying.

As an example, in the case of pears Guinè et al. (2007d) investigated the drying rates for four varieties (Amendoa, Amorim, Carapinheira Branca and S. Bartolomeu). In the experiment the pears were peeled and dried uncut. The drying process was halted when the final water content in pears reached about 20%. The drying experiment lasted 10 days. The data obtained experimentally in the form of moisture content on a dry-basis versus time curves were fitted with various empirical models: a sigmoid function, a first order kinetics and a power equations. The model that best fits the data was a sigmoid function. The value

of the effective diffusivity range from $9.756*10^{-10}$ m^2/s for the variety S. Bartolomeau to $1.160*10^{-9}$ m^2/s for pear of variety Amorim.

1.2.2 Models considering heat and mass transfer

Heat and mass transfer models have been widely used to describe the movement of water and heat transfer during drying. The fruit and vegetables are often modelled as an homogenous medium.

Moisture transport involves two processes: the evaporation of moisture at the solid surface that need heat from the air and the internal diffusion of liquid at the surface.

The physical equations for simultaneous transfer of moisture M(t) and temperature T(t) with no internal sources of moisture are given by the coupled partial differential equations (pde):

$$\frac{\partial \mathrm{M}}{\partial \mathrm{t}} = \nabla \cdot \left(D \nabla \mathrm{M} \right) \tag{1}$$

$$\rho_s cp \frac{\partial \mathrm{T}}{\partial \mathrm{t}} = \nabla \cdot \left(k \nabla \mathrm{M} \right) \tag{2}$$

where D is the diffusion coefficient, ρ_s is the density, cp is specific heat capacity and k is thermal conductivity of food material. Temperature is given from heat conduction, where the conductive temperature flux $q = -k\nabla \mathrm{T}$. Equation 1 represents the moisture movement in the food during drying. Equation 2, instead, represents the temperature evolution in the interior of the food. Generally, equations 1 and 2 may be limited by drying conditions at the surface of the food product or internally: $D = D\left(\mathrm{M},\mathrm{T}\right)$ and $k = k\left(\mathrm{M}\right)$.

For one dimensional geometry with constant diffusivity D_{eff} and constant thermal diffusivity α the pde become:

$$\frac{\partial \mathrm{M}}{\partial \mathrm{t}} = D_{eff} \frac{\partial^2 \mathrm{M}}{\partial \mathrm{x}^2} \tag{3}$$

$$\rho \frac{\partial \mathrm{T}}{\partial \mathrm{t}} = \alpha \frac{\partial^2 \mathrm{T}}{\partial \mathrm{x}^2} \tag{4}$$

where $\alpha = k / \rho\, c_p$.

For a slab that is defined by taking a region $-\mathrm{L}\left(\mathrm{t}\right) < \mathrm{x} < \mathrm{L}(\mathrm{t})$,

initial conditions are given by

$$\mathrm{M} = \mathrm{M}_0 \text{ and } \mathrm{T} = \mathrm{T}_0 \text{ at t=0} \tag{5}$$

symmetry conditions are applied at the centre for equal drying from both slab surfaces:

$$\frac{\partial \mathrm{M}}{\partial \mathrm{x}} = 0 \text{ and } \frac{\partial \mathrm{T}}{\partial \mathrm{x}} = 0 \text{ at x=0} \quad (6)$$

At the surface can be applied two types of boundary conditions, depending on the drying conditions applied: equilibrium boundary conditions or flux boundary conditions.

Equilibrium boundary conditions are given by:

$$\mathrm{M} = \mathrm{M}_e \text{ and } \mathrm{T} = \mathrm{T}_e \text{ at } x = \mathrm{L(t)} \quad (7)$$

where M_e and T_e are moisture and temperature at the equilibrium.

Flux boundary conditions, instead, are given by:

$$D_{eff} \frac{\partial^2 \mathrm{M}}{\partial \mathrm{x}^2} = -h_m \left(\mathrm{M}_{\mathrm{sur}} - \mathrm{M}_{air} \right) \text{ at } x = \mathrm{L(t)} \quad (8)$$

$$\text{And } k \frac{\partial \mathrm{T}}{\partial \mathrm{x}} - \lambda D_{eff} \frac{\partial \mathrm{M}}{\partial \mathrm{x}} = -h \left(\mathrm{T}_{\mathrm{sur}} - \mathrm{T}_{\mathrm{air}} \right) \text{ at } x = \mathrm{L(t)} \quad (9)$$

h_m is the moisture transfer coefficient, h is the temperature transfer coefficient; $\mathrm{M}_{\mathrm{sur}}$ and T_{sur} are moisture and temperature at the surface, $\mathrm{M}_{\mathrm{air}}$ and T_{air} are moisture and temperature of air, λ is the latent heat of evaporation.

All these parameters are based on a bulk transfer model between the values at the surface of the fruit and external conditions.

The effective diffusion coefficient D_{eff} is generally determined experimentally by "the method of slope" approach that is widely used. Experimental data of the effective diffusion coefficient of selected dried fruit are shown in table 2.

Food Product	**Shape**	D_{eff} **(m^2/s)**	**References**
Apple	Cube	From $3.21*10^{-10}$ at 30 °C to $12.67*10^{-10}$ at 60 °C	Simal et al. (1997)
Grape	Cylinder	$2.22*10^{-10}$ at 60 °C	Simal et al. (1998)
Mango	Parallelepiped	$8.56*10^{-10}$ at 60 °C	Hernández et al. (2000)
Cassava	Parallelepiped	$4.93*10^{-10}$ at 60 °C	Hernández et al. (2000)
Carrot	Cylinder	From $0.776*10^{-9}$ at 50 °C to $9.335*10^{-9}$ at 70 °C	Doymaz (2003)

Pineapple	Prarallelepiped	From $1.48*10^{-10}$ at 30°C to $3.24*10^{-10}$ at 50 °C	Rastogi et al. (2004)
Pear	Sphere	$5.10*10^{-10}$ at 30 °C $1.4*10^{-9}$ at 50 °C	Guinè (2006)
Banana	Cylinder	From $3.81*10^{-10}$ at 50 °C to $20.15*10^{-10}$ at 70 °C	Nguyen et al. (2007)
Pear D. Joaquina	Sphere	$8.60*10^{-10}$ at 60°C; $11.88*10^{-10}$ at 70 °C	Guinè et al. (2013)

Table 2 *Moisture diffusivity of many food products at different temperatures.*

It is assumed that the diffusivity is constant during the whole drying period. However, experimental studies also suggest that the transport properties inside the food are dependent on moisture content and temperature. The effective diffusion coefficient varies with moisture $D_{eff} = D(\mathrm{M})$, varies with temperature $D_{eff} = D(\mathrm{T})$ or varies with moisture and temperature $D_{eff} = D(\mathrm{M,T})$.

Moisture diffusivity is widely considered as a function of temperature, usually of an Arrhenius dependence, because there is an increase of molecular kinetics energy when temperature rises. In this case D_{eff} is:

$$D_{eff}(\mathrm{T}) = D_0 \exp\left(-\frac{E_a}{R\mathrm{T}}\right) \qquad (10)$$

where D_0 is the pre-exponential factor (m^2/s), E_a is the activation energy (kJ/mol), T is the temperature of air (K) and R the gas constant (kJ/mol K).

Value of D_0 and E_a are usually estimated from experimental data.

Examples of activation energy are reported in table 3:

Food Product	**E_a (kJ/mol)**	**References**
Carrot	28.36	Doymaz (2003)
Kiwi	20.41	Mhoammadi et al. (2008)
Tomatoe	33.32	Taheri-Garavant et al. (2011a)
Bell pepper	44.49	Taheri-Garavand e al., (2011b)
Pear	44.78	Doymaz & Ismail (2012)
Russian olive	48.18	Abbaszadeh et al. (2012)

Ginger slices	19.31	Akpinar et al. (2013)

***Table** 3 Activation energy of many fruit and vegetables.*

A large number of empirical parametric equations expressing diffusivity as function of moisture content can be found in the literature. An empirical equation proposed by Kiranoudis et al., (1995) to calculate moisture diffusivity for all type of fruits and vegetables is as follow:

$$D_{eff} = a\exp\left(-\frac{b}{\mathrm{M}}\right)\exp\left(-\frac{c}{\mathrm{T}}\right) \tag{11}$$

where:

M is the moisture content ($kg/kg_{d.b.}$), T temperature in °C, $a = 1.29\cdot10^{-6}$, $b = 0.0725$, c=2044.

A compilation of such equations is given by (Zogzas et al., 1996). All authors agree that the temperature effect can be described by an Arrhenius-type relation. Nevertheless, the moisture content effect has not yet been formatted into a general accepted model.

Hassini et al. (2007) for convective drying of potatoes, for moisture content from 2 to 0.25 $kg/kg_{d.b.}$ and for temperature ranging from 40 to 85°C, propose the following empirical equation for potato moisture diffusivity:

$$D_{eff}\left(\mathrm{T},\mathrm{M}\right) = 7.18\cdot10^{-5}\exp\left(-\frac{31580}{R\mathrm{T}}\right)\exp\left[\left(-0.0025\mathrm{T}+1.22\right)\cdot\mathrm{M}\right] \tag{12}$$

that's expressed in the form of:

$$D_{eff}\left(\mathrm{T},\mathrm{M}\right) = a\exp\left(-\frac{b}{\mathrm{T}}\right)\exp\left[\left(-c\mathrm{T}+d\right)\cdot\mathrm{M}\right] \tag{13}$$

The most common modelling in fruits involve heat and moisture transfer, equation 1 and 2, with empirical value of effective diffusivity such as that given by equation 11 and 13.

Guinè et al. (2007a) proposed a model to describe the drying behaviour of pears. The model simulates a significant number of situations resultant from the variation of same of the operating conditions. The temperatures tested were 30, 40 and 50 °C, the air velocities were 0.5, 1.0 and 1.5 m/s, and the relative humidity of the drying air was 40%, 50% and 60%.

The model was composed of two partial differential equations, accounting for the variations of temperature (T) and dry basis moisture content (M) for spherical geometries. Based on the model suggested by Zogzas et al. (1996), the effective diffusion coefficient (D_{eff}) was expressed by Guinè as a modified Arrhenius relationship:

$$D_{eff}\left(\mathrm{T},\mathrm{M}\right)=D_0\left(\frac{1+B\mathrm{M}}{1+CS}\right)\exp\left[\frac{\left(-E_a\right)}{R\mathrm{T}}\right] \quad (14)$$

where M and *S* represent the dry basis moisture and sugar concentrations, respectively. The parameters (D_0, *B*, *C*, E_a) were estimated from experimental data using an orthogonal regression algorithm.

The model results, representing the evolution of moisture (H=M/1-M) with time for different radial positions, confirm the experimental observations that at the periphery the profile is far much steeper (corresponding to a very fast drying rate) than in the centre, where a smooth sigmoid curve was obtained (as a result of the paths for moisture diffusion being longer and more tortuous). This behaviour is totally opposite to that of sugar evolution, where a very fast increase in sugar concentration close to the border was found, making difficult the water diffusion.

1.2.3 Models considering shrinkage

Experimental data show that the final volume of air-dried food is reduced (Barcelos et al., 2011; Yadollahinia et al., 2009), therefore, predicting the shrinkage during dehydration becomes a prerequisite for process design and optimization of the drying conditions.

In literature there are several empirical/theoretical models to predict the size reduction.

This phenomena is the direct consequence of the combination of water elimination and a weak structure forming the solid network of the dried matrixes.

The shrinkage, S_V, is generally defined as the ratio of the volume of the product during drying (V) over the initial volume (V_0) or alternatively as reduced dimensional change of thickness, diameter or the ratio of surface to volume.

Different expressions are used to represent the shrinkage phenomenon. The mathematical relationships between these expressions are reported in table 4.

Model	Product	References
$S_V = a + bM_R$	**1** Banana, apple, carrot, potato **2** Apple **3** Potato **4** Potato **5** Sweet potato **6** Pear **7** Carrot	**1** Krokida and Maroulis (1997) **2** Moreira, et al., (2000) **3** Mulet et al., (2000) **4** Yang, Sakai et al., (2001) **5** Ochoa et al., (2002) **6** Guinè et al., (2006) **7** Madiouli et al., (2007)
$S_V = a + bM_R + cM_R^2$	Apple, potato, carrot	Mayor and Sereno (2004)
$S_V = a + b\frac{M_R}{1+M_R} + c\left[\frac{M_R}{1+M_R}\right]^2$	Mango, banana, pineapple	Yan et al., (2008)
$S_V = a + b\exp(cM_R)$	Apple, potato, carrot	Mayor et Sereno (2004)

Table 4 *Mathematical models to describe the shrinkage coefficient as a function of moisture content in dried fruit and vegetables.*

For some time shrinkage was considered negligible in drying modelling, thus making drying models easier to be solved. However, in food systems shrinkage is rarely negligible, in fact model considering shrinkage fit better experimental data than model without shrinkage.

Mulet et al. (2000) showed that the volumetric shrinkage of potato samples follows a linear relation with moisture content at varying drying air temperatures, which suggests that the shrinkage is predominantly due to the volume of water removed. Such a linear shrinkage behavior of food materials has been reported by many researchers, whereas others reported a two-period phenomenon. In this case, the volume of water removed during the final stages of drying is larger than the reduction in sample volume. This behavior can be explained by the decrease in the mobility of the solid matrix of the material at low moisture contents. At lower drying temperatures, a more uniform moisture distribution exists, inducing less internal stresses that allow the sample to continue to shrink until the last stages of drying. Such a substantial shrinkage results in a low porosity. On the contrary, at higher air

temperatures, case hardening of the surface may occur and the volume of the sample becomes fixed at an earlier stage, inducing less shrinkage and a more intensive pore formation.

Parakeet et al. (2015) affirm that shrinkage and porosity change along with simultaneous heat and mass transfer during process. For potato slices dried for 7 hour at 62°C they observed that shrinkage vary linearly with moisture content and reduction in radial dimension of potato slices was around 35% (Figure 1). Porosity undergoes rapid increase after attaining certain moisture content in final stages of drying.

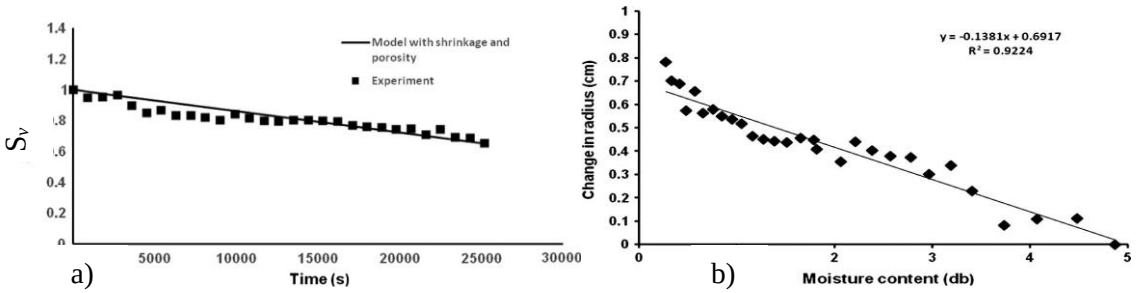

Fig. 1*. a) Experimental measurements fitted with model considering shrinkage for potato, b) Linear fitting of change in radius vs. moisture content, (Parakeet et al., 2005).*

Hernandez et al. (2000), in order to obtain a simplified equation for the mathematical description of drying kinetics, proposed an analytical solution of a mass transfer equation with concentration-dependence shrinkage and a constant average water diffusivity. Experimental drying curves of 4 x 4 cm^2 mango slices, with 0.5, 1.0 and 1.5 cm thicknesses and 10 cm long cassava parallelepipeds with 1, 2 and 3 cm thicknesses, at different air temperatures (50°C, 60°C and 70°C) and 3 m/s of air velocity were obtained in order to fit the proposed model by non-linear least-squares.

The values of effective diffusion coefficient obtained with and without shrinkage are reported in table 5:

Ford Product	D_{eff} (m^2/s) without shrinkage	D_{eff} (m^2/s) with shrinkage
Cassava	From $1.22*10^{-9}$ at 40 °C to $1.66*10^{-9}$ 60°C	From $3.67*10^{-10}$ at 40 °C to $5.24*10^{-10}$ at 60 °C
Mango	From $6.13*10^{-9}$ 40 °C to $8.12*10^{-9}$ 60 °C	From $6.13*10^{-10}$ at 40 °C To $8.69*10^{-10}$ 60. °C

Table 5 *D_{aff} for cassava and mango with and without shrinkage, (Hernandez et al., 2000).*

They obtained an accurate simulation of experimental data using the average water diffusivity and shrinkage parameter.

Hasina et al. (2007) plotted the variation of the experimental volume of potato samples as a function of the mean moisture content (Fig. 2).

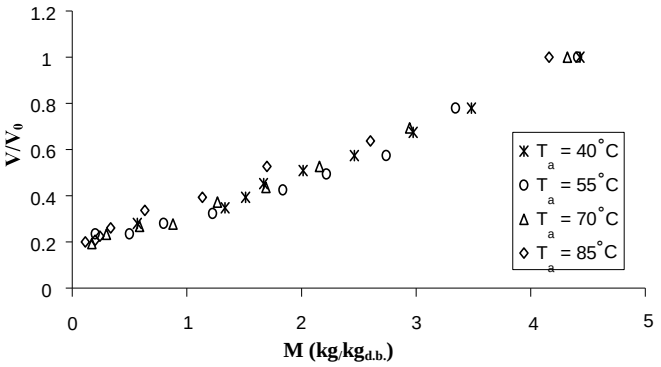

Fig. 2. *Volume of potato slab vs moisture content for different air temperatures, (Hasina et al., 2007).*

They fitted the experimental data by a linear equation:

$$\frac{V}{V_0} = \frac{V_F}{V_0} + \frac{V_F}{V_0}\beta M \qquad (15)$$

where V_F is the final (dry) product volume, V_0 is the initial product volume. The shrinkage coefficient is calculated as the slope of the best fit.

In their experiments $\beta = 1.37$ is calculated on the entire temperature domain: 45-85 °C. It can be compared to 1.35 (Chekhov et al., 2004) for potato, 1.54 for grapes (Venegas, et al., 1990).

The differences between the moisture diffusivity data, corrected and non-corrected for shrinkage, are very significant in the domain of critical value of M, nearly one order of magnitude.

T_{ari} (°C)	a_{ir} (m/s)	D_{eff} (m^2/s), without shrinkage	D_{eff} (m^2/s), with shrinkage	Relative difference (%)
40	0.5	$4.01 \cdot 10^{-9}$	$4.24 \cdot 10^{-10}$	89.27
	1	$4.12 \cdot 10^{-9}$	$4.30 \cdot 10^{-10}$	89.70
55	0.5	$4.39 \cdot 10^{-9}$	$8.12 \cdot 10^{-10}$	81.50
	1	$4.45 \cdot 10^{-9}$	$8.34 \cdot 10^{-10}$	81.25
70	0.5	$5.36 \cdot 10^{-9}$	$1.20 \cdot 10^{-9}$	77.61
	1	$5.43 \cdot 10^{-9}$	$1.29 \cdot 10^{-9}$	76.24
85	0.5	$6.13 \cdot 10^{-9}$	$1.88 \cdot 10^{-9}$	69.33
	1	$6.22 \cdot 10^{-9}$	$1.92 \cdot 10^{-9}$	69.13

Table 6 *Analytically determined moisture diffusivity, with and without shrinkage at different temperatures and air velocities, (Hassini et al., 2007).*

Barcelos et al. (2011) modelled the drying kinetics of potatoes considering shrinkage, adding a low of variation of the radius of the potatoes (a sphere shape with initial radius of 10 mm), obtained fitting the experimental data (equation 16).

$$r = r_0 \left(\frac{0.8 + M}{0.8 + M_0} \right)^{\frac{1}{3}} \qquad (16)$$

During drying, the operating conditions of the oven were: an air temperature of 60ºC and absolute humidity of 5 kg/100 $kg_{dry\ air}$.

They solved the differential equation of mass transfer for moisture content inside the spherical potatoes using the method of finite control volume.

Figure 3 depicts the experimental and simulated data of dimensionless free moisture content as a function of the drying time. In the beginning of drying, the diffusive model, not taking into account the shrinkage, fits better the data. After, this model underestimates the internal mass transfer phenomena as it does not take into account the changes in internal resistance promoted by the size reduction over time, leading to a significant effect on describing the drying kinetics data. Instead, model taking into account shrinkage presents a better agreement to the experimental data.

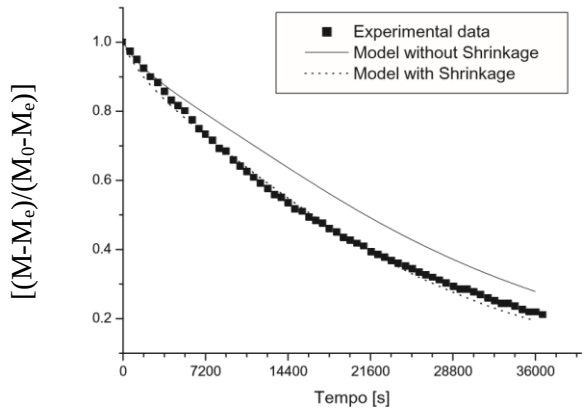

Fig. 3*. Dimensionless free moisture content as a function of drying time, (Barcelos et al., 2011).*

In figure 4 they plotted the moisture content profile along with radius axis. At the beginning of drying (i. e. 3600 s) the moisture content inside the food remains almost spatially uniform and the moisture content shape profile is a sigmoid. From time 10800 s to 36000 s the moisture content shape profiles are parabolic.

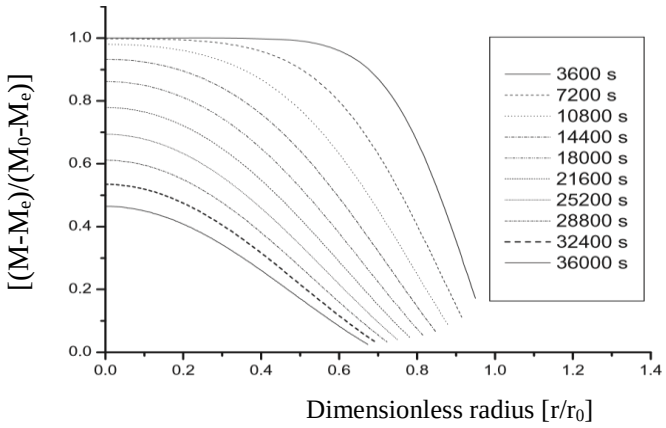

Fig. 4. *Dimensionless free moisture content as a function of dimensionless radius axis at a given drying time, (Barcelos et al., 2011).*

Brasiello et al. (2013) proposed two mathematical models with shrinkage effect describing eggplant drying. In the first model they considered shrinkage effect through a non-constant diffusion coefficient depending on the water content, $D_{eff} = \delta - \beta M_R$, where δ is the intercept of $D_{eff}\left(M_R\right)$ and β the slope of $D_{eff}\left(M_R\right)$.While in the second model they introduced a fictious convective term, $u = \xi \frac{\partial M_R}{\partial x}$, where u is the shrinkage velocity and ξ a parameter linking u and the spatial derivate of M_R. They demonstrated, using suitable boundary conditions, that the two models are equivalent. Then using experimental

data of weight loss and void fraction at different temperature they derived models parameters. The advantage of this model was of describing with sufficient accuracy the drying process in a wide range of conditions using few parameters.

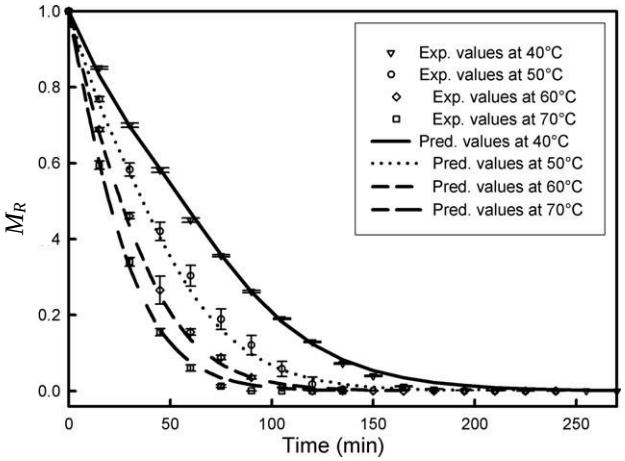

Fig. 5. *Experimental and predicted total dimensionless water content temporal profiles during eggplant drying at different temperatures, (Brasiello et al., 2013).*

In a successive work, Brasiello et al. (2017) analyzed the possibility of prediction MRI spatial profile of water during eggplant's dehydration using the mathematical model developed previously. In figure 6 it's compared the MRI derived moisture spatial profile during the dehydration of a cylindrical sample of eggplant at 323 K with the previous model taking into account the shrinkage effect. It's possible to see that numerical data are close to experimental data, instead applying simple Fick's law in cylindrical coordinate, numerical data are lower than experimental data.

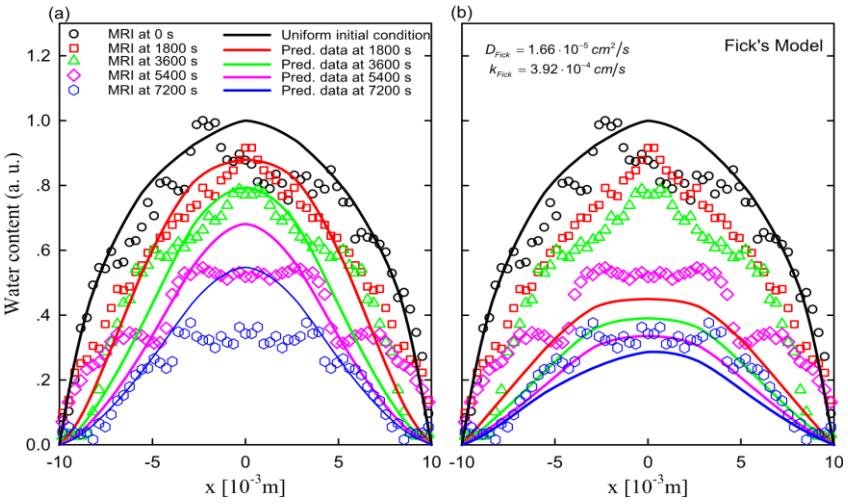

Fig. 6. *Comparison of the MRI derived moisture spatial profiles during the dehydration of a cylindrical sample of eggplant at 323 K with: (a) numerical data; (b) numerical data derived from Fick's model, (Brasiello et al., 2017).*

1.3 Techniques for quality analysis of fruit and vegetable

Laboratory analysis of food quality often involves extensive preparation procedures, during which foods are severely disturbed by size-reducing, deforming, or diluting steps. This is very unlike the way in which food consumers evaluate the quality of food products (i.e., foods are consumed while their integrity is generally intact.). Naturally it would be desirable to be able to analyse food quality in a completely non-destructive and non-invasive way. Nuclear magnetic resonance (NMR) techniques are among those most capable of performing such a task.

Nuclear magnetic resonance (NMR) spectroscopy and magnetic resonance imaging (MRI) are based on the magnetic properties of the atomic nucleus and many elements have isotopes with such properties, above all the omni-abundant proton. NMR and MRI have some distinct advantages over other instrumental methods: they are non-invasive and non-destructive; most systems are transparent for the excitation; they measure volumes instead of surfaces; and the methods allow the extraction of both physical and chemical information. By exploitation of magnetic resonance it is possible to obtain unique knowledge about, for example, flow, diffusion and water distribution without perturbing the system. Similarly, processes such as heating, freezing, salting, hydration and dehydration can be monitored absolutely non-invasively.

Another advantage of these techniques, beside that the sample don't need any pre-treatment, is that once developed, standards protocols based on rapid measurements can be easily transferred to quality control applications.

1.3.1 Basic theory of NMR and MRI

NMR differs from most other forms of spectroscopy in that it is the atomic nuclei that are the subject of study, and the energy absorbed and emitted by the nuclei is in the radio frequency range. Many nuclei possess an angular momentum, which means that they have a characteristic spin quantum number (I), and may be analyzed using NMR. The most common nuclei analyzed by NMR are the proton (H) and the ^{13}C isotope of carbon, as well as ^{19}F and ^{31}P, all of which have a spin $I = 1/2$.

These nuclei are also charged, and a spinning charge generates a magnetic field. Simply put, the nuclei behave like tiny magnets that interact with an applied, external magnetic field.

Once the nuclei are placed within a strong external magnetic field (B_0), the spin of the nuclei will align with that field. Because of quantum mechanical constraints (nuclei of spin I have $2I + 1$ possible orientations in the external magnetic field), there are only two orientations

that the spin 1/2 nuclei can adopt: either aligned with the applied magnetic field (parallel or spin +1/2) or aligned against the field (anti-parallel or spin −1/2). The parallel orientation has a slightly lower energy associated with it and, therefore, has a slightly higher population. It is this excess of nuclei in the spin +1/2 state that produces the net magnetization that is manipulated during an NMR experiment. The spin of the nuclei is not around the center axis, but comparable to a gyration.

The motion of a spinning charged particle in an external magnetic field is known as precession, and there is specific precessional orbit and frequency, the Larmor frequency, which is related to the magnetic properties of the nuclei. The magnitude and direction of the local magnetic field describe the magnetic moment or magnetic dipole of the system. However, due to the precession and the lower energy state excess of nuclei, there is a net vector parallel to the applied field.

All nuclei of the same element, H for example, will have a nearly identical Larmor frequency in a magnetic field. The specific frequency is dependent on the strength of the external magnetic field, and the Larmor frequency of H in this field defines the NMR instrument. For example, a proton has a Larmor frequency of 500MHz in an 11.7 T magnet, so the instrument is termed a "500MHz NMR spectrometer." The strength of the magnet not only governs the Larmor frequency of the nuclei, but also determines the degree of excess nuclei in the parallel orientation. The excess of nuclei in the parallel orientation increases with an increase in the external magnetic field strength, and this in turn impacts the signal intensity of the NMR experiment (i.e., more protons will be detected in a higher field strength instrument). This is one reason researchers seek ever more powerful magnets for NMR. Field strength impacts sensitivity and the signal/noise (signal-to-noise) ratio, and, therefore, the information obtained from the NMR experiment.

One of the major developments in NMR technology was the RF pulse, in which a large range of frequencies is excited by a short pulse of RF energy around a centered carrier frequency, which is at the Larmor, or resonance, frequency of the nuclei under study. This pulse simultaneously excites all of the protons in the sample. The NMR data for all the protons is collected during a short time after the pulse is applied; therefore, it is termed time-domain NMR. In NMR, the carrier frequency, transmitter power, and duration of the RF pulse determine the frequency range of the pulse.

Once the sample is placed in the magnet, the protons align parallel or antiparallel to the applied, external magnetic field, B_0, with an excess in parallel orientation. The net magnetization of the nuclei in the parallel orientation is aligned with the z-axis in an xyz graphical representation of the system, although the precession of each nucleus is random.

However, after a pulse of RF energy is applied to the system, the nuclei precess coherently and individual nuclei absorb energy and shift to a higher energy state. The pulse, which is applied by a transmitter coil perpendicular to the z-axis (B1), tilts the net magnetization vector away from the z-axis and toward the xy plane .

Although the parameters that define a pulse include the transmitter power and the pulse duration, a specific pulse used in an NMR experiment is usually described by the degree to which the net magnetization is tilted. The most common pulse is the 90◦ pulse, which tilts the net magnetization exactly into the xy plane where the receiver coil is located, thereby maximizing the resulting signals.

Many NMR experiments use a series of pulses, termed a pulse sequence, to manipulate the magnetization. Complex pulse sequences are essential for the two-dimensional (2D) NMR experiments that are required for complete structural analyses of complex molecules.

Once the net magnetization has been tilted into the xy plane by a 90◦ pulse, the magnetization begins to decay back to the z-axis. This process is termed NMR relaxation, and it involves both spin–lattice (T1) and spin–spin (T2) relaxation. T1 relaxation is associated with the interaction of the magnetic fields of the excited-state nuclei with the magnetic fields of other nuclei within the "lattice" of the total sample.

T_2 relaxation involves the interactions of neighboring nuclei that lead to a diminishment in the energy state of the excited-state nuclei and the loss of phase coherence.

The mechanisms behind relaxation are complex, but the process can be utilized for some specific NMR experiments that, among other things, take advantage of the fact that samples in different forms, liquids vs. solids for example, relax at different rates.

Like NMR spectroscopy, MRI is a method that exploits the magnetic properties of the atomic nucleus. Magnetic resonance imaging (MRI) is unique in that the sample can be placed into the magnet in the native form, and 2D or 3D images of the sample can be generated.

MRI involves variations in field strength and the center frequency of the pulses over time and space, along with the application of field gradients in different geometric positions relative to the magnet bore (B_0). The end result is a spatial "encoding" of the sample protons with different phase and frequency values. After multidimensional Fourier transformations of multiple FIDs from different spatial "slices" of the sample, an image of the sample is produced that contains information about the state of the material under study.

1.3.2 NMR applied to fruit and vegetables

Low-field ^{1}NNMR relaxometry is an appreciate technique to investigate on the most abundant components of intact foodstuff based on relaxation parameters and amplitude of the NMR signals. ^{1}H pulsed low field NMR allows to obtain information on water compartmentalization and diffusion by detecting proton signal predominantly due to H_2O contained in vegetable tissue.

In literature many fruits such as banana (Raffo et al., 2005), tomato (Musse et al., 2010), kiwifruit (Panarese et. al., 2012) have been investigated by means of low field NMR.

The relaxation signals from vegetal cells have generally been described by a multi-exponential behaviour reflecting different water compartments. The longitudinal T_1 and transverse relaxation T_2 times are known to be related to the water status in the compartments, i.e. water content, water mobility and interactions between water and macromolecules.

Few investigations have been focused on the attribution of the NMR signal components to water compartments.

In tomato fruit Tu et al. (2007) reported a single component of T_2, while four components were found in the tomato pericarp by Duval et al. (2005) and Maringheto et al. (2009). The precise assignment of the NMR signal components to specific subcellular compartments is still a subject of database.

Maringheto et al. (2008) investigated the internal sub-cellular characteristics of Red Delicious apple with novel two-dimensional NMR relaxation and diffusion technique. They found four relaxation peaks. The peak with the longest T_2 and largest area was associated with water in the vacuole, the peak with shortest T_2 was associated to rigid components of cell wall in the apple matrix, and the other two were associate with the water in the cytoplasm and extra-cellular compartments.

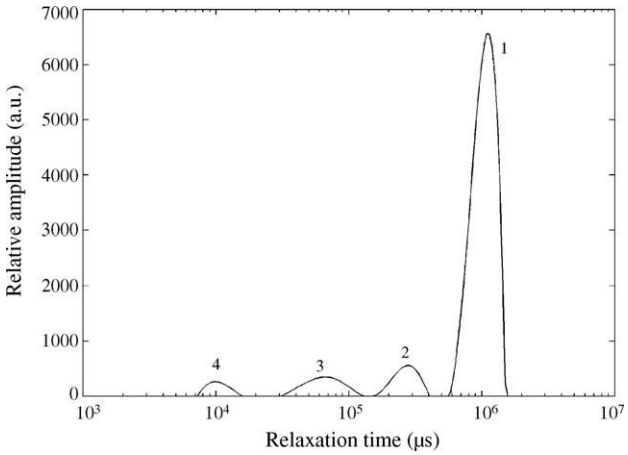

Fig. 7. *Distribution of transverse water proton relaxation times in fresh 'Red Delicious' apple tissue measured at spectrometer frequency of 23.4MHz with a CPMG 90–180◦ pulse spacing of 200s. Numbers refers to relaxation peaks of the water proton in the different cell compartments: 1, the vacuole; 2 and 3, cytoplasm and extra-cellular compartment and 4, cell wall,(Maringheto et al., 2008).*

There are also available portable NMR devices that allow easy sample access, which makes them attractive for quality control in industrial environments and directly on sealed packaged food. In this case, the magnet is placed to one side of the object fully preserving the integrity and the dimension of the sample under investigation and also allowing the measurement to whole packed products.

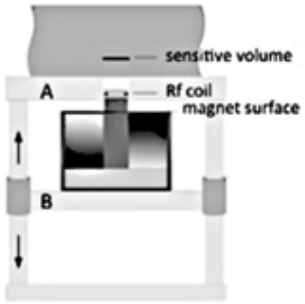

Fig. 8. *Sketch of the geometry of the magnet of the profile NMR mouse.*

Capitani et al. (2010, 2013) monitored the water status of kiwifruits as a function of season using a single-sided NMR sensor. Using this sensor, they measured the entire fruit at a depth of about 0.5 cm from the peel surface without cutting it, as shown in figure 9.

Fig. 9. *Measurement of intact kiwifruit with a single-sided NMR sensor, (Capitani et al., 2010).*

The T_{2eff} distribution of a mature kiwifruit showed three peaks, as reported in figure 10. According to the literature, they assigned the longest T_{2eff} component to protons in vacuole, the intermediate one to proton in cytoplasm and extra-cellular space, and the shortest one to proton in cell walls.

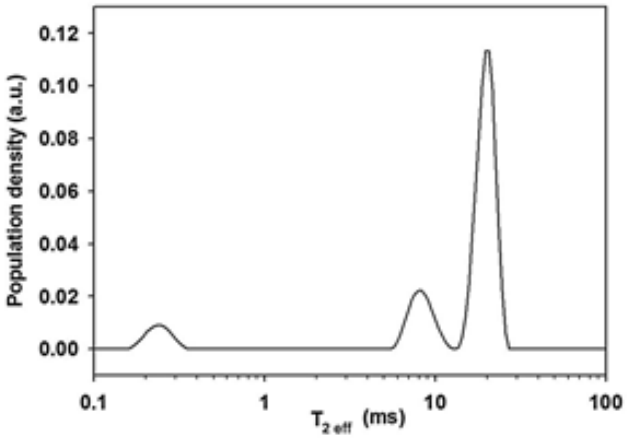

Fig. 10. *Transverse relaxation times distribution measured on ripened kiwifruit, (Capitani et al., 2010).*

In a successive work Capitani et al. (2013), monitored the ripening of kiwifruits in field on fruit attached to the plant during three campaigns of measurement carried out in October, November and December (figure 11).

Fig. 11. *Measurement in field on entire kiwifruit attached to the tree with a portable unilateral NMR instrument, (Capitani et al., 2013).*

Figure 12 show the transverse relaxation decays measured in field on entire kiwifruit attached to the tree, for three cultivars.

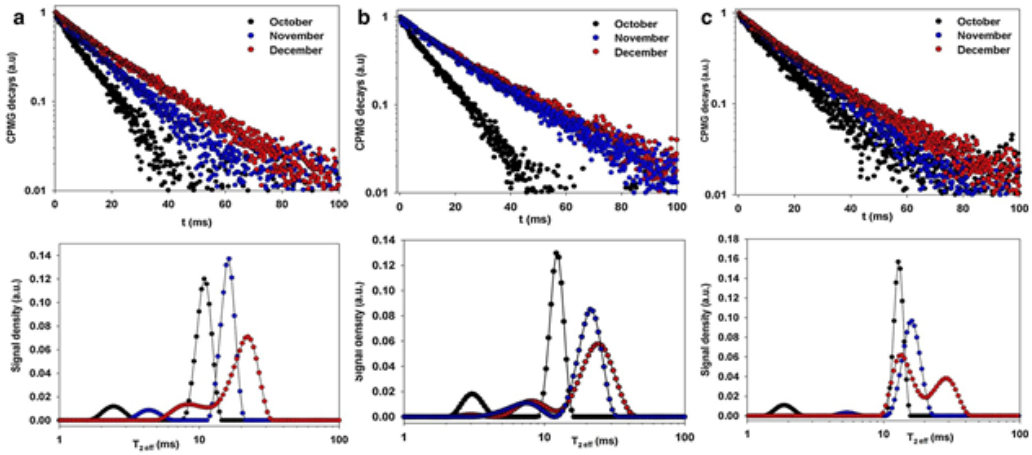

Fig. 12. *Transverse relaxation curves measured in field in October, November, and December on Hayward (a), CI.GI (b), and Zespri (c) with the corresponding relaxation time distribution, (Capitani et al., 2013).*

In all cultivars, a lengthening of decay with the season was observed; already the process was complete in November for Zespri as shown by the perfect overlapping of decay measured in November and December.

Capitani et al. (2014) also applied NMR methodology to the analysis of blueberries.

They plotted the ^{1}H NMR signal as a function of the depth blueberry scanned (figure 13).

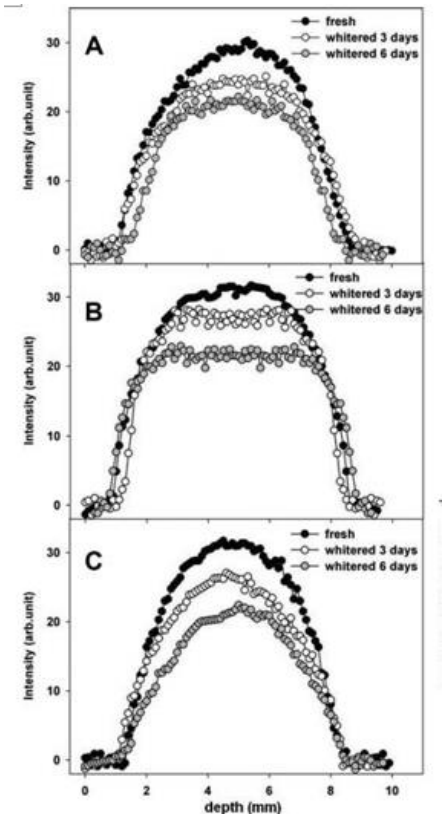

Fig. 13. *(A, B and C) Depth profiles of three fresh blueberries, and profile of the same blueberries let to wither for three and six days, (Capitani et al., 2014).*

They compared profiles of three fresh intact blueberries to those let to wither outside the fridge for three and six days. The amplitude profile of withered blueberries was found to be lower than measured on fresh blueberries, indicating a loss of water.

They calculated the average loss of water in withered blueberries by integrating the profiles. After three days they measured a loss of water of 13 %, 11 % and 16 % in three different blueberries.

Instead, from transverse relaxation time measurement, obtained for the three fresh blueberries and the same let to whiter for three and six days, they found a bimodal and trimodal distribution for fresh and withered blueberries, respectively.

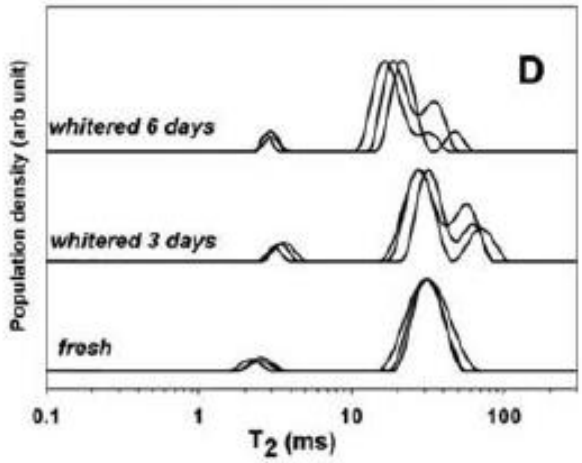

Fig. 14. *T_2 distributions of three fresh blueberries, and the same blueberries let to wither for three days, and for six days, (Capitani et al., 2014).*

In fresh blueberries, the longest component of T_2 was assigned to protons in vacuole and cytoplasm, the shortest in cellular wall.

After three and six days of withering, the shortest T_2 values was assigned to protons in cellular wall, the intermediate in cytoplasm and the longest in protons to vacuole. After withering for six days T_2 value shortened, indicating membranes denaturation and occurrence of water loss due to prolong whitening. This observation may be explained with a reduced permeability of water across membranes.

Adiletta et al. (2015) used the NMR relaxometry to investigate the drying process of parallelepiped samples of pear at T=50°C. Using a portable NMR they measured the amplitude of water profile in fresh and dried samples during time, which resulted in good agreement with gravimetric measurements. Moreover, information on shrinkage was obtained by measuring the depth of NMR profiles during time. The data obtained were well correlated (R^2=0.87) with size measurements made through a vernier caliper.

Adiletta et al. (2014) investigated the effect of hot-air drying (50, 60 °C) on the physical properties of cylindrical eggplant samples. They determined drying kinetics, water profiles along longitudinal and transversal sample sections through nuclear magnetic resonance imaging (MRI) and volumetric shrinkage.

The two-dimensional spin echo images of eggplant samples are shown in figure 15 for both temperatures they investigated (50, 60 °C) at specific times.

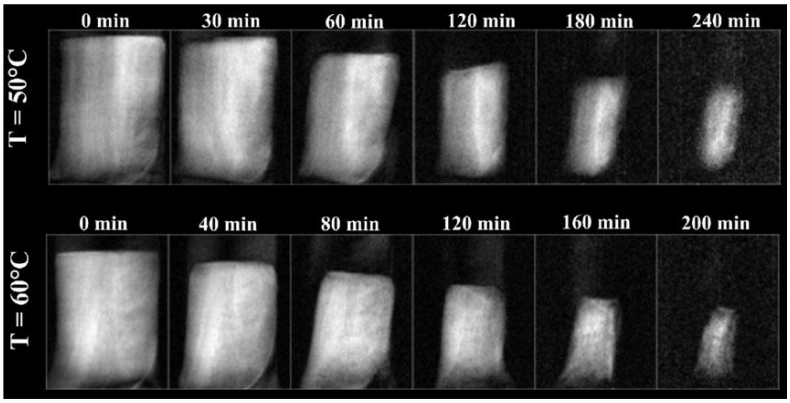

Fig. 15. *Two-dimensional spin echo images of eggplant at both investigated temperatures and selected drying times, Adiletta et al. (2013).*

As expected, during the drying process, the size of brighter regions, which corresponded to higher proton density areas, considerably decreased. For every temperature, they extracted the pixels with the maximum and minimum signal, regardless the drying steps, considering all the images collected. Then they rescaled all the values: the minimum pixel value was set equal to 0 and the maximum value to 1. After that, for each image, they summed all the pixel values and normalized all data to the initial mass of water, to obtain the dimensionless moisture ratio M_R. At the end they compared these values with those obtained with gravimetric method achieving a good agreement, figure 16.

Also, they proposed a power equations ($V/V_0 = a_1 + a_2 M_R^b$) to fit the experimental data of shrinkage, figure 17.

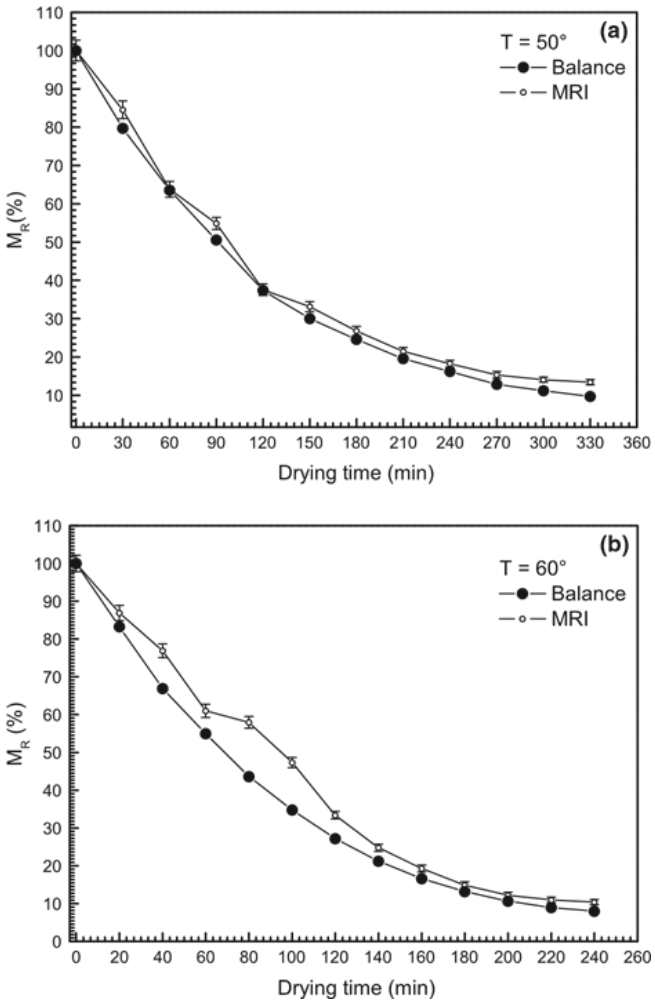

Fig. 16 *Moisture ratio (%) of samples during drying obtained by gravimetric method and MRI at T = 50 °C (a) and 60 °C (b), (Adiletta et al., 2014).*

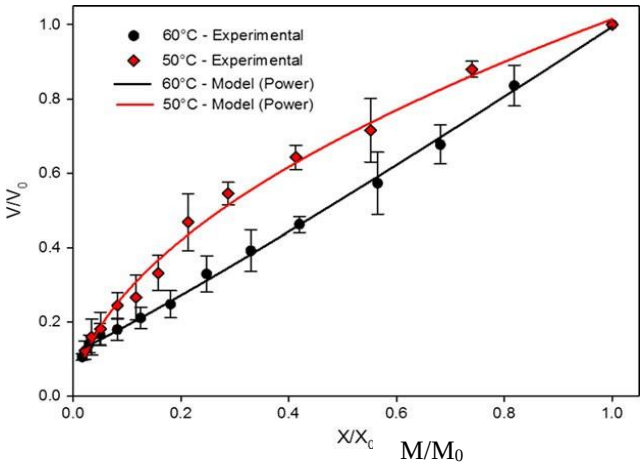

Fig. 17. *Experimental shrinkage data and prediction by power model, (Adiletta et al., 2014).*

1.4 Thesis Objectives

The aim of this thesis is to better understand the effect of drying on the final product quality with respect to the fresh one. Understanding the factors responsible for the decrease in quality of the food during dehydration process is of major relevance.

First objective is to investigate the effect of the main parameters, temperature and time of drying, on the final products.

The most important modification during drying, which was considered, is the reduction of the food external volume due to heating and loss of water that causes stress in the cellular structure. Loss of water and heating causes stress in the cellular structure of the fruit leading to change in shape and decrease in dimensions. Shrinkage has a negative consequence on quality of dehydrated fruit. Changing in shape and hardness cause in most cases a negative impression in the consumer. Another negative consequence of shrinkage is the decrease of the rehydration capability of the product.

In this thesis, hot air drying was applied to fruits such as pear and grape, which are characterized by high initial moisture levels and by cellular internal structure. The drying kinetics of the samples and their volume was measured during drying. Fruit samples were then characterized before and after drying by SEM, NMR relaxometry.

Through NMR relaxometry is possible to study the quality of the food by measuring H^1 NMR depth profile, longitudinal and transverse relaxation time and self-diffusion coefficient. Specifically, relaxation times and self-diffusion coefficient were measured to probe the state of water, whereas ^1H NMR depth profiles allowed to detect and quantify the shrinkage and to detect the presence of sugar gradients in dried fruits.

All these measurements allowed us to model the process in a better way. In fact, in literature the models based on Fick's second law are able to predict in same case the drying evolution of moisture ratio vs time, but are not able to predict the moisture profile along the main coordinate of the product. On the other hand, it is clear that shrinkage is an important parameter to consider in order to properly model the drying process.

The second objective of this thesis is to build a model that consider the shrinkage effect and that can be replicable. As observed in literature, the evaluation of effective diffusion coefficient without considering shrinkage can change considerably. Having a model more complete, it's possible to use it to estimate drying parameters as first step for other operating conditions and reduce experimental costs.

Finally, the effect of physical pre-treatment (abrasion) on the drying kinetics of grape was analysed in order to reduce the drying time, without changing food quality, and with the final objective to reduce the cost production.

1.5 Thesis Structure

In this chapter is given a brief overview of drying methods applied to fruit and vegetables, the mathematical models developed, their application and their results. In chapter two are presented all the experimental measurements carried out on pear samples: drying experiments, thickness reduction measurements, ^{1}H NMR depth profiles, longitudinal and transverse relaxation time, self-diffusion coefficient and SEM analysis. In chapter three are reported mathematical models used to describe pear drying. First, the analytical solution of the Fick's law in regular geometries, sphere and parallelepiped is reported, and the results in terms of moisture ratio vs time and moisture profile along the main coordinate are compared with the experimental data. Then it is presented a model considering the shrinkage effect and its comparison with experimental results. Chapter four presents the study carried out on the drying of grapes. There is a brief overview of the characteristics and quality of grapes under physical pretreatment presented in literature, and the experimental drying kinetics, shrinkage measurements and SEM images performed were reported. Then it is presented a mathematical model in cylindrical and spherical coordinate based on Fick's law and a model considering shrinkage in spherical coordinate. The results of the models are compared to the experimental data.

In the end, chapter five gives the conclusions of the thesis and future work suggestions.

CHAPTER 2

Pear Drying: experiments

2 Materials and Methods

The pear (*Pyrus communis* L. cv. 'Conference') is a typical fruit of temperate zones and is cultivated in Europe, among other regions. It has nutritive properties, good taste and low caloric level. Pears can be consumed fresh, dried and they are also used in processing techniques such as in syrup conserves, purees for use in nectars and yogurts and drying (Park et al., 2002). Hence the pear are highly considered by consumers.

2.1 Sample preparation

Drying experiments are conducted on pears of cultivar Conference.

Samples are taken in two different geometries. Pears are peeled and with a spoon were taken spherical samples of a diameter of 1.4 cm with initial moisture content of 5.73 ± 0.12 $kg/kg_{d.b.}$. Then using a suitable steel mould, samples with dimensions of 2.5x2.5x2 cm^3 and initial moisture of 7.53±1.10 $kg/kg_{d.b.}$ were also obtained from peeled fruit, figure 18.

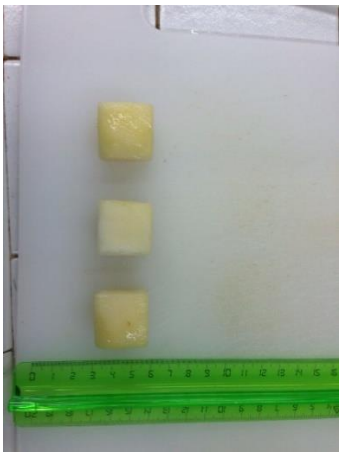

Fig. 18. *Parallelepiped sample of fresh pear.*

Then the samples were placed over a metal grating in a convective dryer, with air velocity of 2.3 m/s, operating at a constant temperature, figure 19.

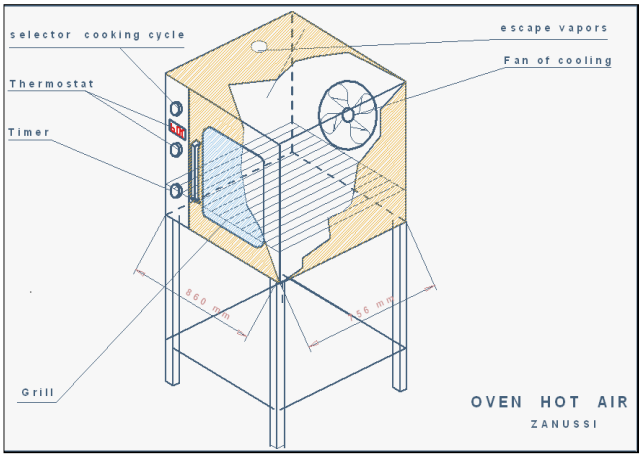

Fig. 19. *Convective oven with a constant air velocity of 2.3 m/s used for the experiment.*

2.2 Results

2.2.1 Drying experiments

Drying experiments were carried out at three different temperatures: 45, 50 and 55°C, typically used temperature in industrial environment. At one our interval the sphere samples were removed and their weight loss was measured by means of a digital balance. The procedure was repeated until the weight remained constant. A total drying time of 52 hours was necessary to reach a constant value of 0.025 ± 0.013 kg/$Kg_{d.b.}$ for the sample in spherical geometry. Instead, sample of parallelepiped geometry were put on a perforate network and the drying kinetics was continuously recorded by means of a weight sensor (Phidgets INC., Canada), figure 20. This sensor is a load cell made of a transducer that converts mechanical force into electrical signals.

A time of 48 h was necessary to reduce the moisture content of pear parallelepiped samples to a constant value of 0.39 ± 0.12 kg/$Kg_{d.b.}$.

Moisture ratio (M_t/M_0) was calculated as the ratio between the actual (M_t) and the initial (M_0) moisture content on dry basis.

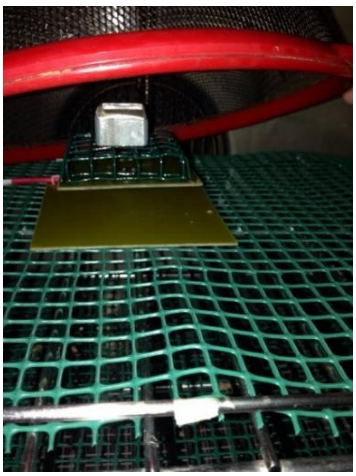

Fig. 20. *Weight sensor on which there is a perforated network where lie the sample.*

In figures 21, 22, 23 are reported the experimental result of drying kinetics during time for spherical pears sample and in figures 24, 25, 26 for parallelepiped samples at the three temperatures evaluated, 45, 50 and 55°C.

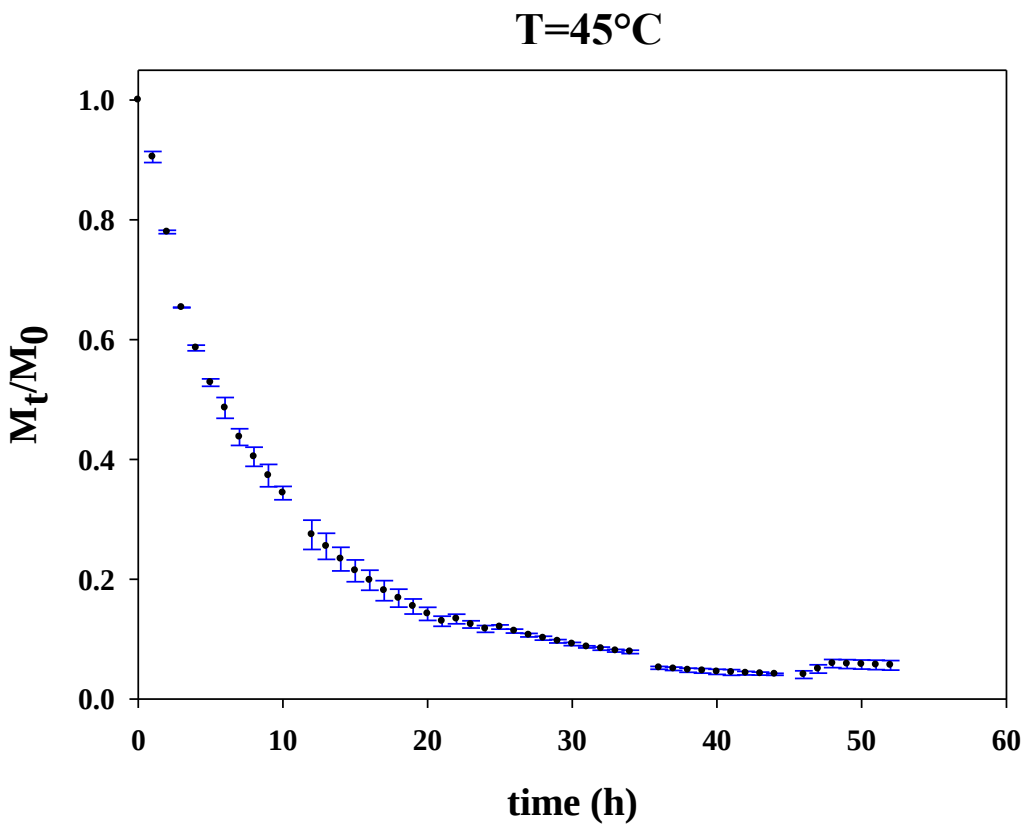

Fig. 21. *Moisture ratio of spherical pear sample during drying at T=45°C.*

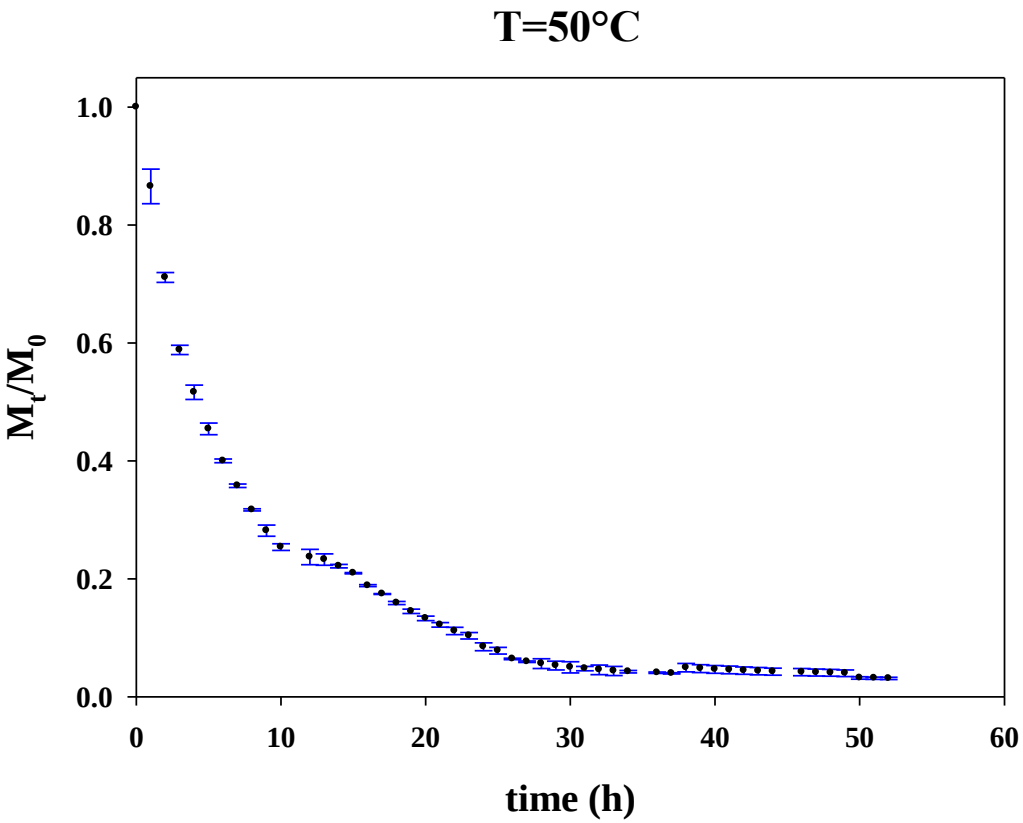

Fig. 22. *Moisture ratio of spherical pear sample during drying at T=50°C.*

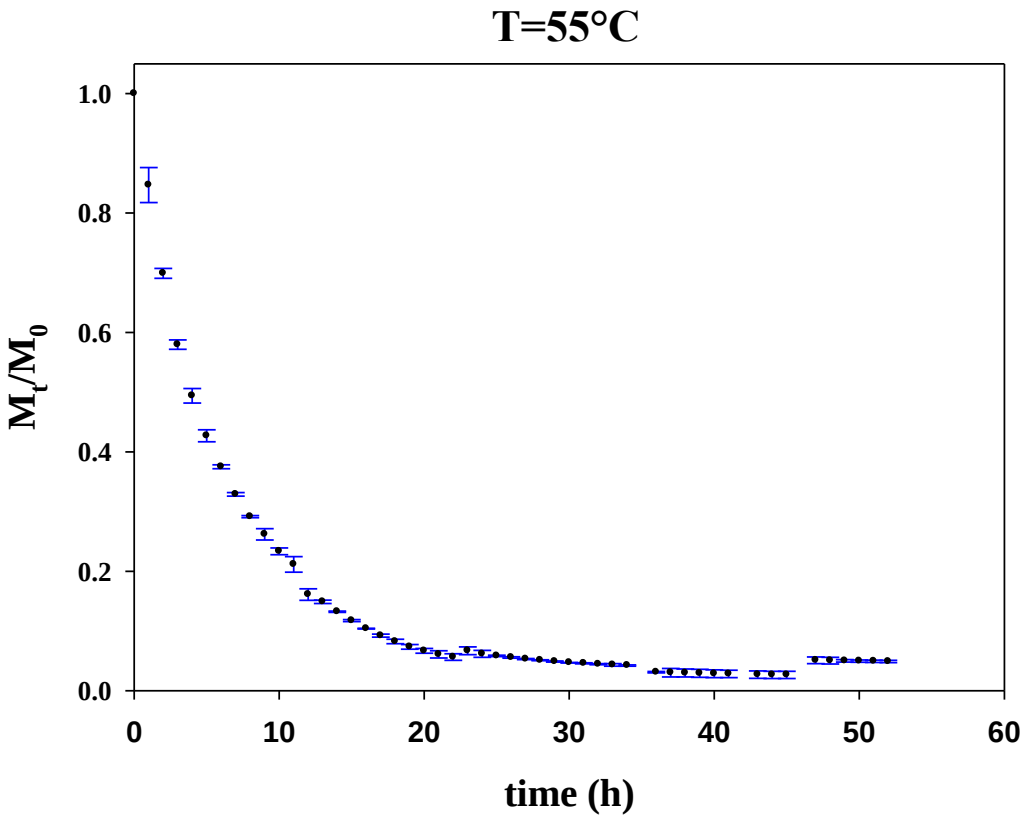

Fig. 23. *Moisture ratio of spherical pear sample during drying at T=55°C.*

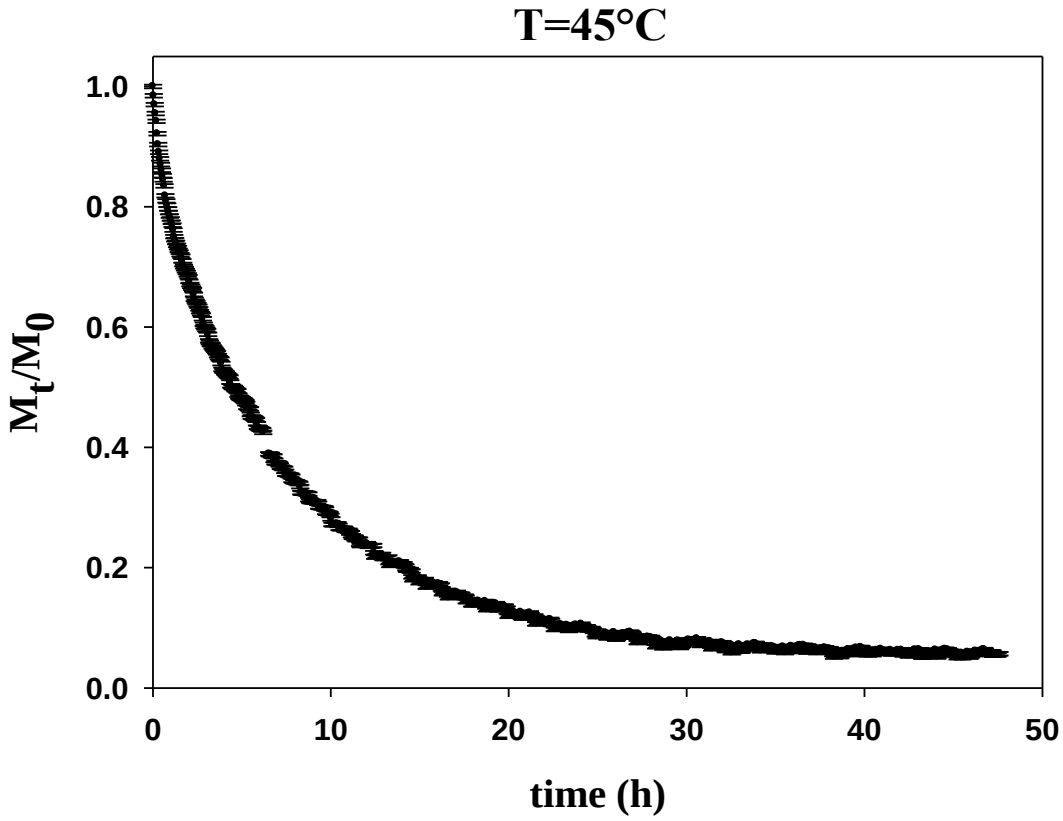

Fig. 24. *Moisture ratio of parallelepiped pear sample during drying at T=45°C.*

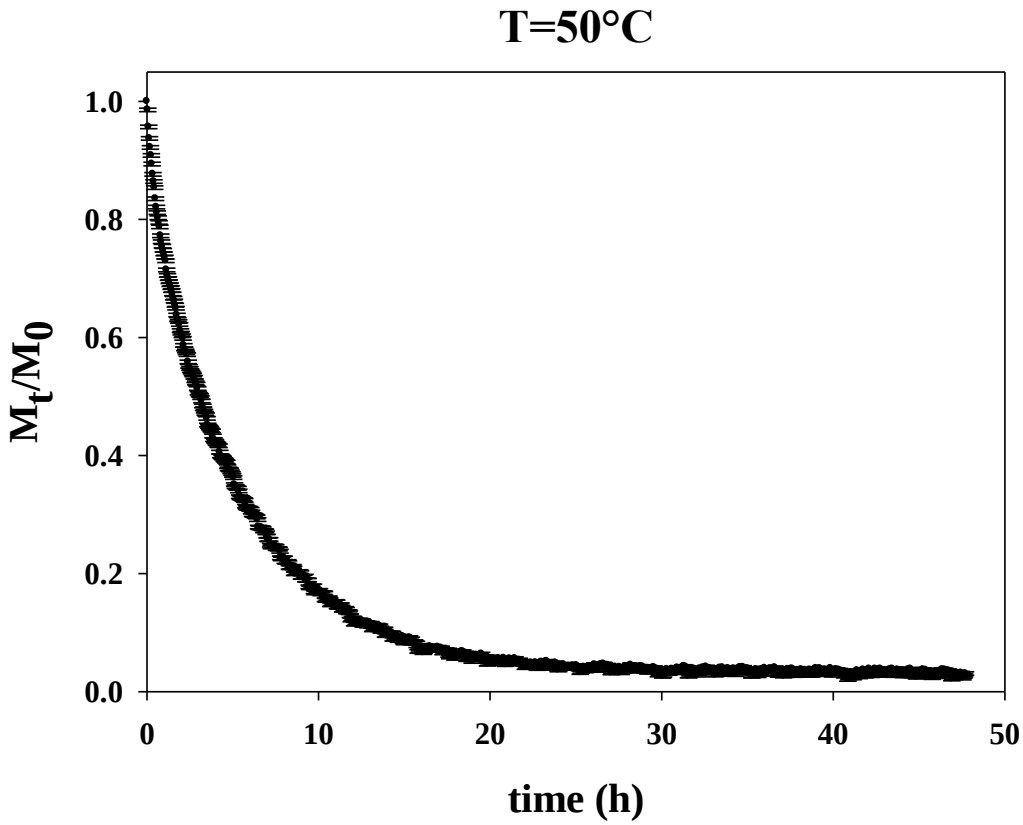

Fig. 25. *Moisture ratio of parallelepiped pear sample during drying at T=50°C.*

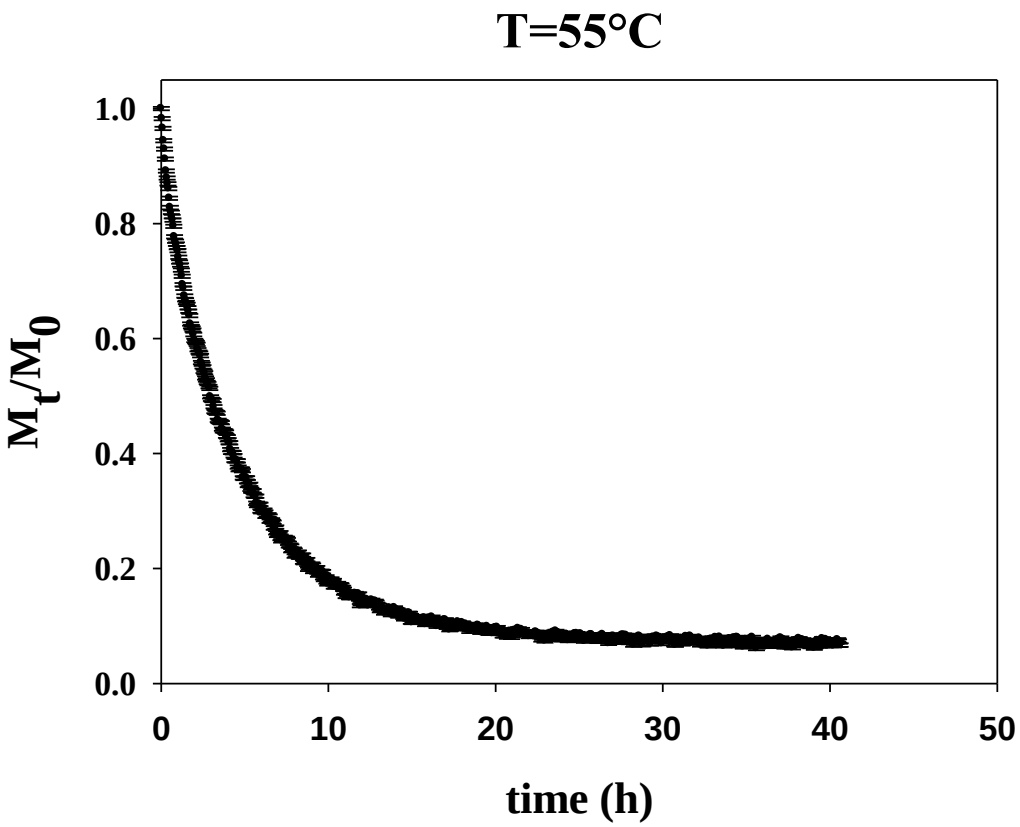

Fig. 26. *Moisture ratio of parallelepiped pear sample during drying at T=55°C.*

2.2.2 Thickness reduction measurements

At each drying time pear samples in parallelepiped geometry were removed from the oven and their dimensions were measured by means of a vernier caliper. Three measurements were carried out on each sample, one measurement was performed on the right end of the sample, another on the left end of the sample and another one in the middle. Then the thickness L of the sample at various drying time was obtained from the average of the three values.

The shrinkage of sample was expressed as the ratio between the sample thickness at a given drying time (L) and initial one (L_0).

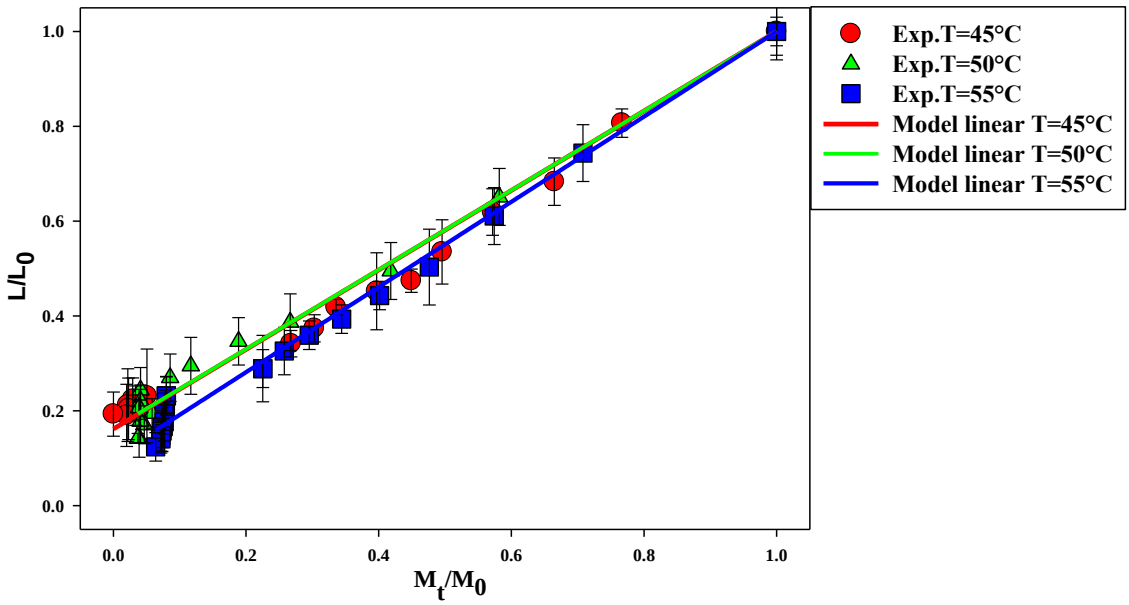

Fig. 27. *Experimental data of average thickness reduction L/L_0 vs Mt/M_0.*

The shrinkage results were reported as function of moisture fraction for the different temperature in figure 27. A linear equation (17) with constants and fitting parameter in table 7 can be used.

$$\frac{L}{L_0} = a + b\frac{M_t}{M_0} \qquad (17)$$

	Temperature		
	45 °C	**50 °C**	**55 °C**
a	0.1617	0.1627	0.1018
b	0.8383	0.8373	0.8982
R^2	0.9795	0.9812	0.9877

Table 7 *Constants and fitting parameter for the linear correlation of L/L_0 vs M/M_0*

During the drying process some shrinkage is observed as a function of the evaporated water volume because water migrates from the center of the sample towards the surface. As a consequence, the size of pear samples measured reduce considerably.

A linear relationship between the thickness reduction $\left(\frac{L}{L_o}\right)_{NMR}$ obtained by NMR, and obtained by size measurements $\left(\frac{L}{L_o}\right)_{VC}$ were found at the three temperature evaluated.

Figure 28 reports this relationship for the temperature of 50°C. The coefficient of determination R^2 was found to be 0.98. The same order of the coefficient of determination was found for the other two temperatures. The thickness L_{0NMR} of the fresh sample and the thickness L_{NMR} of dried samples were directly obtained from depth profiles reported in figure 30.

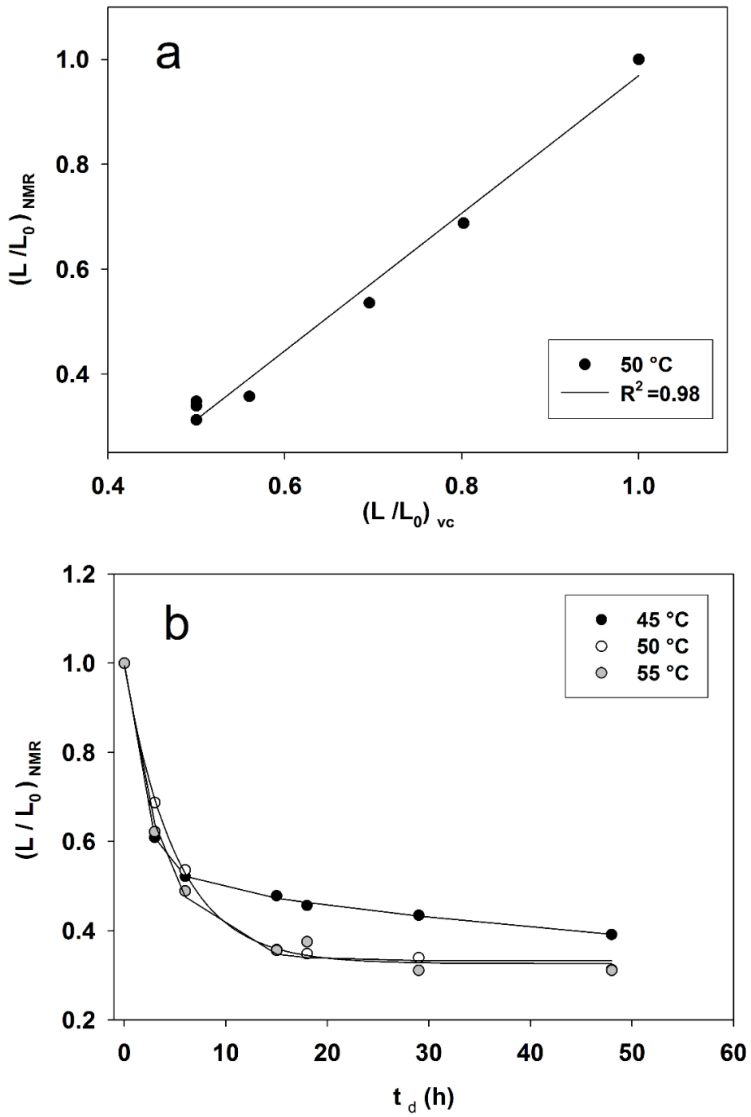

Fig. 28. *a) Linear relationship obtained by NMR and vernier caliper measures at T=50°C, b) thickness reduction obtained by NMR at 45, 50 and 55°C.*

It was possible to see that the size of pear samples decreased sharply until 15h of drying, then the reduction was smoother. The thickness reduction $\left(\frac{L}{L_o}\right)_{NMR}$ as a function of the drying time was fit to the following equation:

$$\left(\frac{L}{L_o}\right)_{NMR} = C * e^{-S_r t} \quad (18)$$

where S_V indicates the rate of thickness reduction with the drying time (t_d). S_r was found to be 0.37 h^{-1} in the case of data collected at the drying temperature of 45°C, whereas it was found to be 0.2 h^{-1} in the case of data collected at 50 as well as 55°C. These results indicate that the rate of thickness reduction is definitely slower at 45°C than 50 and 55°C.

2.3 NMR relaxometry

^{1}H pulsed low resolution NMR measurements in homogeneous field were performed with a Minispec mq 20 pulsed NMR spectrometer (Bruker Spectrospin Company, Germany), operating at a frequency of 23 MHz for protons (magnetic field strength 0.47 T). Before measurements, samples were inserted in 10 mm NMR tubes and let to equilibrate until achieving thermal equilibrium (ca. 20 min). Transverse relaxation times were measured by the Carr–Purcell–Meiboom–Gill (CPMG) pulse sequence (Farrar and Becker, 1971) with an echo spacing 2τ of 200 μs between two pulses.

Measurements in inhomogeneous field were carried out at 13.62 MHz with a portable NMR instrument from Bruker Biospin interfaced with a purposely built single-sided sensor by RWTH Aachen University, Germany (Perlo et al., 2005). This sensor generates a magnetic field with an extremely uniform magnetic field gradient to resolve the near surface of arbitrary large samples. Fresh and dried pear samples were wrapped in a transparent film to prevent further water/moisture loss during the measurement.

All profiles were obtained measuring both sides of pear samples with a total field of view of 20 mm. The recycle delay was 10 s, and 64 scans were collected.

Longitudinal relaxation times T_1 were measured with the Aperiodic Saturation Recovery sequence, using a logarithmic increment, 64 blocks were collected in each experiment (Farrar and Becker, 1971).

Effective transverse relaxation times T_{2eff} were measured using the CPMG pulse sequence with an echo time 2τ of 104 μs, 4096 echoes. Measurements were carried out at 1 mm and 5 mm of depth inside the pear sample. Because the field generated by unilateral NMR is inhomogeneous, transverse relaxation times obtained are shorter than those measured in a homogeneous field. Using the CPMG sequence for measuring T_2, only water components are observed, whereas T_2 of the rigid macromolecular matrix which is of the order of a few tens of μs is disregarded.

Diffusion measurements were carried out at 0.36 T (13.62 MHz) with a steady gradient (SG) of 14.28 T/m using a Hahn echo (SGSE) and a stimulated echo (SGSTE) pulse sequence followed by a CPMG echo train to improve the signal to noise ratio (SNR) (Stejskal and Tanner, 1965). For calibration purpose, SGSE sequence was applied to measure the

diffusivity of bulk water whose self-diffusion coefficient D_0 was found to be 2.055×10^{-9} m^2/s. The self-diffusion coefficient D_{juice} of pear juice obtained by homogenization and centrifugation of fresh pear, was found to be 1.39×10^{-9} m^2/s.

2.3.1 NMR data processing

The amount of moisture content in fresh and dried pears at different drying times was calculated by numerical integration of ^1H NMR depth profiles applying the Newton–Cotes quadrature rule.

The longitudinal relaxation times T_1 were obtained fitting the magnetization to the following equation:

$$M_z(t) = M_{ze}\left(1 - e^{\frac{-2t}{T_1}}\right) \tag{19}$$

Where M_{ze} is the magnetizaion at the equilibrium.

The transverse relaxation times T_2 were obtained fitting the magnetization decay to the following equation

$$Y = \sum_{i=1}^{n} W_i e^{\frac{-t}{T_{1,2i}}} \tag{20}$$

where n is the number of components of the decay, W_i is the weight of i^{th} component, and $T_{1,2i}$ is the relaxation time of i^{th} component and t is the time of the magnetization decay. Before fitting, the sum of weights of each component was normalized to 100%.

A regularized inverse Laplace transformation (Press et a., 1994) was applied to invert the CPMG decay using a software implemented within the Matlab (MathWorks) framework. After the transformation, data were represented as a distribution of relaxation times. In this representation, the peaks of the distribution are centered at the corresponding most probable T_2 values, whereas peak areas correspond to the relative weights of each component.

2.3.2 ^1H NMR depth profiles

Because the proton signal detected is predominantly due to water contained in the vegetable tissue, the full thickness of the parallelepiped sample was analysed with a micrometic resolution, figure 29. The magnet is placed on a lift that moves the sensitive slice step by step inside the object.

Fig. 29. *Direction of the magnetic field.*

Information on drying kinetics can be obtained analyzing the profiles collected as a function of the drying temperature and time, figure 30. It shows the comparison among profiles of fresh pear and pears dried for 3, 6, 15, 20, 29 and 48 h for the three temperature investigated. Specifically, the outer regions of the sample correspond to the left-side (≈ 0 mm) and the right-side (≈8-20 mm) of figure 30.

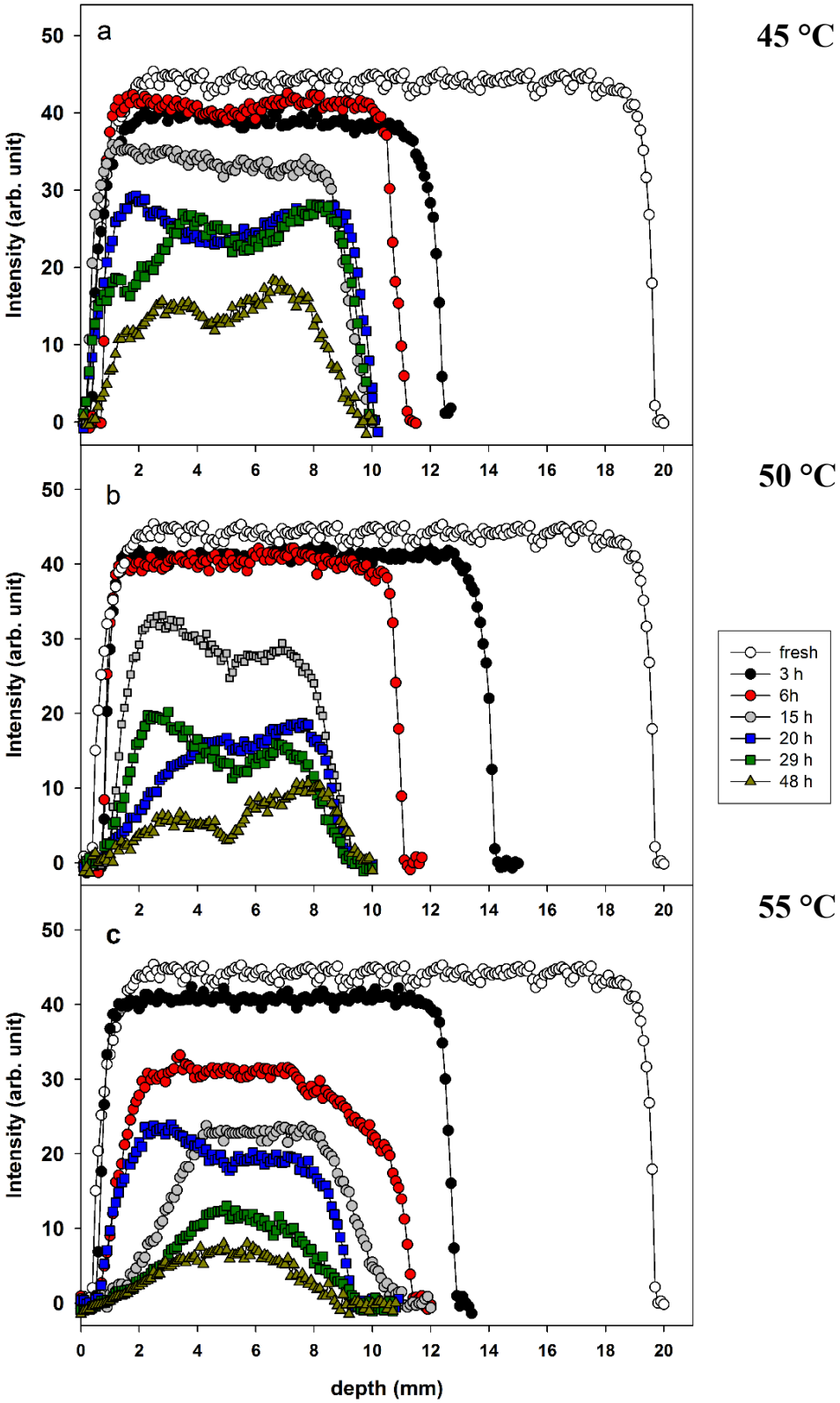

Fig. 30. *Depth profiles of fresh and dried pear samples for 3, 6, 15, 20, 29, 48 at* a *45,* b *50 and* c *55°C.*

The amplitude of ^{1}H NMR signal is directly proportional to the moisture content of pear samples (Adiletta et al., 2015). The amplitude of profiles, their shape and thickness are affected by both the drying time and temperature. Profiles collected in all dried samples indicated a progressive loss of water accompanied by a shrinkage of samples. The reduction of the amplitude, thickness, and changes in the shape of profiles depended on the drying temperature. In fact, profiles of samples dried at 45 and 50°C showed a net reduction of the amplitude after 15 h of drying, whereas in samples dried at 55°C the net reduction occurred early just after 6 h of drying. Furthermore, the thickness reduction was more pronounced in samples dried at 55°C than in those dried at 45 and 50°C. From figure 30, it's possible to see that the modification of the shape of profiles also indicated that the water loss did not occur evenly along the whole sample thickness. Sometimes the water loss seemed more pronounced in the internal part of the sample, whereas sometimes it seemed more pronounced in the external parts of the sample. This effect might likely to be due to the presence of sugar gradients which might hinder water loss in some regions of the sample, whereas in other regions where the sugars concentration was lower the water loss might be not hindered.

Then the ratio of I_t/I_0 vs drying time is calculated and reported in Fig. 31. The trend is very similar to that found in the case of M_t/M_0 curves (figures 21, 22, 23). In fact, a very good agreement (R^2=0.94, 0.98, 0.94 respectively at 45, 50 and 55°C) was found between M_t/M_0 values, obtained by gravimetric measurements, and I_t/I_0 values obtained by integrating NMR profiles.

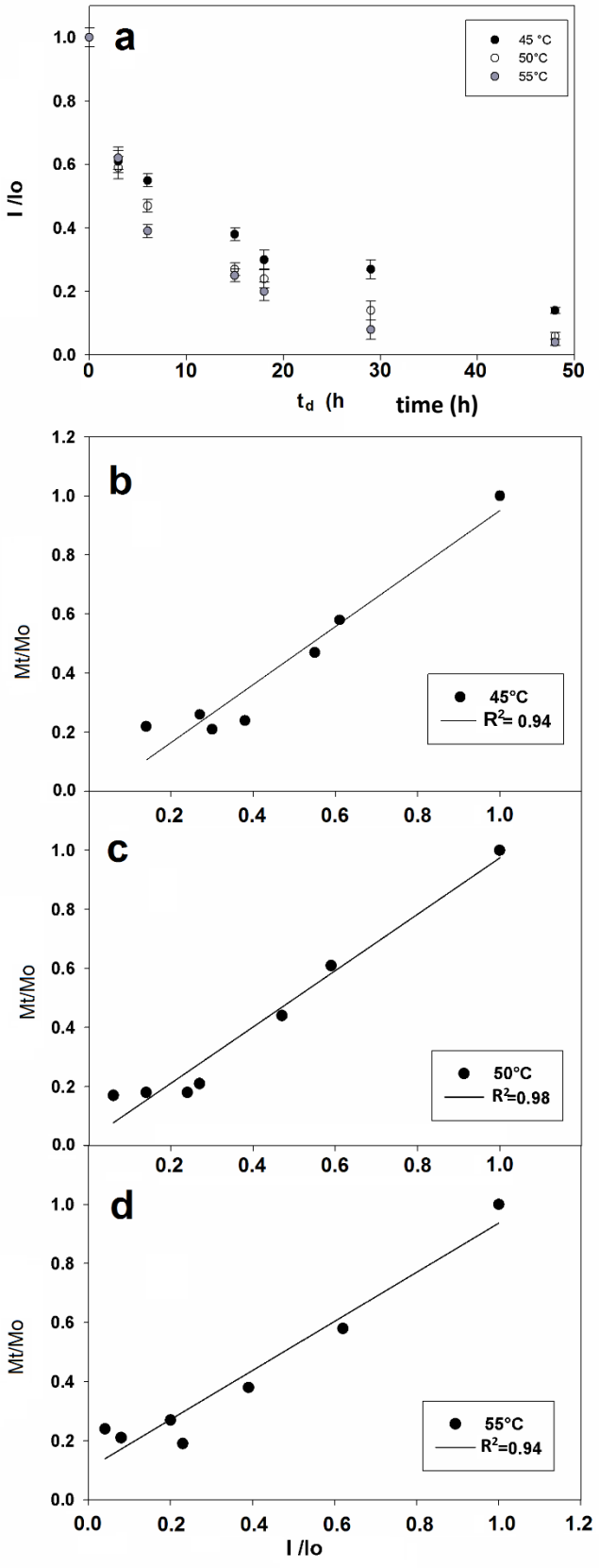

Fig. 31. *Variation of moisture content (I_t/I_0) measured by NMR* ***a****, relationship between NMR integral ratio I_t/I_0 and M_t/M_0 at* ***b*** *45°C,* ***c*** *50°C and* ***d*** *55°C.*

2.3.3 Longitudinal relaxation time

Results of the T_1 relaxation times of pears dried at temperature of 45, 50 and 55 °C as a function of the drying time are reported in figure 32.

The T_1 values were normalized respect to the fresh value, T_{1fresh}=1440 ±30 ms in order to compare the trend during drying for the three temperatures.

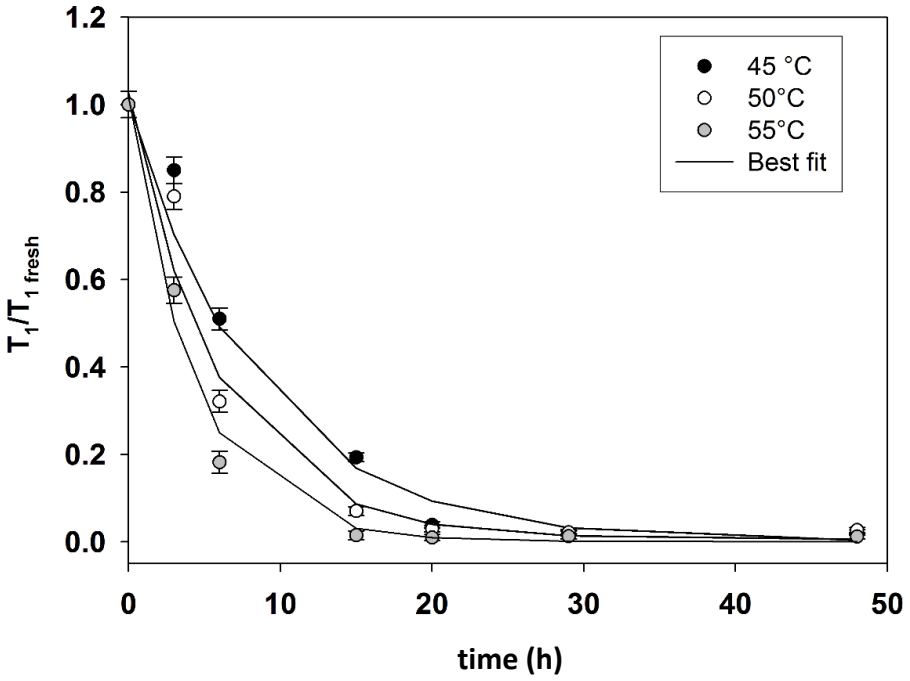

Fig. 32. *T_1 /T_{1fresh} of pear samples at different drying time at 45, 50 and 55°C and best fit.*

The decay curve were found to be mono-exponential, which corresponds to a single T_1 value in fresh pear as well as in all dried pears. As expected, the exchange among water from different compartments of pear tissue averaged T_1 values to a single, rather long value in fresh pear and pears dried for a short time. At long drying time, the amount of water was very low and pear tissue became a "solid-like" tissue exhibiting a single, very short T_1 value. In all cases T_1 values shortened increasing the drying time as well as the drying temperature. After 29 h of drying all T_1 values collapsed to an average value of 24±2 ms, and remained constant at the longest drying time. This behaviour may be easily interpreted considering that, during the drying process, at long drying times, fresh pear transforms in a "solid-like" matrix. In fact, small, fast rotating molecules like free water exhibit a long relaxation time of the order of seconds, as molecular motion slows T_1 and T_2 shorten.

Data reported in figure 32 were fit to the following equation:

$$\frac{T_1}{T_{1fresh}} = A * e^{-Rt_d} \quad (21)$$

where R_s indicates the rate of $\frac{T_1}{T_{1fresh}}$ shortening with the drying time t_d. R_s was found to be 0.12 h^{-1} in the case of data collected at the drying temperature of 45°C, 0.17 h^{-1} at 50°C, and 0.20 at 55°C. These results indicate that, by increasing the drying temperature, the rate of $\frac{T_1}{T_{1fresh}}$ shortening increased.

2.3.4 Transverse relaxation time

T_2 measurements yield a more detailed information on the partitioning of water in vegetable tissue than T_1, as water exchange among compartments results in a partial averaging which depends on the size of compartments and on membranes water permeability.

To investigate in detail the effect of drying temperature and time on the state of water in pears, we have determined transverse relaxation times (T_{2i}) and relative weight (W_i). According to the literature, the water state in raw fruits and vegetables are usually categorized into ‘‘bound water’’, ‘‘immobilized water’’, and ‘‘free water’’, which correspond to different cell compartments, namely cell walls, cytoplasm and extracellular space, and vacuoles.

The distributions of transverse proton relaxation times in fresh pear tissue measured in homogenous field are shown in figure 33a. Three relaxation peaks (A, B, C) can be seen. The parenchyma tissue of pear is representative of multi-compartment cellular tissue. The peak exhibiting the fastest T_2 (peak C) at 680 ms is associated with water in the vacuole, the intermediate peak (peak B) at 290 ms is associated with the water in the cytoplasm and extra-cellular compartments and the peak exhibiting the slowest T_2 (peak A) at 28 ms is assigned to water in cell walls. The relative weights of relaxation peaks were 77% (W_c), 20% (W_b) and 3% (W_a), indicating that most water resided in the vacuolar compartment. These results agree with those recently reported for pears by Khan et al. (2016).

T_2 distributions obtained by portable NMR are shown in figure 33b. Due to the inhomogeneity of the magnetic field of unilateral NMR, peaks are centred at definitely shorter values than those obtained in homogeneous field (figure 33a). Also in this case, we observed three relaxation peaks. Therefore, samples were analysed only by portable NMR.

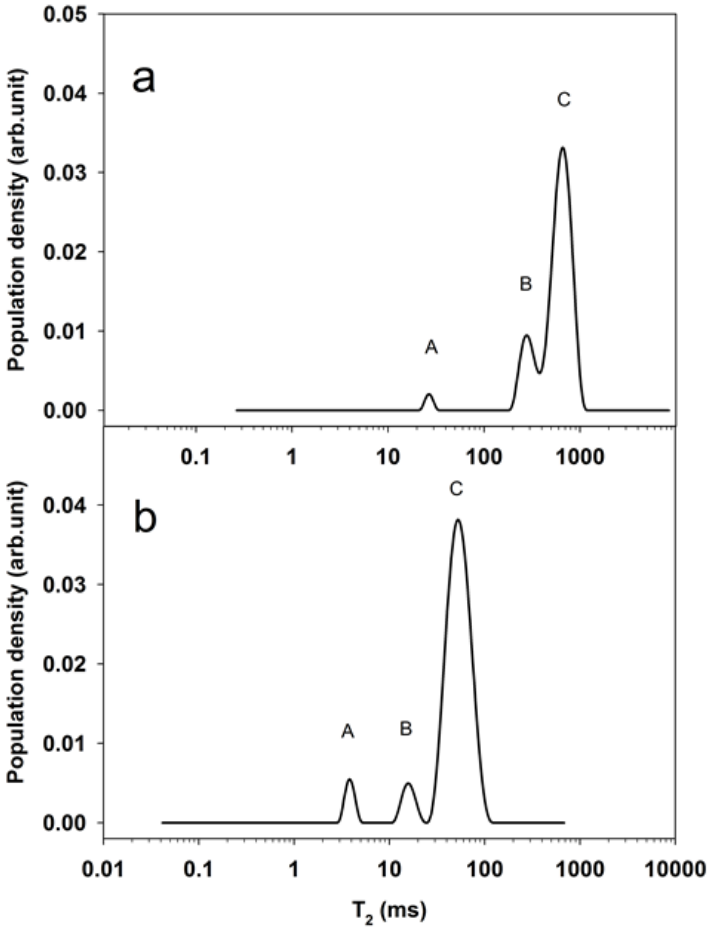

Fig. 33. *T_2 values of fresh pear samples in homogeneous a and not homogeneous field NMR b.*

Figure 34 reports T_2 distributions obtained at drying temperatures of 45, 50 and 55°C as a function of the drying time. Distributions reported in a, b and c were obtained at 1 mm of depth (external part of the sample), whereas those reported in d, e, and f were at 5 mm of depth (internal part of the sample).

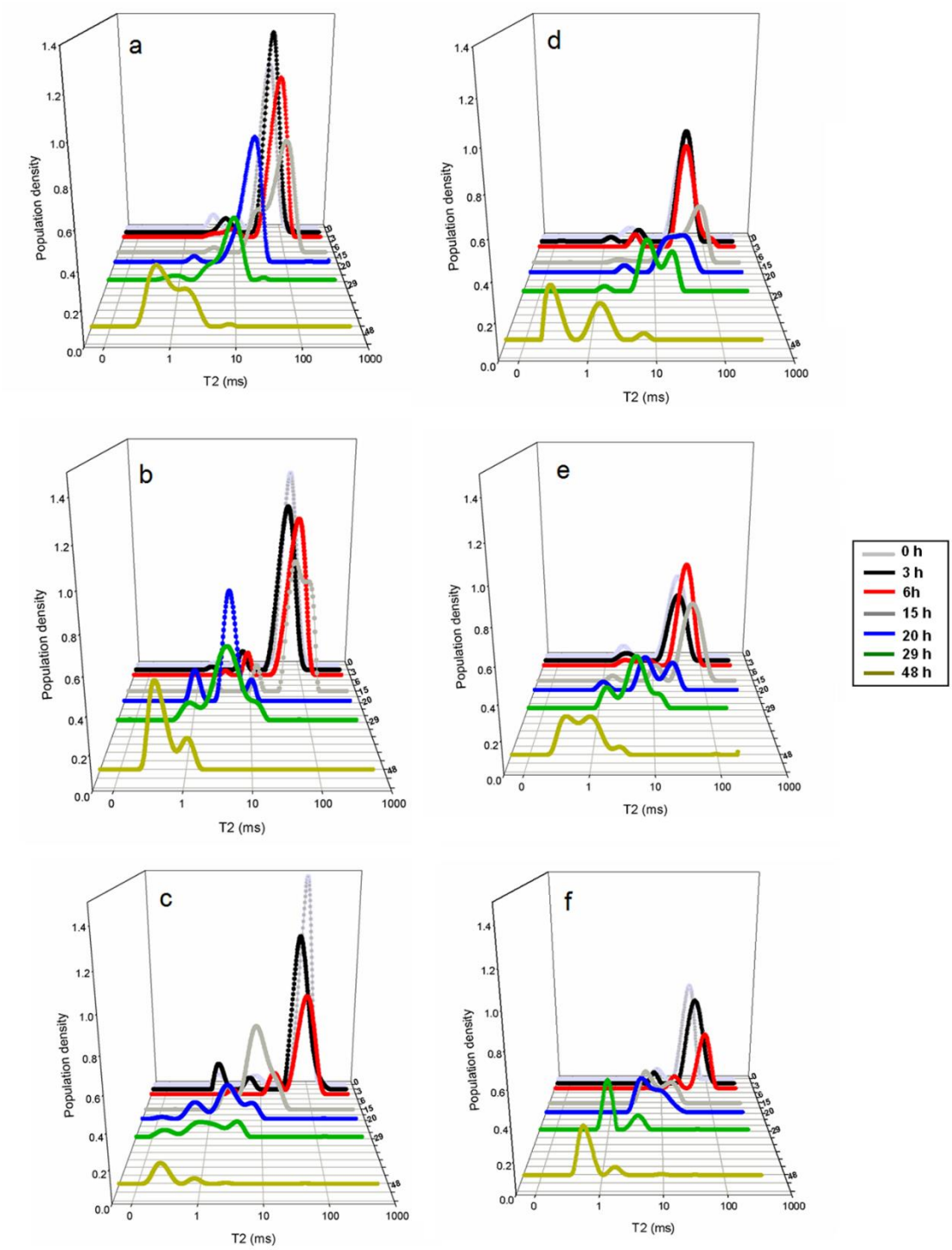

Fig. 34. *T_2 distribution at a 45°C, b 50 °C and c 55°C at 1 mm of depth, T_2 distribution at d 45°C, e 50 °C and f 55°C at 5 mm of depth.*

By increasing the drying time a gradual shift of all relaxation peaks to shorter values was observed, which is closely associated with changes in water status during drying. The shortening affected deeply the slowest T_{2c} component and, to a lesser extent, the intermediate and the fastest components. We also observed a net loss of the population W_c associated to the slowest component assigned to water in vacuole, suggesting that most of water lost during drying is removed from the vacuolar compartment. As a consequence, one may expect a shortening of the transverse relaxation time ascribed to water in vacuole as the vacuolar content is concentrated by drying. Such a behavior was observed both by performing measurements in the internal part of the sample (5 mm of depth) and in the external part of the sample (1 mm of depth). The decrease of water in vacuole under drying suggested that this compartment may undergo shrinkage due to water loss during drying.
Figure 35 reports the loss of population associated to water in vacuole as a function of the drying time at drying temperatures of 45, 50, and 55°C. The solid lines is obtained applying a linear regression to data.

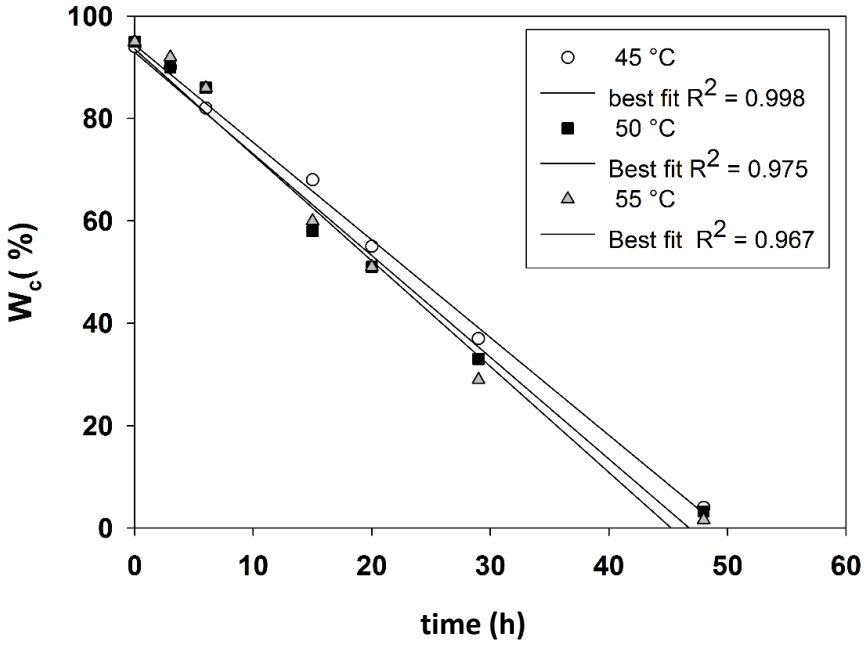

Fig. 35. *Loss of population associated to water in the vacuole as a function of the drying time at drying temperature of 45, 50 and 55°C and their best fit.*

The slope of the straight lines obtained from the best fit slightly increased with the drying temperature being 1.90, 1.99 and 2.1 h^{-1} respectively at 45, 50 and 55°C, indicating that the rate of water loss from vacuole slightly increased increasing the drying temperature. Besides,

the amount of water lost from the vacuole at any drying time might be extrapolated from the straight lines obtained applying the best fit procedure.

2.3.5 Self-diffusion coefficients

In SGSTE pulse sequence, the attenuation of the stimulated echo caused by the dephasing of nuclear spins allows the study of the translational motion of molecules by measuring the self-diffusion coefficient D (Casanova and Perlo, 2011). The dependence of echo attenuation (A_t) on the self-diffusion coefficient and relaxation times is expressed by the following equation:

$$\ln\left(\frac{A_t}{A_0}\right) = -\gamma^2 G^2 \tau_1^2 \left(\Delta + \frac{2}{3}\tau_1\right) D - \frac{2\tau_1}{T_2} - \frac{\Delta}{T_1} \quad (22)$$

where A_0 is the amplitude of the echo at the shortest time τ_1, A_t is the amplitude of the echo at time t (s), Δ is the diffusion time (s), G (14.28 T/m) is the magnetic field gradient, and γ is the ^1H gyromagnetic ratio (2.6752×10^8 $s^{-1}radT^{-1}$), D is the self diffusion coefficient (m^2/s) and T_1 and T_2 (s) are the longitudinal and transverse relaxation time, respectively.

In the case of large D values, strong magnetic field gradient, $\tau_1 << T_2$, and $\Delta << T_1$, diffusion terms dominate over relaxation terms, and the equation can be approximated as follows:

$$\ln\left(\frac{A_t}{A_0}\right) \cong -\gamma^2 G^2 \tau_1^2 \left(\Delta + \frac{2}{3}\tau_1\right) D \quad (23)$$

Because water confined in a vegetable tissue comes in contact with cell walls, barriers and membranes which restrict diffusion, the self-diffusion coefficient D of the confined liquid usually decreases with increasing the diffusion time, deviating from D_0 measured in the bulk liquid.

Figure 36 shows the plot of NMR echo amplitude $\ln\left(\frac{A_t}{A_0}\right)$ vs $-\gamma^2 G^2 \tau_1^2 \left(\Delta + \frac{2\tau_1}{3}\right)$ at a fixed diffusion time Δ of 0.01 s; A_0 is the echo amplitude measured in the case of fresh pear, and A_t is the amplitude at the drying time t. Solid lines reported in figure 36 were obtained by applying a linear regression to data. Self-diffusion coefficients D of water molecules were obtained from the slope of the straight lines, data are reported in Table 7 along with standard deviations (SD) and coefficients of determination (R^2).

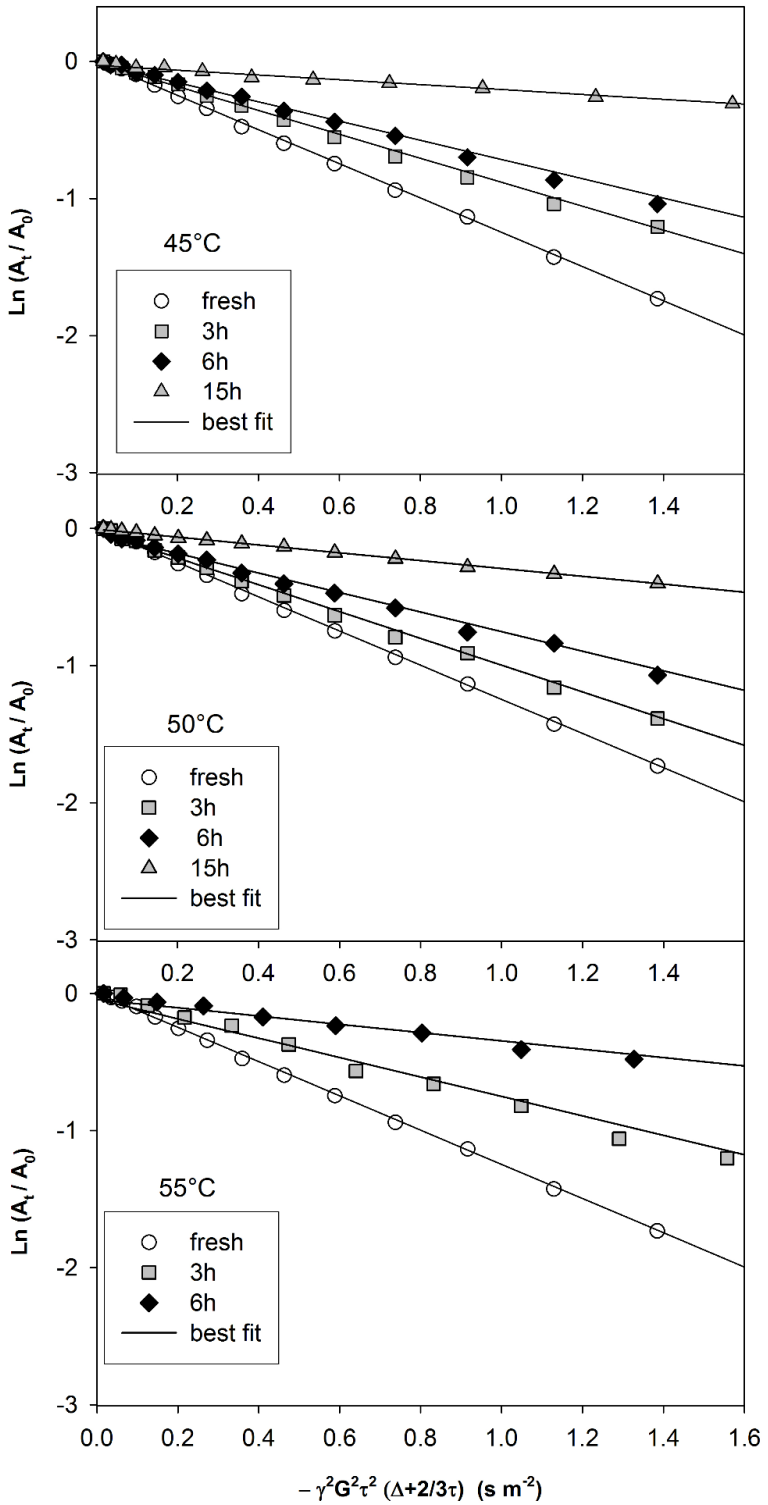

Fig. 36. *Dependence of echo attenuation (A_t) on the self-diffusion coefficient and relaxation time at 45, 50 and 55°C.*

Sample	($D \pm$ SD) x 10^{-9} m^2/s	R^2
Pear juice	1.39 ± 0.01	0.998
Fresh pear	1.25 ± 0.01	0.999
45 °C		
3 h	0.87 ± 0.03	0.997
6 h	0.70 ± 0.01	0.994
15 h	0.19± 0.03	0.997
50 °C		
3 h	0.98 ± 0.03	0.998
6 h	0.71± 0.01	0.995
15 h	0.017± 0.03	0.998
55 °C		
3 h	0.71 ± 0.01	0.991
6 h	0.301 ± 0.008	0.991

Table 8 *Self-diffusion coefficients obtained by fitting data collected at drying temperatures of 45, 50, and 55 °C, and drying times of 3, 6, and 15 h to equation (3). SD=standard deviation, R^2=coefficient of determination.*

In Table 8 was also reported the self-diffusion coefficient of bulk pear juice as a reference. In pear juice the value of the self-diffusion coefficient depended only on the sugar concentration, therefore it shortened its value with respect to that measured in bulk water. Besides, due to the presence of barriers in pear tissue, the self-diffusion coefficient was found to be faster in pear juice than in pear tissue. In all pear samples, as the drying time increased, a reduction of the self-diffusion coefficient was observed, due to the reduction of vacuolar water and, consequently, to the increase of sugars concentration which hindered water motion. At drying temperatures of 45 and 50°C and drying times longer than 15 h, due to the water loss, the pear tissue was transformed in an almost “solid-like” tissue where water motion was greatly slowed down. As a consequence, the water self-diffusion coefficient decreased dramatically to a value below the limits measurable by PFG-NMR methods. At a drying temperature of 55°C the same effect occurred already after 6 h of drying indicating that the slowdown of water motion took place earlier than at drying temperatures of 45 and 50°C.

Preliminary data suggested the occurrence of restricted diffusion in fresh and dried pears, as the apparent self-diffusion coefficient depended on the diffusion time.

2.4 SEM analysis

To investigate the effect of dehydration at different temperatures on texture characteristics of pear, we had captured images of pear structure during drying with a scanning electron microscope. The area observed was obtained by cutting a cross-sectional cut made in a central zone and parallel to the sample surface. Before examined with the microscope, samples of pear were coated with a thin layer of gold under high vacuum condition. Micrographs were taken at 27 Kv accelerating voltage, 10 mm working distance and 350X magnification.

The tissue of fresh pear is composed of numerous cells, small intercellular space and a high degree of cell compartmentalization. In the early phase of drying, the properties of the tissue are almost the same on the surface and in the centre of the pear. During drying water is removed from the solid material and tissue are not able to maintain their structure as consequence of continuous water removal. The pressure difference between the inner and the external of the material generates a stress that may lead to material shrinkage or collapse. On the other hand, the surface deforms due to viscoelastic behavior of the solid food. Therefore, drying treatment modifies the cell which become deformed, contracted and collapsed.

As evidenced by SEM micrograph of figure 37, pores and cracks in the pear structure can be well observed, instead it's difficult to distinguish between cells and intercellular spaces.

At 45°C after 15 and 20 h drying, we have observed pores with an average size of the order of 100 μm (figure 37, a, b) After 29 h of drying appeared some micro-cracks (figure 37c) while at longest drying the pore size increase with an average size of 200-300 μm (figure 37d).

At 50°C at 20 h appeared few pores (figure 37f) while micro crack were evident after 29 h of drying (figure 37g), these micro-cracks transformed into large pores at the longest drying time (figure 37h).

Instead at highest temperature of 55°C the micro-cracks occurred already after 15 h of drying (Fig. 37i) and progressively become larger as the drying time increased (figure 37l-37n). These differences in the porous structure at different drying temperatures significantly influences the mechanism of transport of water during drying.

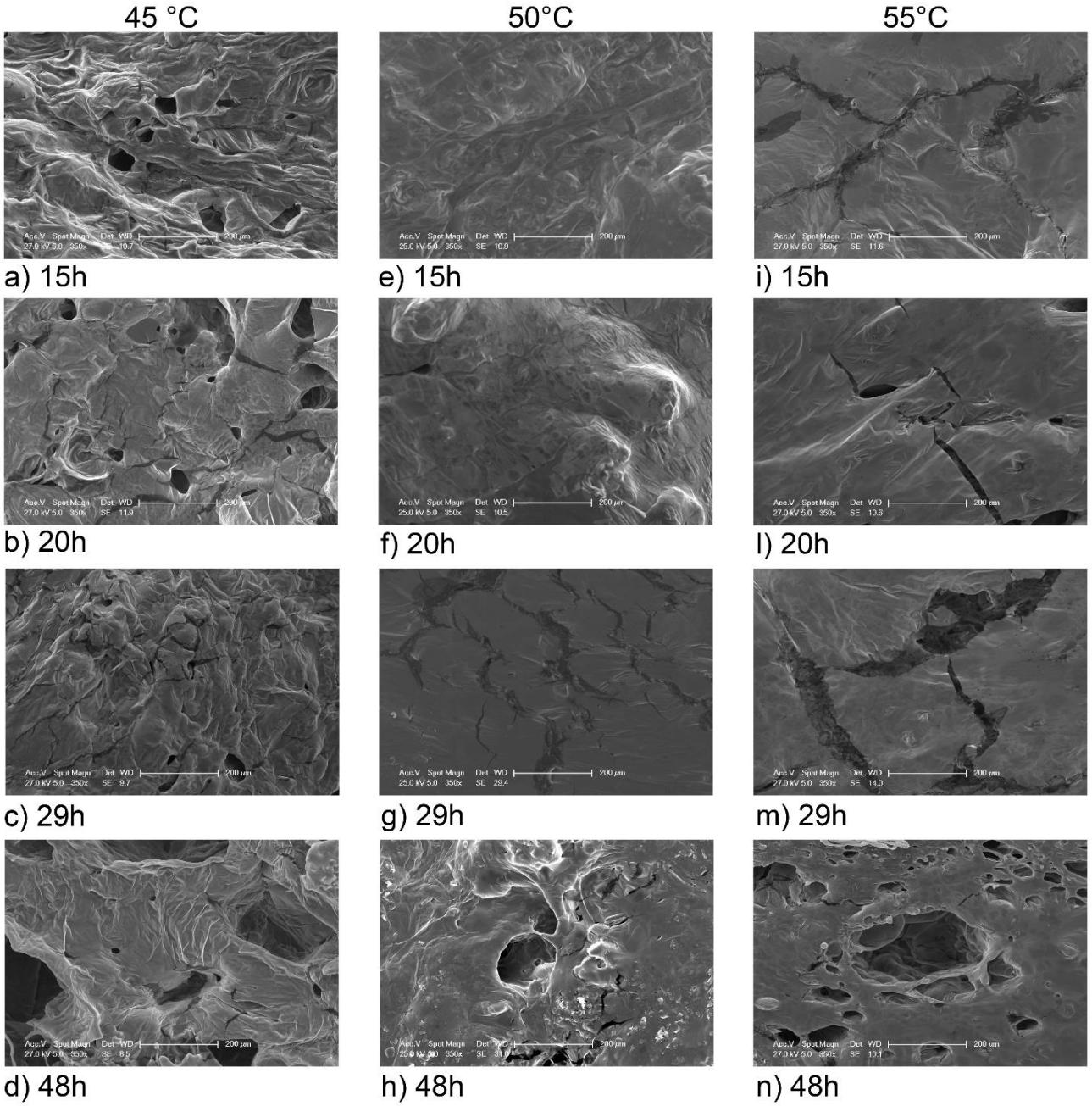

Fig. 37. *SEM images of pear sample at:*
45 °C after a) 15 h, b) 20 h, c)29 h, d) 48 h;
50 °C after e) 15 h, f) 20 h, g)29 h, h) 48 h ;
55 °C after i) 15 h, l) 20 h, m)29 h, n) 48 h.

2.5 Conclusions

Portable NMR technique allowed to monitor changes of water state in pears during the drying process. ^{1}H NMR depth profiles of dried samples indicate a progressive loss of water accompanied by a shrinkage of samples. From these profiles the average moisture content was obtained and compared with that obtained by standard gravimetric method. These two methods exhibited a very good agreement. Independently on drying temperature, at the end of the drying process the total amount of water in pear tissue reduced to about 20% percent of its initial value. The amplitude of profiles, their shape and thickness are affected by both the drying time and temperature. In particular, the modification of the shape of profiles indicated that the water loss did not occur evenly along the whole thickness of samples, possibly due to the presence of sugar gradients which might hinder water loss in some regions of the sample, whereas in other regions where the sugars concentration was lower the water loss might be not hindered.

The most regular shape is obtained in the case of profiles collected on samples dried at 55°C suggesting a more uniform concentration of sugars. These data indicated that 55°C is probably the best drying temperature to avoid the formation of sugar gradients which might hinder water evaporation as the drying time increases.

The thickness reduction obtained by portable NMR and size measurements were found to be in a good agreement. Our results indicated that the rate of thickness reduction was slower at 45 than 50 and 55°C.

The distribution of transverse relaxation times exhibited three components assigned to different compartments in pear tissue, namely cell walls, cytoplasm and extra-cellular space, and vacuole. From the distributions, the quantitative analysis of the components was also obtained. The monitoring of transverse relaxation times as a function of drying temperature and time demonstrated that the drying process affected all compartments, however most of water lost during drying was removed from the vacuolar compartment, and the rate of water loss from vacuole slightly increased increasing the drying temperature. The net decrease of water in vacuole under drying suggested that this compartment may undergo shrinkage during drying.

In all pear samples, as the drying time increased, a reduction of the self-diffusion coefficient was observed, due to the concomitant reduction of vacuolar water and, consequently, to the increase of sugars concentration which hindered water motion. Preliminary data suggested the occurrence of restricted diffusion in fresh and dried pears, as the apparent self-diffusion coefficient depended on the diffusion time.

CHAPTER 3

Modelling of pear drying

3 Analytical solution of Fick second law of diffusion

As first, the modelling analysis of the drying process of pear samples was carried out applying the Fick second law of diffusion for a sphere and a cube.

The simplified hypotheses in this case are:

- the pear sample is spherical or cubical;
- the shrinkage and other structural modification phenomena that may occur during drying are neglected, so it is assumed that shape and size (radius or axis) remain constant;
- the sample is homogeneous and isotropic;
- transport properties are constant compared to space and time;
- mass transfer takes place radially or axially (across the surface of the sample), according to diffusion mechanism within the sphere or cube and a convective transport at the surface;
- the initial humidity content of the samples (M_0) is distributed uniformly and constant along the radial (axial) direction;
- the concentration of the water vapour in the surrounding environment is negligible ($M_e \rightarrow 0$);
- the process is studied under isothermal conditions, the thermal transient is generally faster than the transport of matter (which is the limiting stage), the sample immediately reaches the drying temperature and remains constant.

In spherical coordinate the mathematical model consists of one-dimensional diffusion equation, along the radial coordinate:

$$\frac{\partial M}{\partial t} = D_{eff}\left(\frac{\partial^2 M}{\partial r^2} + \frac{2}{r}\frac{\partial M}{\partial r}\right) \qquad (24)$$

M is the concentration of water in the differential volume (ie. the amount of water at time t), t is the time coordinate, r is the spatial coordinate along which material transport take place; D_{eff} is the effective diffusion coefficient.

The initial and boundary conditions are:

$$\text{I.C } t = 0 \quad M(0,r) = M_0 \quad \text{in the domain } 0 \le r \le r_0 \qquad (25)$$

B.C1 $\mathrm{r}=0 \quad \mathrm{M}(0,\mathrm{t})=\mathrm{M}\big|_{\mathrm{r}=0}\neq 0 \ \forall t>0$ (26)

B.C2 $-D_{\mathrm{eff}}\left.\dfrac{d\mathrm{M}(\mathrm{t},\mathrm{r})}{d\mathrm{t}}\right|_{r=r_0}=\mathrm{h_m}\left(\mathrm{M}(\mathrm{t},\mathrm{r_0})-\mathrm{M}_e\right)\forall \mathrm{t}>0$ (27)

The solution of the Fick's law for spherical geometry with these conditions is: (Crank, 1975)

$$\frac{\mathrm{M}(\mathrm{t},\mathrm{r})-\mathrm{M}_e}{\mathrm{M}_0-\mathrm{M}_e}=\frac{2Sh\mathrm{r}_0}{\mathrm{r}}\sum_{n=1}^{\infty}\frac{e^{-D_{\mathrm{eff}}B_n^2\mathrm{t}/\mathrm{r}_0^2}}{B_n^2\left[B_n^2+Sh(Sh-1)\right]}\frac{\sin\left(B_n\mathrm{r}/\mathrm{r}_0\right)}{\sin B_n} \tag{28}$$

while the time evolution of the average concentration is expressed by:

$$\frac{\bar{\mathrm{M}}(\mathrm{t})-\mathrm{M}_e}{\mathrm{M}_0-\mathrm{M}_e}=\sum_{n=1}^{\infty}\frac{6Sh^2e^{-D_{eff}\beta_n^2\mathrm{t}/\mathrm{r}_0^2}}{\beta_n^2\left[\beta_n^2+Sh(Sh-1)\right]} \tag{29}$$

where B_n are the roots of the following equations:

$$\beta_n\cot(\beta_n)+Sh-1=0 \tag{30}$$

and

$$Sh=\frac{r_0h_m}{D_{eff}} \tag{31}$$

In a solid of cubic shape $2\mathrm{R}=2\mathrm{R}_1=2\mathrm{R}_2=2\mathrm{R}_3$, the mathematical model consists of a three-dimensional diffusion equation, along the three axes:

$$\frac{\partial \mathrm{M}}{\partial t}=D_{eff}\left(\frac{\partial^2\mathrm{M}}{\partial x^2}+\frac{\partial^2\mathrm{M}}{\partial y^2}+\frac{\partial^2\mathrm{M}}{\partial \mathrm{z}^2}\right) \tag{32}$$

It's possible to consider only 1/8 of the volume for symmetry.

The initial, symmetry and boundary conditions are as follows:

Initial condition:

$$\mathrm{M}(x,y,z,t=0)=\mathrm{M}_0,\ 0<x<\mathrm{R}_1,0<y<\mathrm{R}_2,0<z<\mathrm{R}_3 \tag{33}$$

Symmetry conditions:

$$\frac{\partial \mathrm{M}(x=0,y,z,t)}{\partial x}=\frac{\partial \mathrm{M}(x,y=0,z,t)}{\partial y}=\frac{\partial \mathrm{M}(x,y,z=0,t)}{\partial \mathrm{z}}=0,\forall t>0 \tag{34}$$

Boundary conditions:

$$-D_{eff}\frac{\partial \mathrm{M}}{\partial x}=h_m(\mathrm{M}(t,x=\mathrm{R}_1,y,z)-\mathrm{M}_e) \tag{35}$$

$$-D_{eff}\frac{\partial \mathrm{M}}{\partial x}=h_m(\mathrm{M}(t,x,y=R_2,z)-\mathrm{M}_e) \tag{36}$$

$$-D_{eff}\frac{\partial \mathrm{M}}{\partial x}=h_m(\mathrm{M}\left(t,x,y,z=R_3\right)-\mathrm{M}_e) \tag{37}$$

The solution of the Fick's law for a cube is: (Crank, 1975)

$$\frac{\mathrm{M}-\mathrm{M}_e}{\mathrm{M}_0-\mathrm{M}_e}=\sum_{n=1}^{\infty}\left[\frac{2Sh}{\left(\beta_n^2+Sh^2+Sh\right)\cos\beta_n}\right]^3\cos\left(\frac{\beta_n}{\mathrm{R}_1}\right)\cos\left(\frac{\beta_n}{\mathrm{R}_2}\right)\cos\left(\frac{\beta_n}{\mathrm{R}_3}\right)e\left(-\beta_n^2D_{\mathrm{eff}}t\left(\frac{3}{\mathrm{R}^2}\right)\right) \tag{38}$$

while the time evolution of the average concentration is:

$$\frac{\bar{\mathrm{M}}-\mathrm{M}_e}{\mathrm{M}_0-\mathrm{M}_e}=\sum_{n=1}^{\infty}\left[\frac{2Sh^2}{\beta_n^2\left(\beta_n^2+Sh^2+Sh\right)}\right]^3e\left(-\beta_n^2D_{\mathrm{eff}}t\left(\frac{3}{\mathrm{R}^2}\right)\right) \tag{39}$$

where B_n are the roots of the following equation:

$$\beta_n\tan\left(\beta_n\right)=Sh \tag{40}$$

and

$$Sh=\frac{\mathrm{R}\cdot\mathrm{h}_\mathrm{m}}{D_{\mathrm{eff}}} \tag{41}$$

3.1 Drying kinetics

Model parameters were estimated using a numerical procedure based on non-linear regression methods, with the use of the software MatLab.

The normalized experimental data were compared with the roots of the diffusion equation implemented in the software. In this way, it was possible to determine the effective diffusion coefficient D_{eff} (m^2/s) and the mass transport coefficient h_m (m/s) for the three experimental temperatures.

Then to validate the results, the residual was calculated which is the difference, normalized, between the experimental value and that predicted by the model.

The statistical values were calculated as follow:

$$\mathrm{R}^2=1-\frac{\left(y_i-\hat{y}_i\right)^2}{\left(y_i-\bar{y}\right)} \tag{42}$$

$$\chi^2=\sum_{i=1}^{N}\left(y_i-\hat{y}_i\right)^2\frac{1}{\sigma_i^2} \tag{43}$$

$$RMSE=\sqrt{\left[\frac{1}{N}\right]\sum_{i=1}^{N}\left(\hat{y}_i-y_i\right)^2} \tag{44}$$

where:

y_i are the observed data;

$\bar{y}$ is the mean of the observed data;

$\hat{y}_i$ are the data estimated by the model obtained from regression;

N is the number of observations;

σ standard deviation of y_i.

The lower the values of the reduced χ-square, the better the goodness of the fit.

The $RMSE$, root mean square error, gives the deviation between the simulated and experimental values and it is required to reach zero.

In the following figures 38-40 for spherical samples and 41-43 for cubical ones, the experimental and predicted total dimensionless water content vs time and the residual are shown for each investigated temperature.

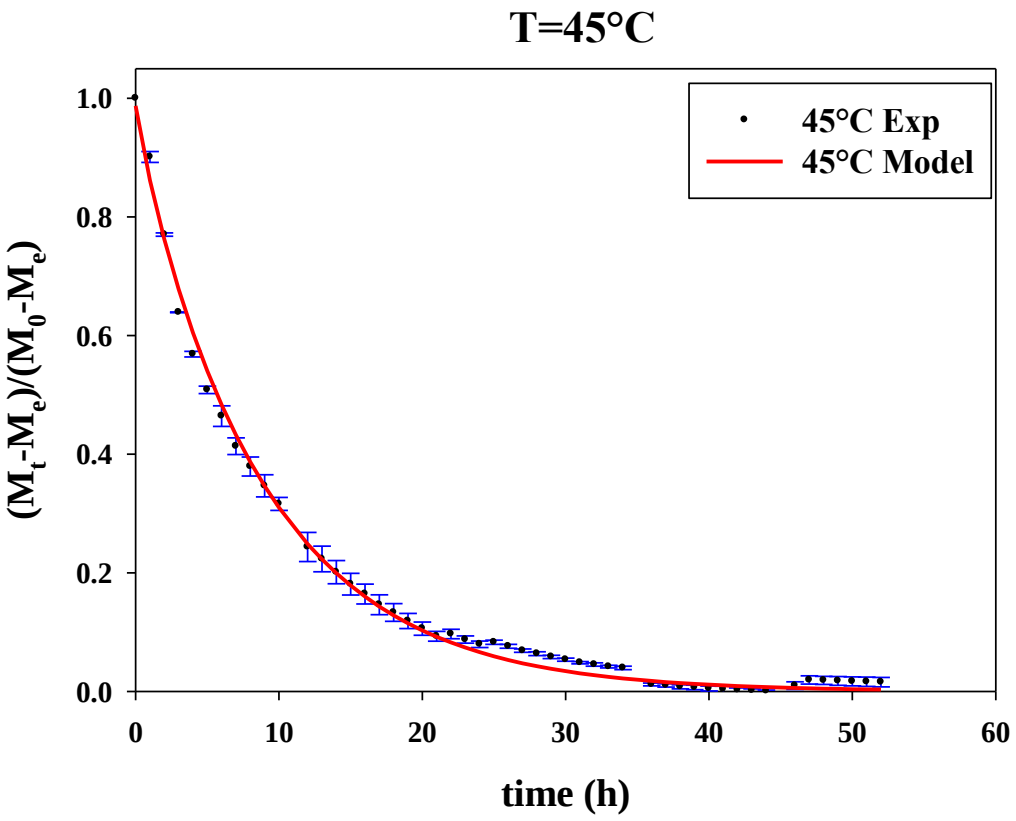

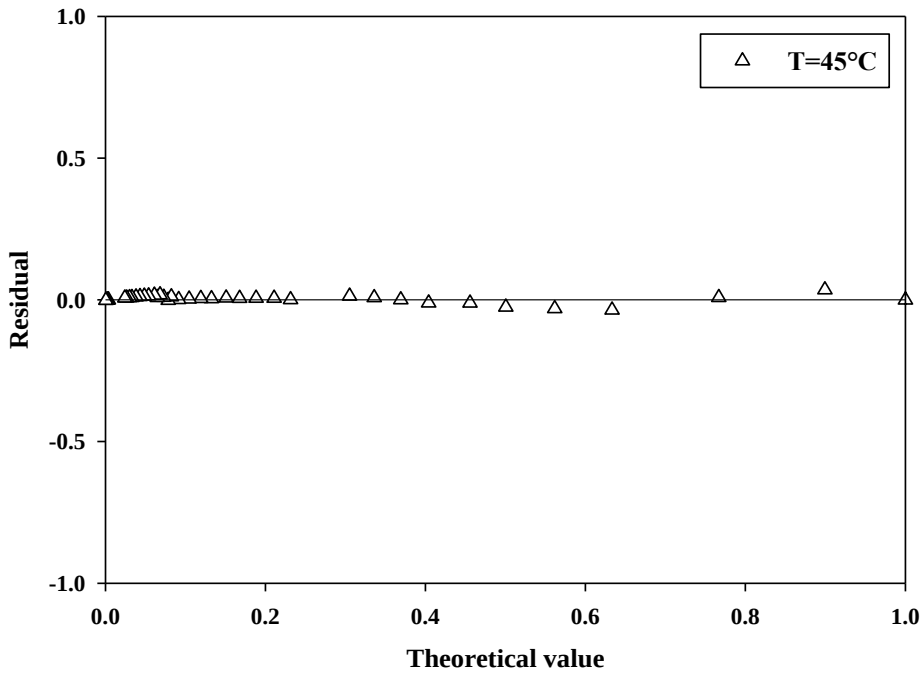

Fig. 38. *Experimental and predicted total dimensionless water content vs time at T=45°C and the residual for spherical pear sample.*

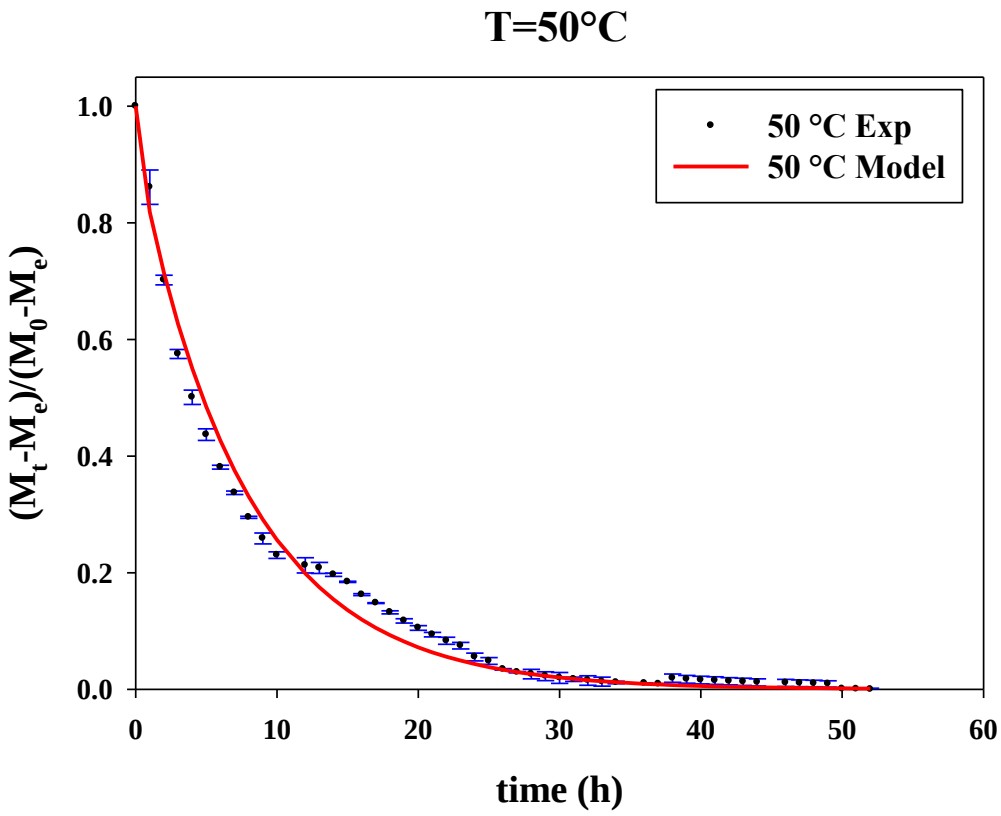

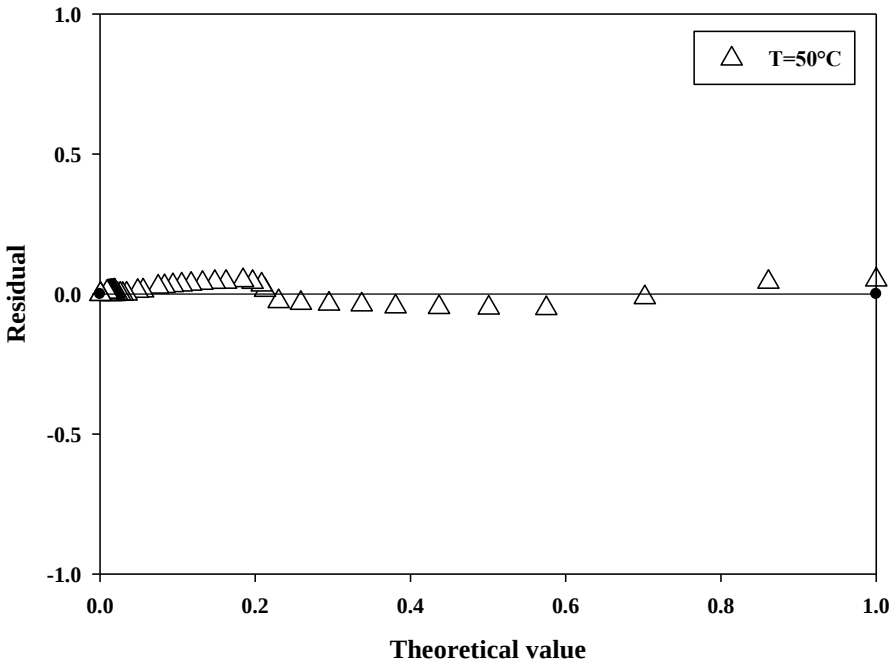

Fig. 39. *Experimental and predicted total dimensionless water content vs time at T= 50°C and the residual for spherical pear sample.*

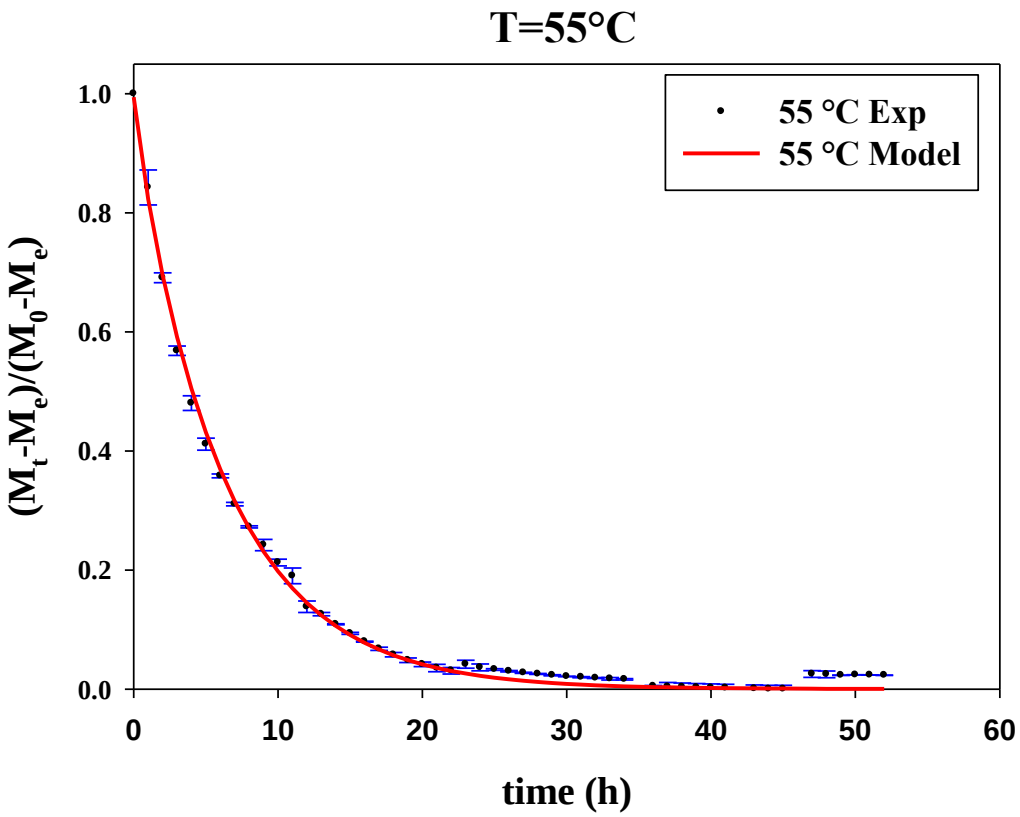

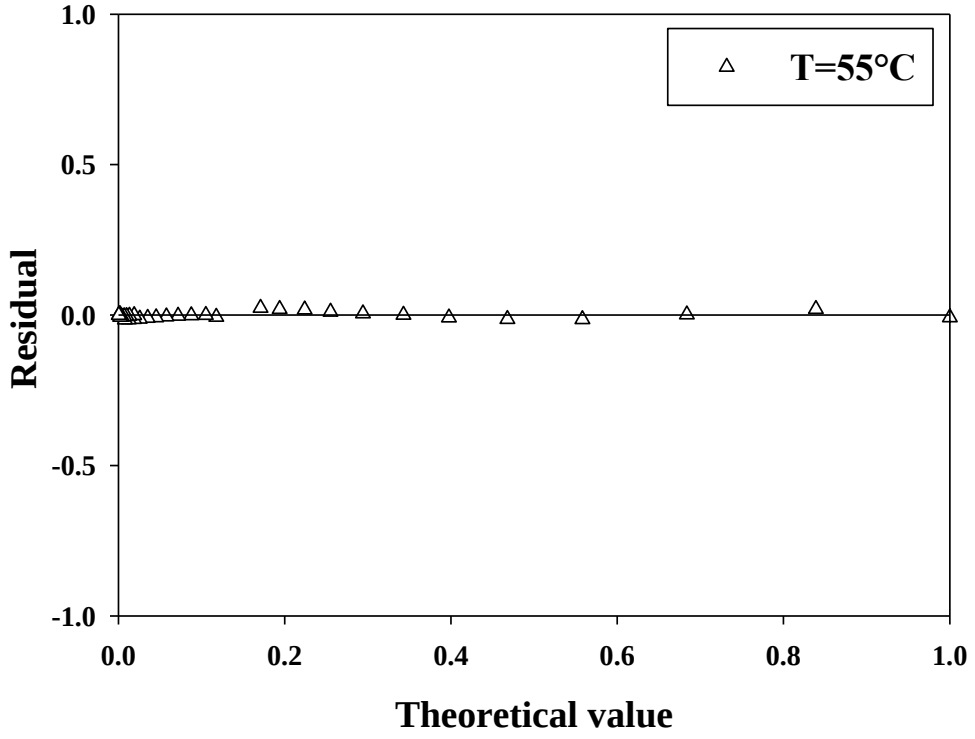

Fig. 40. Experimental and predicted total dimensionless water content vs time at T=55°C and the residual for spherical pear sample.

The value of the parameters D_{eff} , h_m, Sh calculated for spherical and cubical samples are reported in Table 9 and 11, respectively, while in Table 10 and 12 the statistical parameters are shown:

T (°C)	D_{eff} (m^2/s)	h_m (m/s)	Sh
45	$3.43*10^{-10}$	$1.07*10^{-7}$	2.17
50	$4.49*10^{-10}$	$1.11*10^{-7}$	1.73
55	$4.73*10^{-10}$	$1.54*10^{-7}$	2.28

Table 9 *Values of D_{eff}, h_m and Sh obtained at the three temperatures for spherical pear sample.*

T(°C)	R^2	χ^2	RMSE
45	0.99566	0.012558	0.015848
50	0.98633	0.034925	0.026429
55	0.99663	0.008399	0.01296

Table 10 *Statistical values obtained for spherical pear sample.*

It is possible to observe for spherical samples that the effective diffusion coefficient increases by increasing the temperature from $3.43*10^{-10}$ to $4.73*10^{-10}$ m^2/s in agreement with data reported in literature: $5.10*10^{-10}$ to $1.14*10^{-9}$ m^2/s from 30 to 50°C (Guinè, 2006); $8.65*10^{-10}$ to $11.88*10^{-10}$ m^2/s from 60 to 70°C (Guinè et al., 2013); 2-8 $*10^{-10}$ m^2/s in the range 40-80°C (Park et al., 2002).

For cubical samples the effective diffusion coefficient is higher than that for spherical sample of one order of magnitude; it also increases from $4.81*10^{-9}$ m/s^2 to $8.95*10^{-9}$ m^2/s (it is about double) by increasing the temperature from 45 to 55°C.

The calculated fitting parameters R^2, *RMSE* and χ-square (Table 10 and 11) showed the good accuracy of the model to predict the experimental data for both geometries.

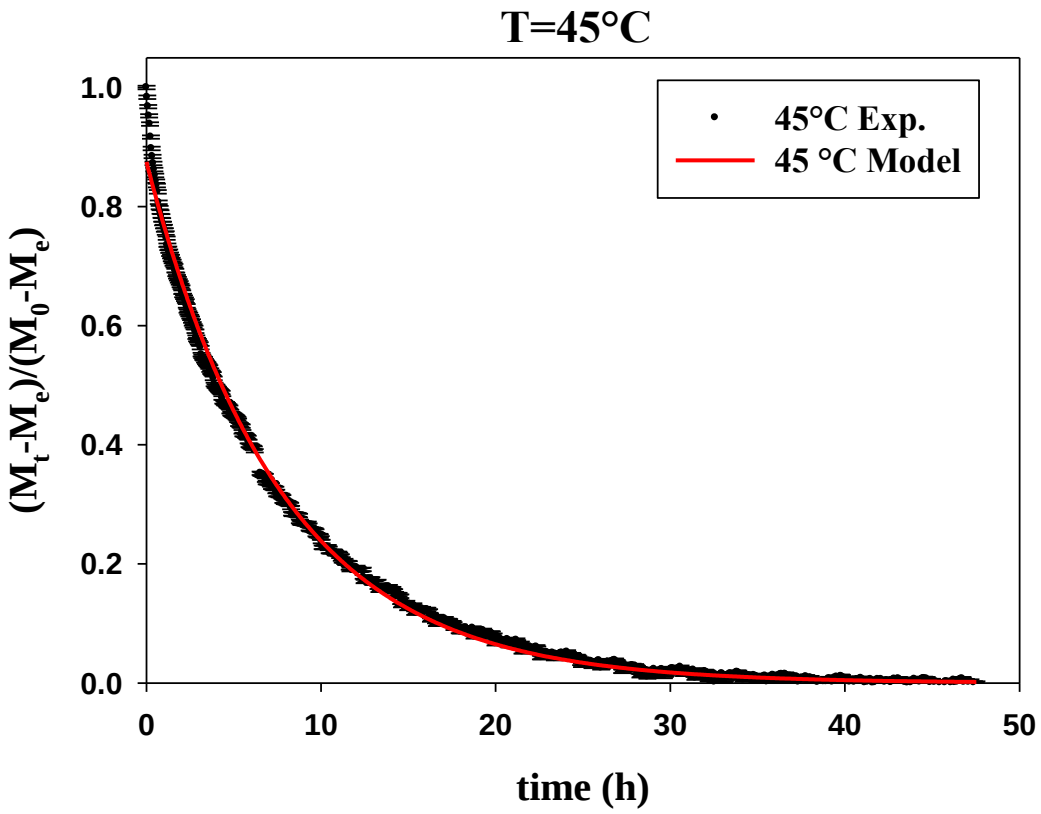

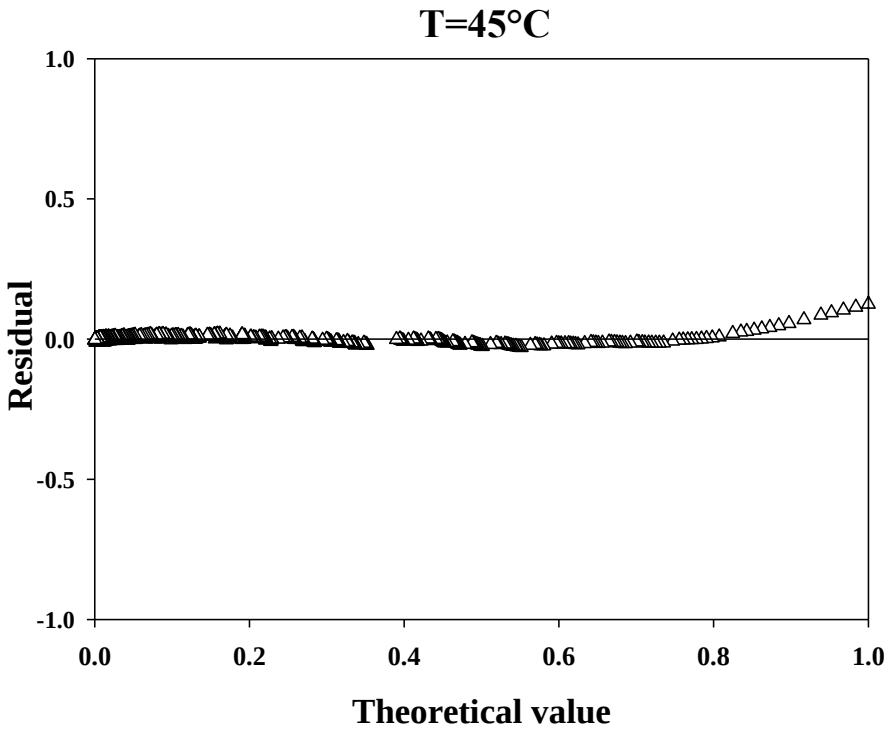

Fig. 41. *Experimental and predicted total dimensionless water content vs time at T=45°C and the residual for cubical pear sample.*

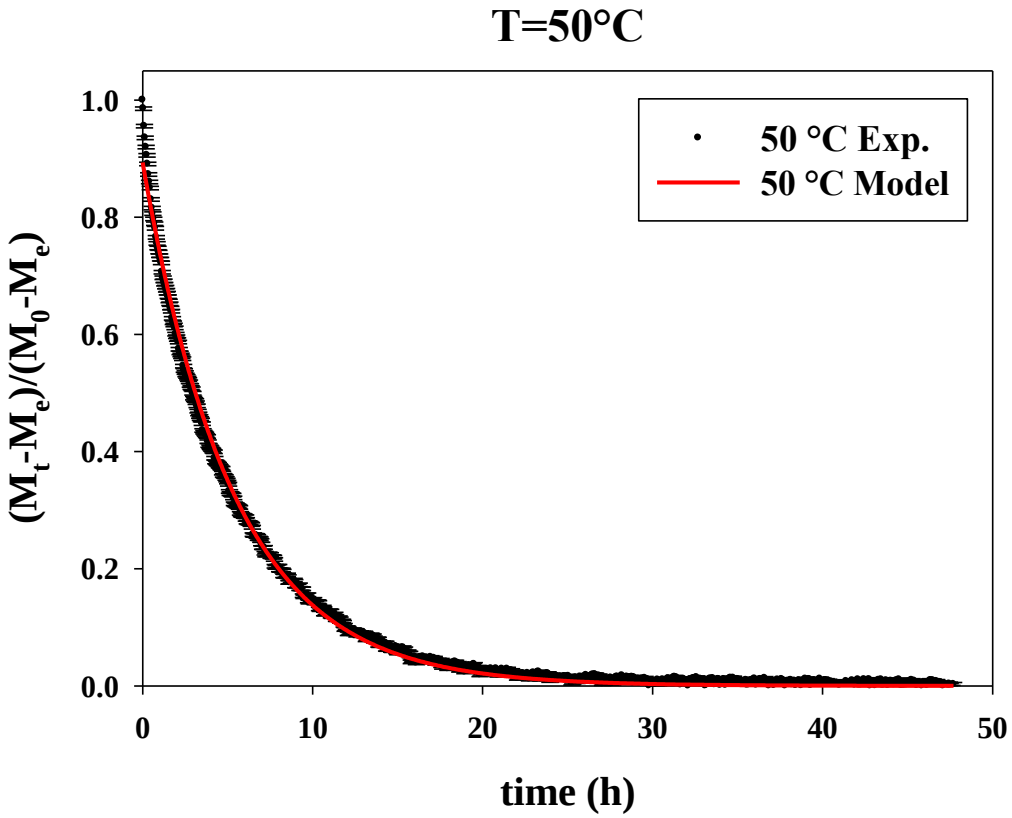

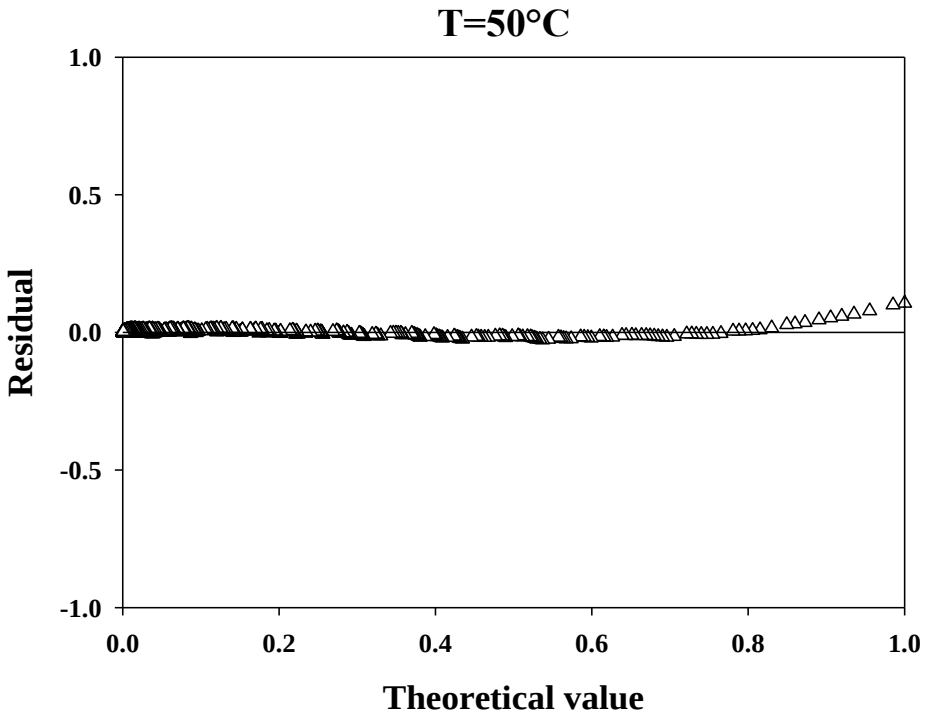

Fig. 42. *Experimental and predicted total dimensionless water content vs time at T=50°C and the residual for cubical pear sample.*

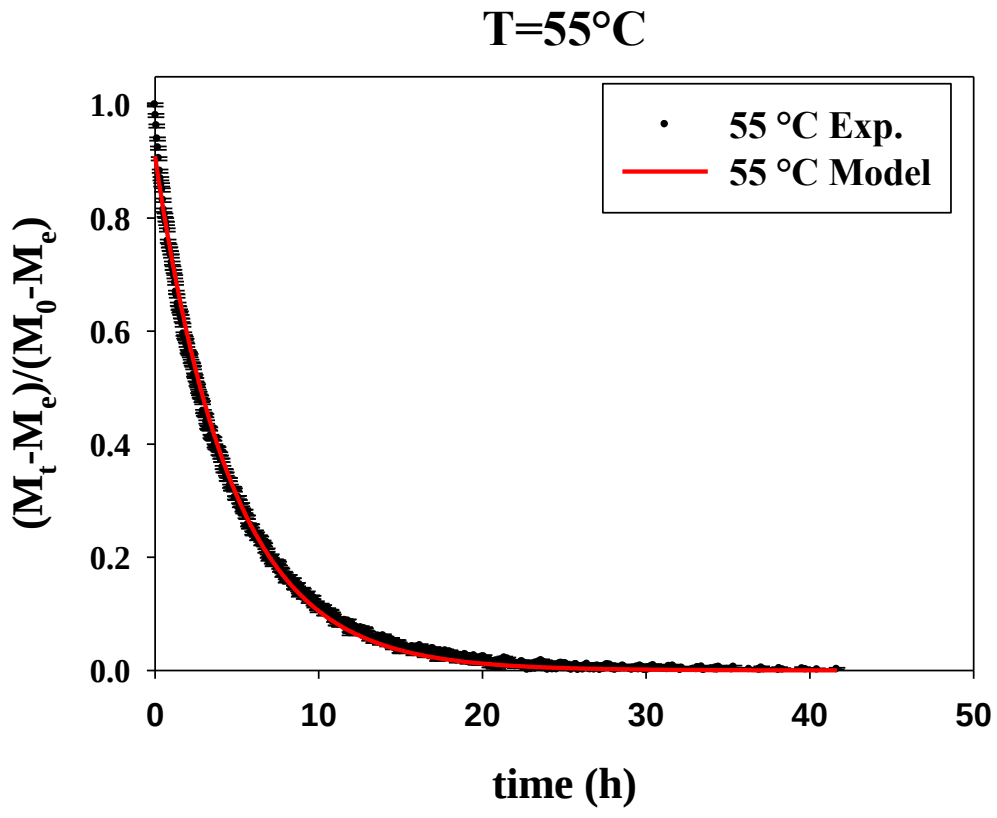

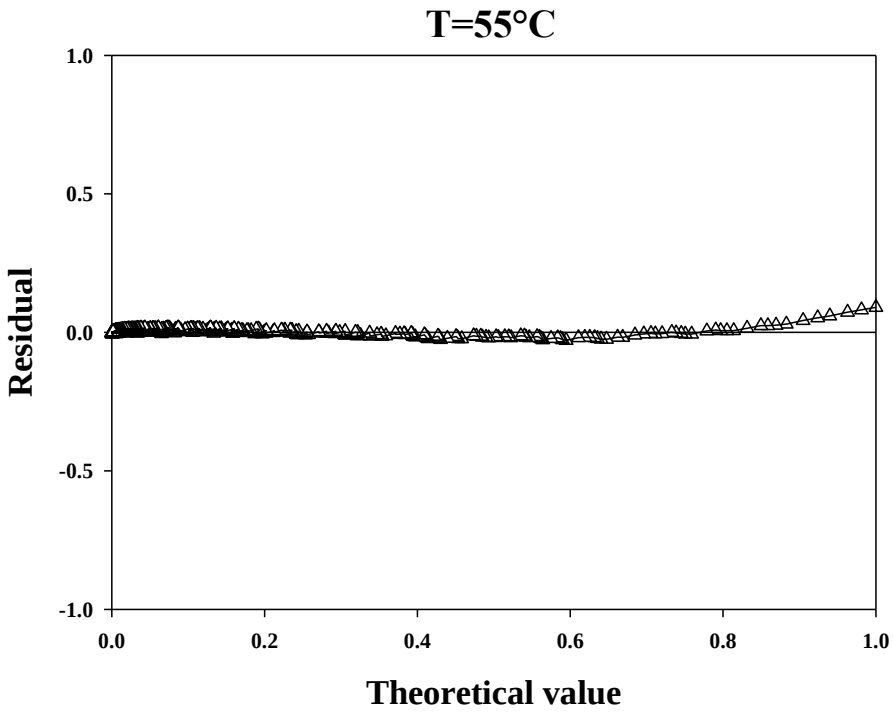

Fig. 43. *Experimental and predicted total dimensionless water content vs time at T=55°C and the residual for cubical pear sample.*

T (°C)	D_{eff} (m^2/s)	h_m (m/s)	Sh
45	$4.81*10^{-09}$	$1.68*10^{-07}$	0.44
50	$7.54*10^{-09}$	$2.43*10^{-07}$	0.40
55	$8.95*10^{-09}$	$2.77*10^{-09}$	0.40

Table 11 *Values of D_{eff}, h_m and Sh obtained at the three temperatures for cubical pear sample.*

T(°C)	R^2	χ^2	RMSE
45	0.99654	0.132940	0.0016760
50	0.99726	0.086734	0.0029367
55	0.99716	0.076239	0.0021509

Table 12 *Statistical value calculated for cubical pear sample.*

The effective diffusion coefficient is temperature dependent according Arrhenius equations:

$$D_{eff} = D_0 \exp\left(-\frac{E_a}{RT}\right) \quad (45)$$

with E_a=33±18 kJ/mol.

3.1.1 Moisture profiles during drying

The water concentration profile as a function of the sphere radius was calculated by applying the equation 28 for spherical samples.

Figures 44, 45 and 46show the profiles of the moisture content at various drying times from 1 h to 50 h and at temperature of 45, 50 and 55°C, respectively. Profiles of moisture content have an initial parabolic shape, which become flat at the end of the drying.

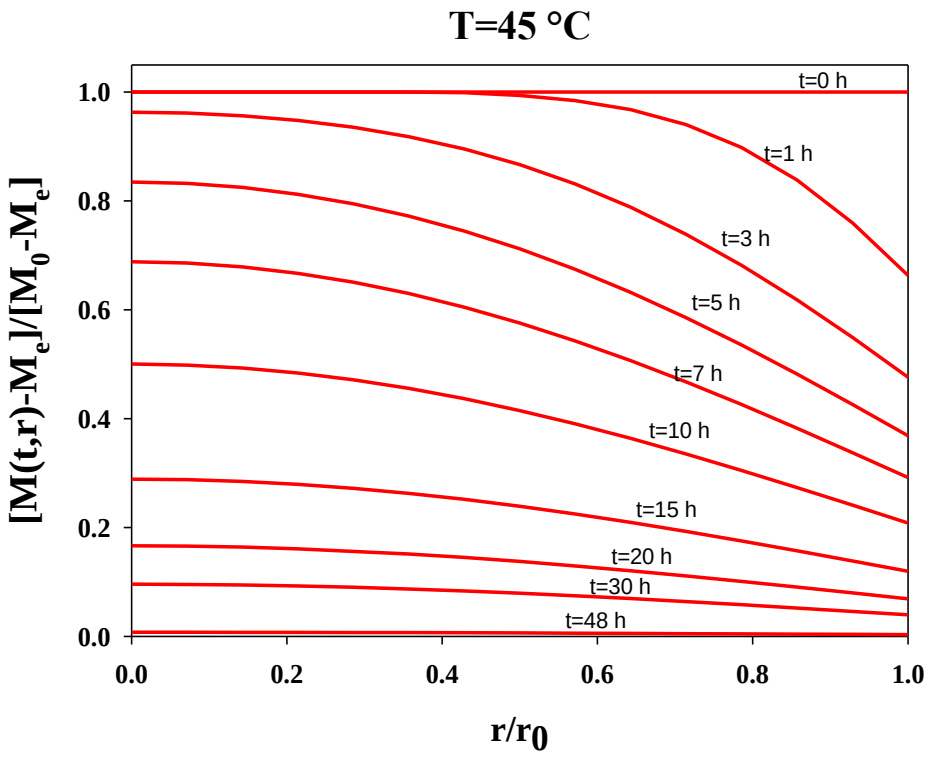

Fig. 44. *Predicted concentration distribution at various times in a spherical pear sample at T=45°C.*

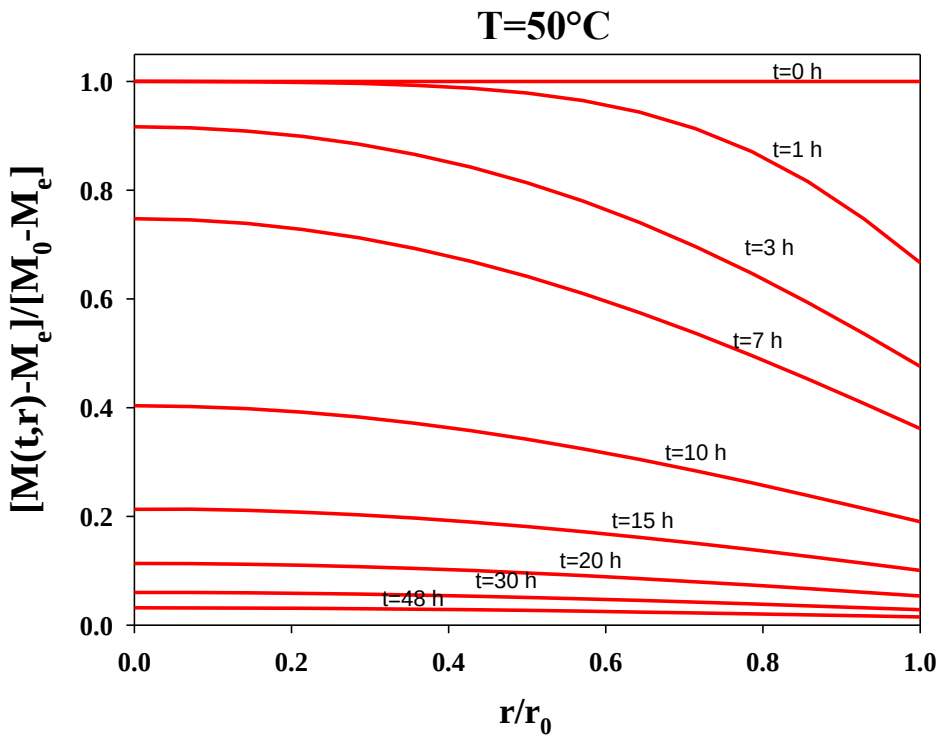

Fig. 45. *Predicted concentration distribution at various times in a spherical pear sample at T=50°C.*

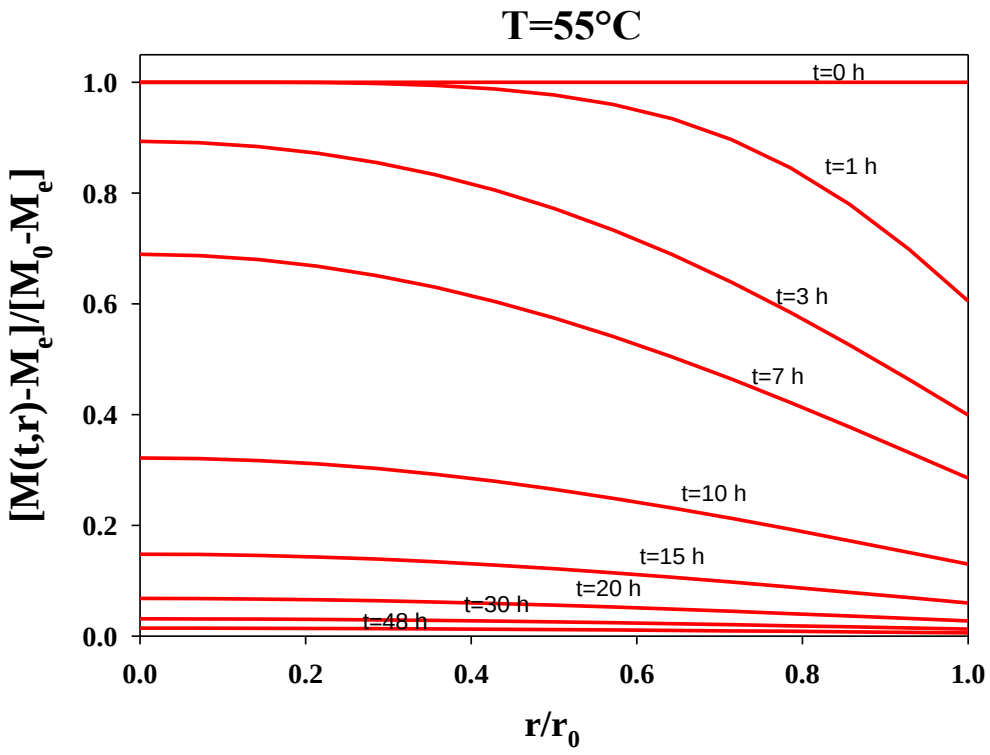

Fig. 46. *Predicted concentration distribution at various times in a spherical pear sample at T=55°C.*

Similarly, form equation 38 it is possible to obtain the water concentration profiles in the cube sample.

Figure 47, 48 and 49 show axial water concentration distribution at various drying times (3, 6 15, 20, 29 and 48 h) at the three investigated temperatures.

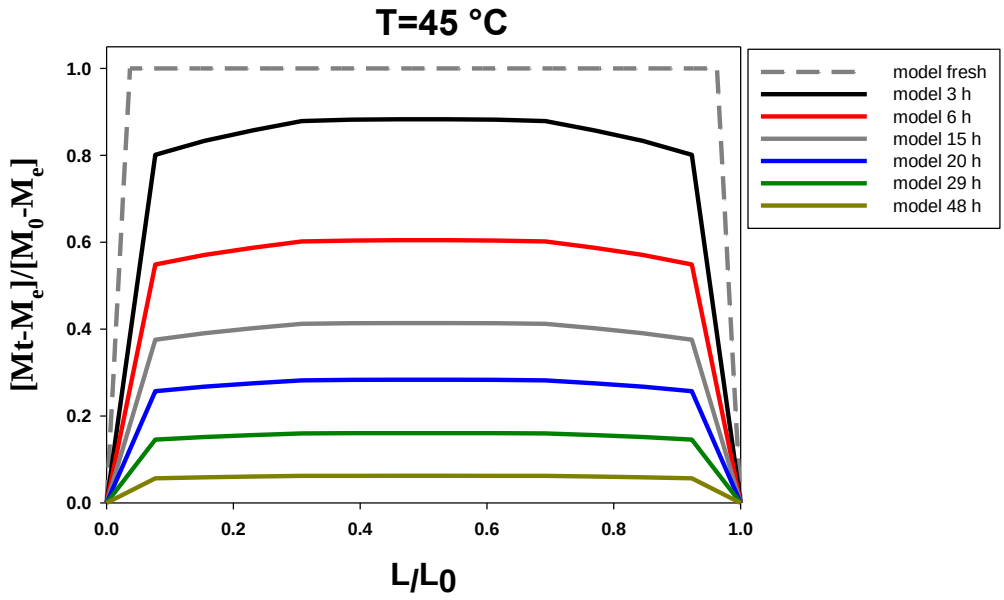

Fig. 47. *Predicted concentration distribution at various times in a cubical pear sample at T=45°C.*

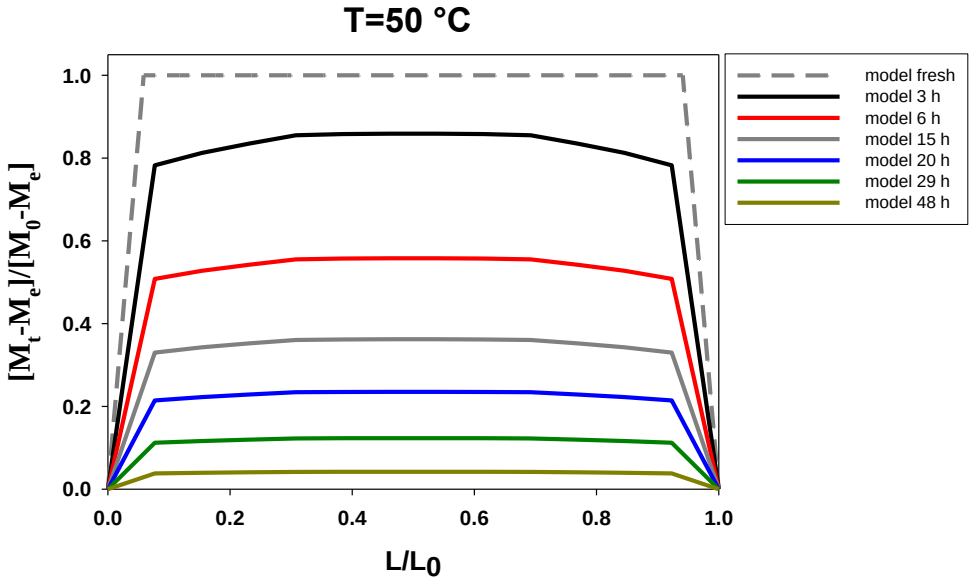

Fig. 48. *Predicted concentration distribution at various times in a cubical pear sample at T=50 °C.*

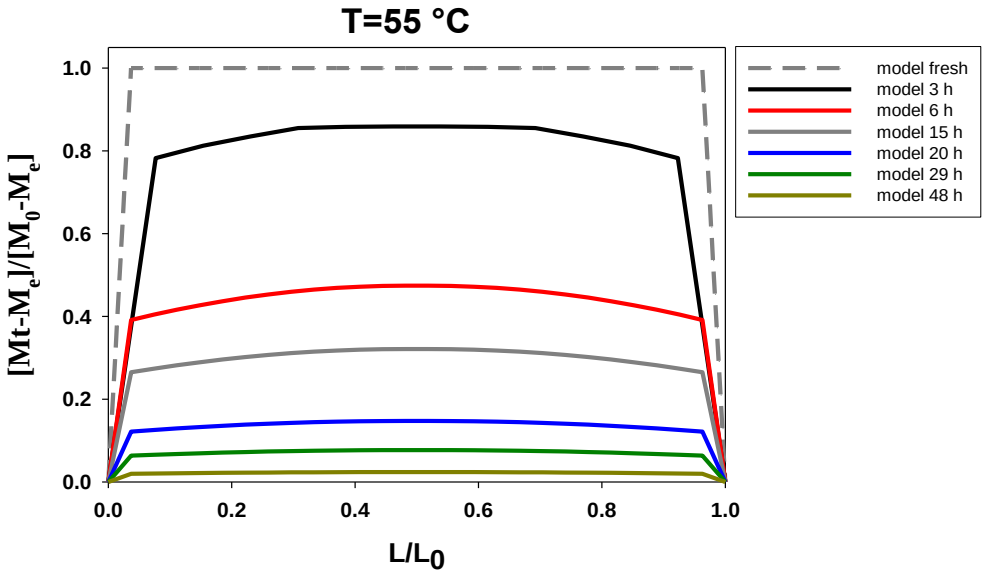

Fig. 49. *Predicted concentration distribution at various times in a cubical pear sample at T=55°C.*

Initially at time 0 the moisture content is assumed constant along the length of the sample. Then, the moisture profile is almost constant in the sample except the zone closest to the surface and decreases with time (after 6 hours it is about half of the initial value).

The model results were compared with experimental ones obtained through NMR relaxometry, in Figure 50 for 45°C. It's evident from comparison that the experimental values were significantly higher than those predicted by the model at the same time. Furthermore, the shrinkage effect is not predicted by the model.

In my opinion, the observed differences cannot be ascribed to the assumption of cubic geometry in the model for the sample of parallelepiped shape (2.5cm x 2.5cm x 2cm) used in the experiments.

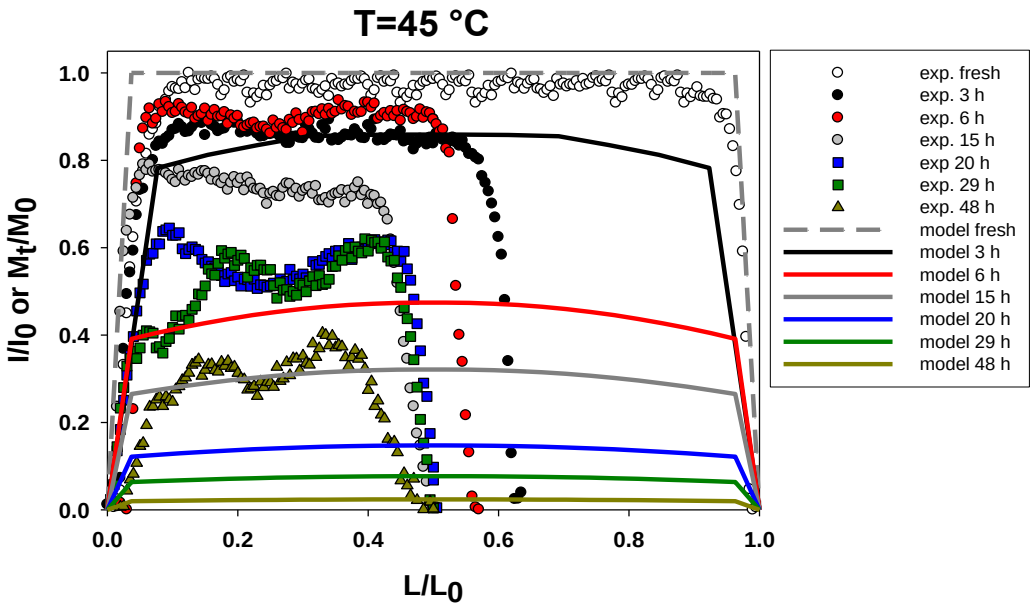

Fig. 50. *Comparison between experimental (I/I_0) depth profile by NMR and predicted moisture ratio (Mt/Mo) for cubical geometry at T=45°C.*

It can be concluded that Fick's second law is not adequate to describe the real moisture profile in a sample. For this reason in the next paragraph, a new model that takes into account the shrinkage effect is presented.

3.2 Mathematical modelling with shrinkage effect

In this model, it is assumed that all water in pear matrix, that is removed during drying, is bulk (free) water. This hypothesis is in agreement with the result of NMR relaxometry indicating that most of the water (77%) is in vacuoles and a net loss of this population occurred during drying. In this model, an isothermal condition is considered since in drying condition here analysed the characteristic time of thermal transient was far less than that of mass transport. The model considers changes in all three dimensions of the pear sample as measured during experiment, by including an empirical correlation.

The Fick's second law is used to predict moisture content distribution inside the pear during drying process.

For a solid of parallelepiped shape, of dimensions $2R_1 \cdot 2R_2 \cdot 2R_3$, the general differential equation, written in Cartesian coordinate, that describes the mass diffusion phenomenon (i.e. water during drying) is the Fick's second law of diffusion, as follows:

$$\frac{\partial M}{\partial t} = \frac{\partial}{\partial x}\left(D_{eff} \frac{\partial M}{\partial x} \right) + \frac{\partial}{\partial y}\left(D_{eff} \frac{\partial M}{\partial y} \right) + \frac{\partial}{\partial z}\left(D_{eff} \frac{\partial M}{\partial z} \right) \quad (46)$$

where D_{eff} is the diffusion coefficient (m^2/s) and M is the moisture content on a dry basis ($kg_r/kg_{d.b.}$).

Using the symmetry of the pear around the x, y and z-axis, it is possible to consider only 1/8 of the volume of the solid. The initial, symmetry and boundary conditions are as follows:

Initial condition inside the solid: the moisture content is constant and uniform

$$M(x, y, z, t = 0) = M_0 \text{ for } 0 < x < R_1, 0 < y < R_2, 0 < z < R_3 \quad (47)$$

Plane of symmetry: the gradient of moisture content are equal to zero at the planes of symmetry

$$\frac{\partial M(x = 0, y, z, t)}{\partial x} = \frac{\partial M(x, y = 0, z, t)}{\partial y} = \frac{\partial M(x, y, z = 0, t)}{\partial z} = 0 \text{ for } t > 0 \quad (48)$$

Free surface: diffusive mass transfer is equal to convective mass transfer at the surface of the solid at the three surfaces: $(x=R_1,y,z);(x,y=R_2,z);(x,y,z=R_3)$, for $t>0$:

$$-D_{eff}\rho_s \frac{\partial M}{\partial x} = h_m \rho_s (M_{sur} - M_e) \quad (49)$$

$$-D_{eff}\rho_s \frac{\partial M}{\partial y} = h_m \rho_s (M_{sur} - M_e) \quad (50)$$

$$-D_{eff}\rho_s \frac{\partial M}{\partial z} = h_m \rho_s (M_{sur} - M_e) \quad (51)$$

where ρ_s is the solid density (kg/m^3) considerate constant; h_m is the moisture transfer coefficient (m/s); M_{sur} is the moisture at the surface of the parallelepiped and M_e is the equilibrium moisture content ($kg/kg_{d.b.}$) (i.e the moisture required to maintain equilibrium with the surrounding atmosphere).

Introducing the dimensionless variables:

$$\bar{x} = \frac{x}{R_1}, \bar{y} = \frac{y}{R_1}, \bar{z} = \frac{z}{R_1} \text{ and } \bar{M} = \frac{M}{M_0} \quad \bar{M}_e = \frac{M_e}{M_0} \quad (52)$$

the equation (44) become:

$$\frac{\partial \bar{M}}{\partial \tau} = \frac{\partial^2 \bar{M}}{\partial \bar{x}^2} + \frac{\partial^2 \bar{M}}{\partial \bar{y}^2} + \frac{\partial^2 \bar{M}}{\partial \bar{z}^2} \quad (53)$$

where τ is the dimensional time $\tau = \frac{t \cdot D_{eff}}{R_1^2}$ (54)

The initial, symmetry and boundary conditions become:

$$\bar{M}\left(\bar{x},\bar{y},\bar{z},\tau=0\right)=1 \text{ for } 0<\bar{x}<1,\ 0<\bar{y}<\frac{R_2}{R_1},\ 0<\bar{z}<\frac{R_3}{R_1} \quad (55)$$

$$\frac{\partial\bar{M}\left(\bar{x}=0,\bar{y},\bar{z},\tau\right)}{\partial\bar{x}}=\frac{\partial\bar{M}\left(\bar{x},\bar{y}=0,\bar{z},\tau\right)}{\partial\bar{y}}=\frac{\partial\bar{M}\left(\bar{x},\bar{y},\bar{z}=0,\tau\right)}{\partial\bar{z}}=0 \text{ for } \tau>0 \quad (56)$$

and at: $\left(\bar{x}=1,\bar{y},\bar{z}\right);\left(\bar{x},\bar{y}=\frac{R_2}{R_1},\bar{z}\right);\left(\bar{x},\bar{y},\bar{z}=\frac{R_3}{R_1}\right)$, for $\tau>0$

$$\frac{\partial\bar{M}}{\partial\bar{x}}=\text{-Sh}\left(\bar{M}_{sur}-\bar{M}_e\right) \quad (57)$$

$$\frac{\partial\bar{M}}{\partial\bar{y}}=\text{-Sh}\left(\bar{M}_{sur}-\bar{M}_e\right) \quad (58)$$

$$\frac{\partial\bar{M}}{\partial\bar{z}}=\text{-Sh}\left(\bar{M}_{sur}-\bar{M}_e\right) \quad (59)$$

The convective mass transfer coefficient and the effective diffusion coefficient are correlated with the dimensionless Sherwood number:

$$Sh=\frac{h_m \cdot R_1}{D_{eff}} \quad (60)$$

The finite element method is applied to solve the non-linear partial differential equation (Eq. 53) subject to the initial and boundary conditions (Eq. 55-59).

7300 cells and 11100 nodes were used in the simulations, and the convergence criterion $\left|\bar{M}^{k-1}-\bar{M}^{k}\right|\le 10^{-8}$ (where k represent the k-th iteration) at each node of the computational domain was adopted, figure 51.

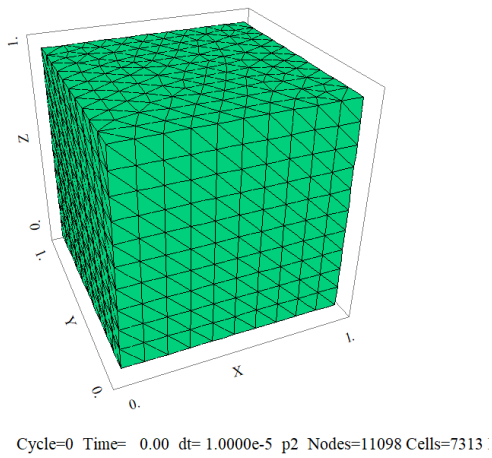

Fig. 51. *Generation of initial mesh for 1/8 of parallelepiped.*

The value of the mass transfer coefficient h_m (m/s) was in agreement with the values reported in literature (Silva et al., 2014, 2016).

In order to determinate the optimum value of the D_{eff}, the coefficient of determination of the fit (R^2), the reduced χ-square of the fit (χ^2) and the root mean square error of the fit $\left(RMSE\right)$ were used as objective functions.

As already described in the experimental section, pear shrinkage occurs during drying.

The experimental data obtained through the measurement with a vernier caliper of the three sizes of the pear and by NMR (along z-axis) showed that, after 15-20 h of drying, each size was half of the initial value.

In order to take into account the effect of shrinkage, a law of variation of the sample size was adopted, (figure 51). The law of size reduction (i. e. L/L_0 along the z-axis) is expressed as an exponential decay law, equation (59), with correlation parameters and coefficient of determination (R^2) reported in table 13.

$$\frac{L}{L_0} = y_0 + a \cdot \exp(-b \cdot \tau) \qquad (61)$$

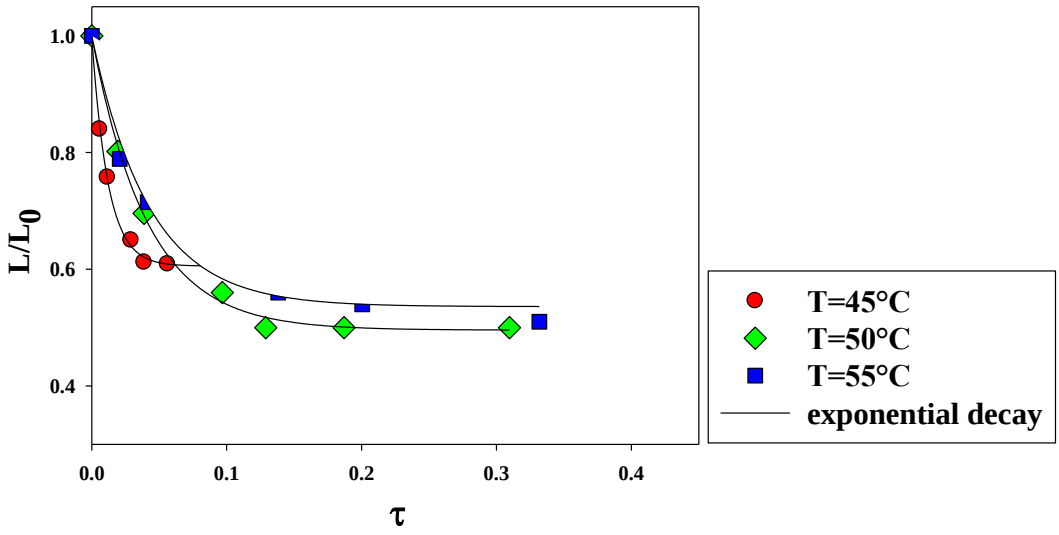

Fig. 52. *Experimental data of thickness reduction L/L_0 during τ .*

	Temperature		
	45 °C	**50 °C**	**55 °C**
y_0	0.61	0.50	0.50
a	0.39	0.50	0.43
b	72.470	18.284	23.84
R^2	0.9982	0.9954	0.9814

Table 13 *Model parameters and fitting parameter for the model with shrinkage.*

Using these conditions, the size of samples is adjusted at each time step during the calculation of the mass governing equation and an adaptive grid was used for simulations. Figure 53 shows the mesh reduction and adaption to the simulation domain in the case of drying temperature of 45°C.

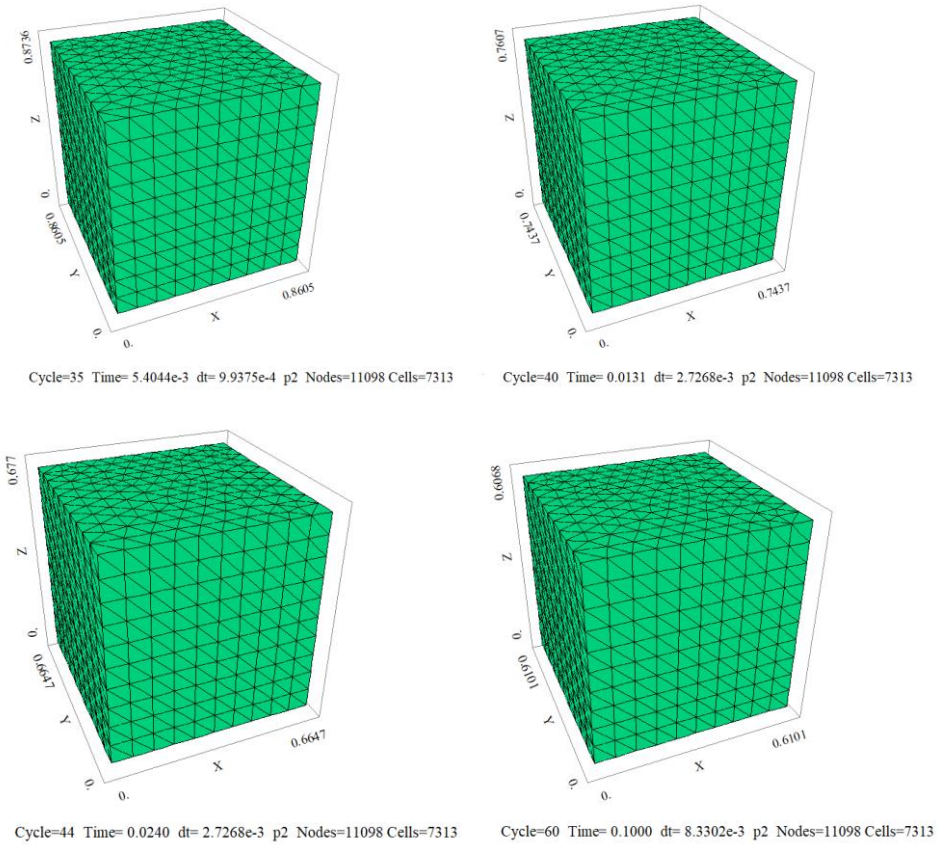

Fig. 53. *Evolution of the mesh for 1/8 of parallelepiped during simulation.*

3.3 Results of the model considering shrinkage

3.3.1 Drying kinetics

Before to calculate the optimum value of D_{eff} it was evaluated the effect of its variation at fixed value of h_m, and the effect of variation of h_m at fixed value of D_{eff}.

As example, it is reported the results for the temperature of 50 °C.

Figure 55 (a) show the effect of variation of D_{eff} at fixed h_m. It is possible to see that by increasing D_{eff} from $1*10^{-8}$ to $1*10^{-11}$ m^2/s the drying kinetics go faster. Instead at fixed value of D_{eff}, the increasing of h_m from $1*10^{-8}$ to $1*10^{-5}$ m/s less influence the variation of velocity of the drying kinetics. This confirm the good choice of the value of h_m adopted (in agreement with the literature).

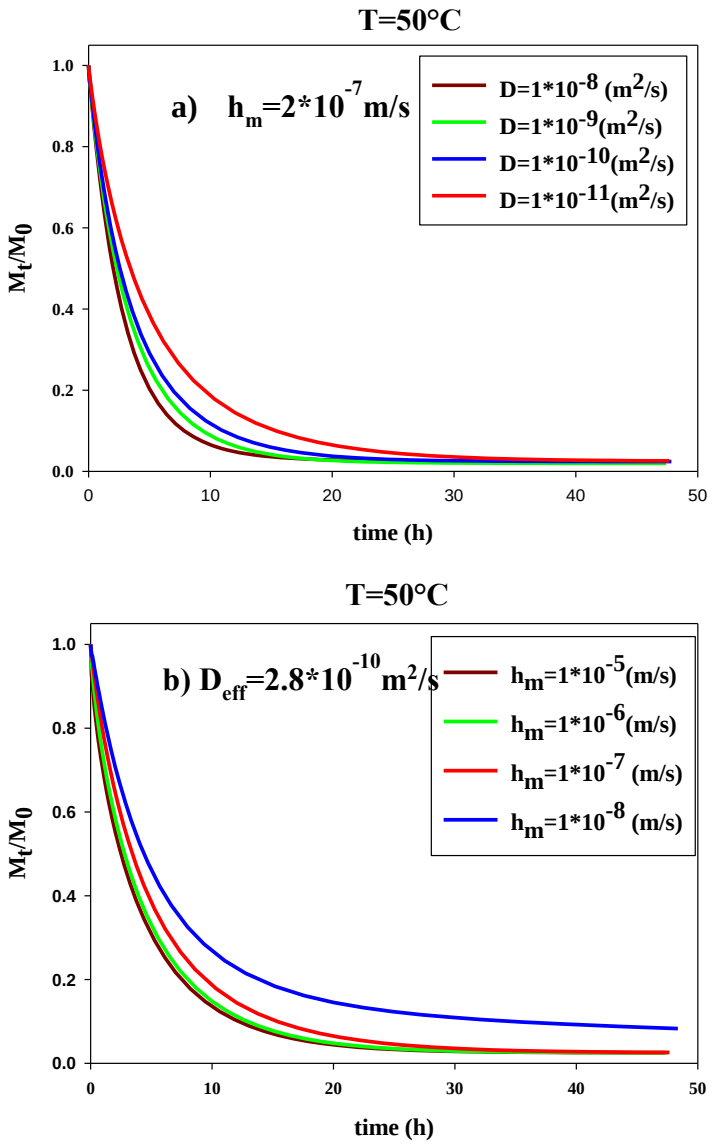

Fig. 54. *Moisture ratio during drying at fixed h_m and different value of D_{eff} (a); at fixed D_{eff} and different value of h_m (b) for T=50°C.*

Model results are compared with experimental moisture ratio data reported in figure 54. Table 14, reports the value of the D_{eff} calculated by the model taking into account the shrinkage, together with the fitting parameters (R^2, $RMSE$, χ-square). A very good agreement between experimental and theoretical data was observed (R^2>0.99; χ-square and RMSE of the order of 10^{-4} and 10^{-2}, respectively).

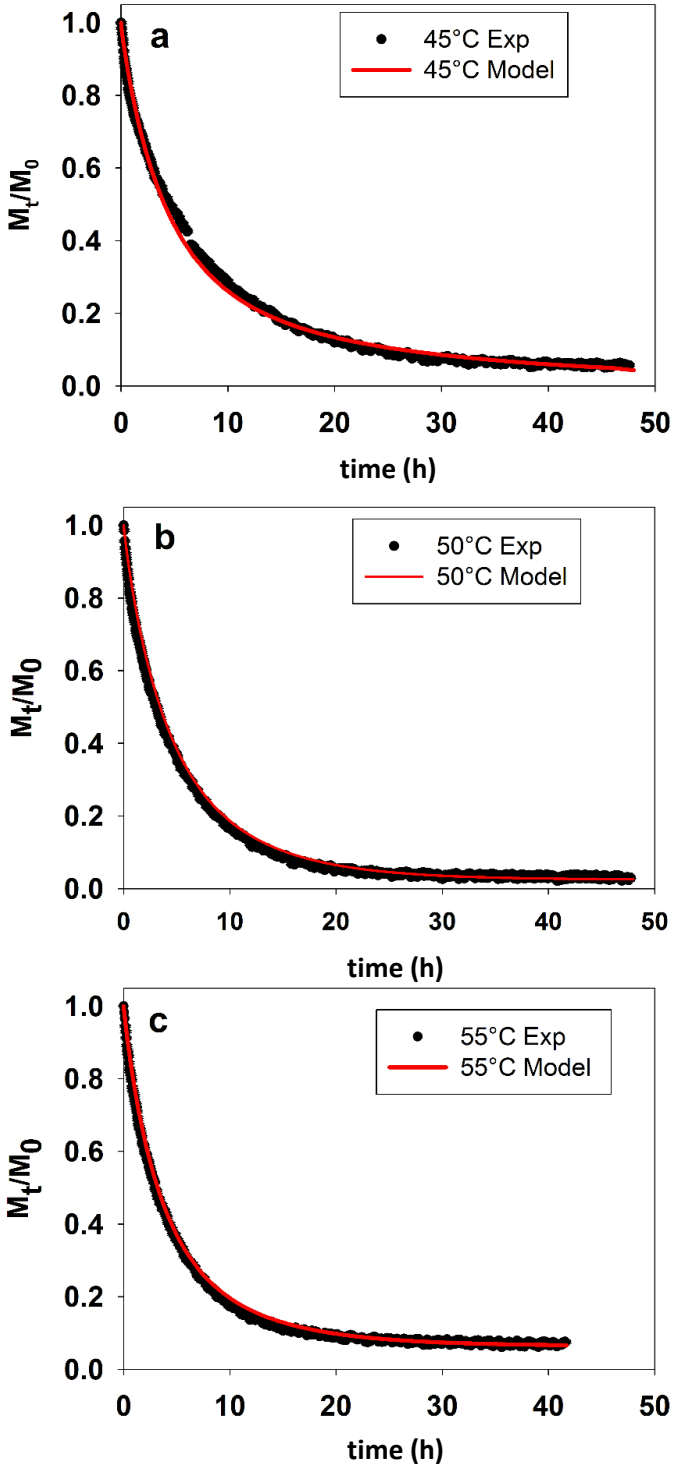

Fig. 55. *Moisture ratio of parallelepiped pear samples during drying at (a) 45, (b) 50 and (c) 55°C.*

	Temperature		
	45 °C	**50 °C**	**55 °C**
Sh	8.0	6.0	4.0
D_{eff} **(m²/s)**	0.84×10^{-10}	2.8×10^{-10}	3.00×10^{-10}
h_m **(m/s)**	2.00×10^{-7}	2.00×10^{-7}	2.00×10^{-7}
R^2	0.990	0.993	0.995
χ-square	4.32×10^{-4}	5.84×10^{-4}	2.32×10^{-4}
RMSE	2.07×10^{-2}	1.61×10^{-2}	1.68×10^{-2}

Table 14 *Model and fitting parameters obtained by comparison with kinetics data.*

The value of the effective diffusion coefficient estimated by the model considering shrinkage ranging from $0.84*10^{-10}$ to $3*10^{-10}$ m^2/s in the range of temperature 45-55 °C. These value of diffusivities are comparable with those found by Park et al. (2002) for the convective drying of pear d'Anjou in the range of temperature 40 to 80 °C (D_{eff} vary from 2 to $8*10^{-10}$ m^2/s) and slightly lower than those predicted by Guinè (2006) (D_{eff}=5.11-11.4*10^{-10} m^2/s) in the range 30-50 °C.

3.3.2 Predicted M_t/M_0 profiles along z-axis

The results of the model in term of M_t/M_0 profiles along z-axis are compared with NMR data of the proton intensity ratio (I/I_0) as function of the thickness ratio (L/L_0) of the sample (figure 56). The comparison was reported for fresh pear and pear samples dried for different times at the three drying temperatures.

At 45°C the model is able to predict the experimental data with good accuracy, especially in the initial drying phase (up to 15 h). In fact, model profiles are very similar to the experimental ones. At longer drying time (20-48 h) some differences between the experimental and model profiles at the center of the sample were observed. At higher temperatures, 50°C and 55°C, these differences were observed at lower drying times (about 15 h).

The observed differences in the trend of moisture profiles may be ascribed to the presence of other components (i.e. sugar) except of water in pear that are not taken into account in the model. As observed previously, during drying the transport of water from the inside to the surface of the sample is influenced by the concentration gradient of sugar which changes during time and along the sample thickness.

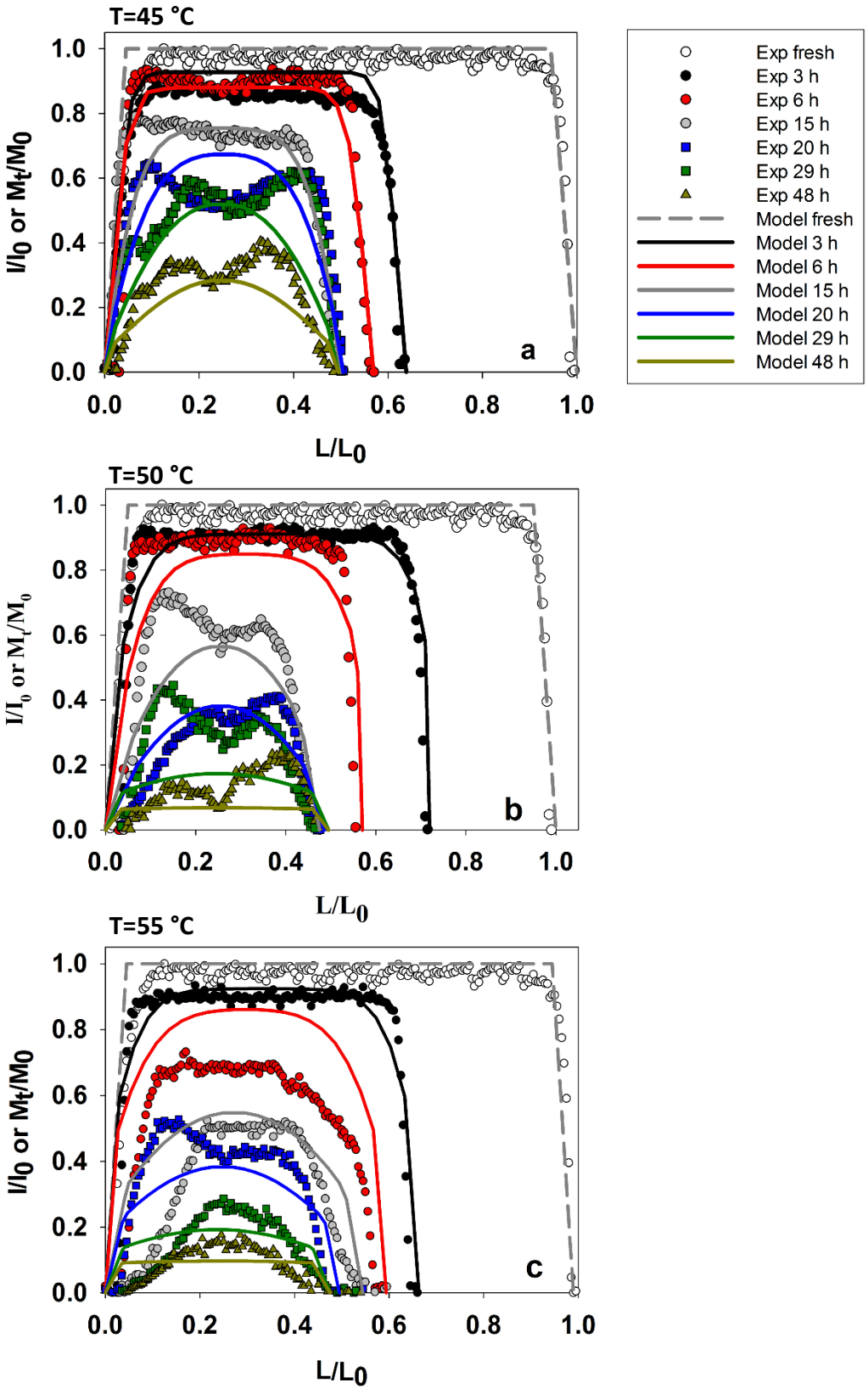

Fig. 56. *Comparison of depth profile of fresh and dried pear obtained with NMR with simulated M_t/M_0 profile along z-axis, at a 45, b 50 and c 55°C.*

3.4 Conclusions

The diffusion model developed including the effect of shrinkage was able to describe the drying process of pear. A very good agreement between experimental and theoretical data of moisture ratio during drying was found. The model also well predicted the moisture profile along the pear thickness especially at first stages of drying (<15 h), when the effect of sugar gradients is less pronounced. The estimated values of the effective diffusion coefficient, ranging from $0.84x10^{-10}$ to $3x10^{-10}$ m^2/s in the range of temperatures 45-55°C, were in agreement with those reported in literature for pear in similar drying conditions.

In conclusion, theoretical model allowed us to elucidate the effect of drying on textural and physical structure of fruit and to select the best drying condition.

CHAPTER 4

Drying of grape

4 Introduction

Grape is an important Italian horticultural product dried for safe storage over an extended period and known as the best source of carbohydrate, organic compounds and minerals. In fact, grapes offer health benefits because contain large amount of phytochemicals including phenols, flavonoids, anthocyanins and resveratrol (Wang et al., 1997).

Grape drying is a slow and very energy intensive process because the waxy peel has low permeability to moisture. Grapes have relatively high sugar and moisture content and are very sensitive to microbial spoilage during storage. For this reason, after harvest they must be consumed or processed into various products in few weeks in order to reduce economic losses.

Grapes drying is carried out using traditional (solar) or industrial methods, a pretreatment with different chemical solutions is also applied prior to drying. Traditionally raisins are obtained by sun drying of the fruit for 8-10 days, which substantially reduces water content. This drying method is cheap, but there is a risk of damage due to dust and insect infection (Pangavhane and Sawhney, 2002).

An alternative to it is hot air drying. In general, the dehydration causes damage in texture, color, taste and nutritional value of food due to the high temperatures (60-75°C) and long drying times required in the process (2-3 days) (Singh et al., 2012). According to Carranza-Concha et al. (2012), the dehydration of grapes affects their content of polyphenols, ascorbic acid and antioxidant activity.

That is why efforts should be made to reduce drying times but also to decrease the temperatures used in the drying process in order to obtain better quality products.

In particular, in the following the effect of a physical pretreatment of peel is considered before drying in order to facilitate water diffusion.

4.1 Effect of physical pretreatment process on the drying kinetics

The major processing method in all grape-growing country is the drying of grapes into raisins. This process is very slow due to the peculiar structure of the grape peel that is covered by a waxy layer, which acts as a barrier to moisture movement across the membrane. With elimination of the wax outer peel layer it is possible to accelerate the drying rate.

Cinquanta et al. (2002) and Doymaz et al. (2004) studied the effect of drying rate applying a chemical pretreatment on grape samples. In particular dipping grapes in oil emulsion: ethyl oleate and K_2CO_3 for several minutes, the wax dissolved and the resistance to water diffusion through the peel reduced.

Di Matteo et al. (2000) proposed an alternative physical pre-treatment, consisting of abrasion of the peel of grapes. It consists of the superficial abrasion of the peel using abrasive material. Seedless white grapes (var. Nevado) were dried in a convective oven at 50°C, with an air speed of 0.5 m/s, so as to reduce the average moisture of grape to about 20% wt. Before drying they submitted about 50 grape berries to one of the following pretreatments: i) immersion in aqueous solution at 2% vol ethyl oleate and 2.5% vol K_2CO_3 at 40 °C for 3 min (TR-EtOl); ii) abrasion in the shaker for 10 min (Abr). White untreated grape (UTR) was used as reference.

They showed that at the end of the drying process the original structure of the berries was maintained independently of the pretreatment used. Results of drying curves of pretreated and control grape berries are shown in figure 57.

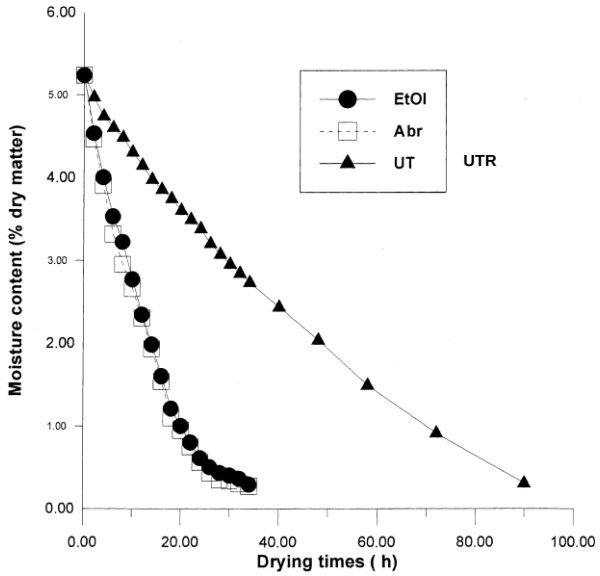

Fig. 57. *Experimental values of humidity (% dry matter) vs drying times for grape berries the peel of which was untreated (UTR) or pre-treated by dipping into ethyl oleate (EtOl) or by abrasion (Abr), (Di Matteo et al., 2000).*

For both chemically and physically treated samples the pattern of the drying curves was quite similar, and also the drying time needed to reduce the average moisture of the grape berries from 84 % to 20% w/w at 50°C was the same (35 h). The drying time was about one third of the time required to dry the untreated grape berries.

Then they showed that the abrasion method was as effective as the traditional chemical method and even though gave rise to a darker final product, which is less attractive to consumer, but avoiding the use of chemical additives allows safer raisins to be produced.
Then they also proposed a mathematical model that describe the diffusion of water through whole grape berries, both in the pulp both in the peel.
The process was described by the model equation:

$$\frac{\partial \mathrm{M_i}}{\partial \mathrm{t}} = D_\mathrm{i}\left\{\frac{\partial^2 \mathrm{M_i}}{\partial r^2} + \frac{2}{r}\frac{\partial \mathrm{M_i}}{\partial \mathrm{r}}\right\} \qquad (62)$$

where the index i =1 refers to the pulp [i.e., for $r \in (0; \mathrm{R_1})$] and i =2 to the peel [i.e., for r $\in (\mathrm{R_1}; \mathrm{R_2})$], figure 58.

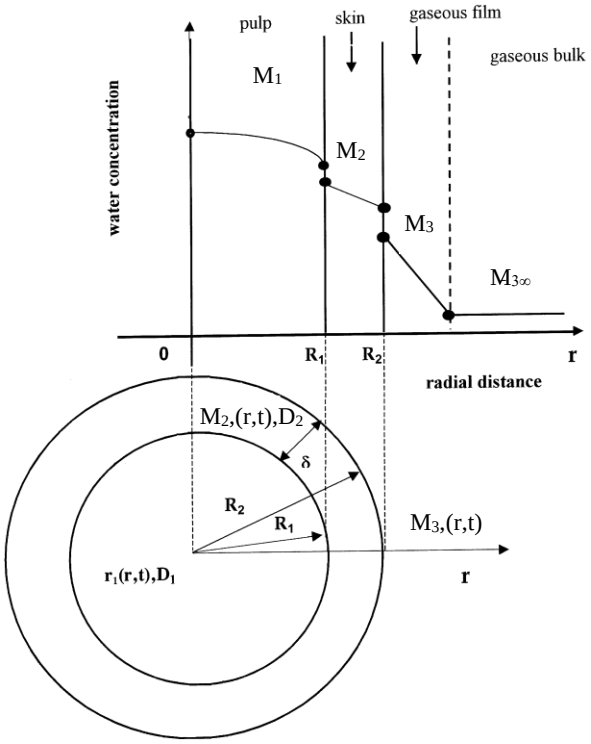

Fig. 58. *Schematic diagram of water (or steam) concentration profiles in the grape pulp and peel, and in the gaseous film surrounding each grape berry, (Di Matteo et al., 2000).*

D_1 is the water diffusivity in the grape pulp, which is much higher than that in the grape peel (D_2). They estimated water concentration in the pulp by solving differential equation (62) for i=1 with the following initial and boundary conditions:

$$\mathrm{M_1}(\mathrm{r},0) = \mathrm{M_{10}} \quad \mathrm{r} \in [0, \mathrm{R_1}],\ \mathrm{t} = 0 \qquad (63)$$

$$\frac{\partial \mathrm{M_i}}{\partial \mathrm{r}} = 0,\ \mathrm{r}=0,\ \mathrm{t} > 0, \qquad (64)$$

$$D_1 \frac{\partial M_1}{\partial r} = D_2 \frac{\partial M_2}{\partial r},\ r=R_1,\ t > 0 \tag{65}$$

$$M_1 = k_1 M_2,\ r=R_1,\ t > 0 \tag{66}$$

where the equilibrium distribution curve relating water concentrations in the pulp/peel interface was assumed to be a linear one characterized by the equilibrium constant K_1. At the same time they obtained water concentration in the grape peel by solving Eq. (60) for i=2 with the following initial and boundary conditions:

$$M_2(r,0) = \frac{M_{10}}{K_1} \quad r \in [R_1, R_2],\ t = 0 \tag{67}$$

$$-D_2 \frac{\partial c_2}{\partial r} = h_m \left[\frac{c_2(R,t))}{K_2} - c_{3\infty} \right] \quad r=R_2,\ t > 0, \text{ if } h \neq \infty \tag{68}$$

$$M_2(R_2,t) = k_3 M_\infty,\ r=R_2,\ t > 0, \text{ if } h \to \infty \tag{69}$$

where the equilibrium-distribution curve relating water concentration at peel/outer environment interface was assumed to be a linear one, characterized by the equilibrium constant K_2. Water diffusion in the gaseous film around the grape berry was described by means of the convective mass transfer coefficient h_m.

They neglected the water accumulation in the peel and considered a steady-state distribution of $c_2(r, t)$ in the peel for any time. For this case, the second boundary condition for the diffusion in the pulp (if $h \neq \infty$) (Eq. 65) becomes:

$$-D_1 \left. \frac{\partial M_1}{\partial r} \right|_{r=R_1} = B \left[\frac{c_1(R,t))}{K_1} - M_{2e} \right] \tag{70}$$

with

$$B = \frac{D_2}{\delta} \left(1 - \frac{D_2/\delta}{h/K_2 + D_2/\delta} \right) \tag{71}$$

$$M_{2e} = K_2 M_{3\infty} \tag{72}$$

For $h \to \infty$ Eq. (70) reduced to

$$-D_1 \left. \frac{\partial M_1}{\partial r} \right|_{r=R_1} = k\left(c_1(R_1,t) - M_e\right) \tag{73}$$

with

$$k = \frac{D_2}{\delta k_1} \tag{74}$$

$$\mathrm{M}_{1e} = K_1 K_2 \mathrm{M}_{3_\infty} \tag{75}$$

In their experiments the gaseous velocity was quite high, so they could neglect the resistance to the mass transport out of the grape. Under this hypothesis they applied an analytical solution (in series) that integrated over the whole volume of any grape berry and at the end they derived the distribution of humidity:

$$\frac{H - H_e}{H_0 - H_e} = 6L^2 \sum_{n=1}^{\infty} \frac{\exp\left(-D_1 \beta_n^2 t / R_2^2\right)}{\beta_n^2 \left(\beta_n^2 + L\left(L-1\right)\right)} \tag{76}$$

with

$$L = \frac{R_2 k}{D_1} \tag{77}$$

where β_n is the n-th root of the following transcendental equation:

$$\beta_n \cot\left(\beta_n\right) + L - 1 = 0 \tag{78}$$

For peeled grape they expressed the dehydration process mathematically by accounting only for the diffusion of water in the grape pulp and water vapour in the gaseous film surrounding the grape berry. The diffusion of water in the pulp was described by differential equation (60) with i=1 together with the following initial and boundary conditions:

$$\mathrm{M}_1\left(\mathrm{r}, 0\right) = \mathrm{M}_{10} \quad \mathrm{r} \in \left[\mathrm{R}, \mathrm{R}_1\right], \ \mathrm{t} = 0 \tag{79}$$

$$\frac{\partial \mathrm{M}_1}{\partial r} = 0 \ \mathrm{r}=0, \ \mathrm{t} > 0 \tag{80}$$

$$D_1 \frac{\partial \mathrm{M}_1}{\partial r} = h_m \left[\mathrm{M}_3\left(R_1, t\right) - \mathrm{M}_{3\infty}\right], \ \mathrm{r}=\mathrm{R}_1, \ \mathrm{t} > 0, \text{ if } \mathrm{h} \neq \infty \tag{81}$$

$$\mathrm{M}_1\left(R_1, t\right) = \frac{\mathrm{M}_1\left(R_1, t\right)}{k_3}, \ \text{ if } \mathrm{h} \neq \infty \tag{82}$$

or

$$\mathrm{M}_{1eq} = K_3 \mathrm{M}_{3\infty} \text{if } \mathrm{h} \to \infty \tag{83}$$

Also in this case, neglecting the resistance to the mass transport out of the grape (i.e. $h \to \infty$), they used an analytical solution (in series) that integrated over the whole volume of any grape berry devoid of its peel derived the following distribution of humidity:

$$\frac{H - H_e}{H_0 - H_e} = \frac{6}{\pi^2} \sum_{n=1}^{\infty} \frac{1}{n^2} \exp\left(- \frac{n^2 \pi^2 D_1 t}{R_1^2} \right) \tag{84}$$

They estimated the value of the unknown parameters of the models fitting the experimental drying data collected when using untreated and chemicaly and physically treated grape berries. The unknown parameters estimated were D_1 and c_{1eq} for all three kinds of grape berries, and k for the untreated or treated ones.

The optimal value of water diffusion in the pulp was found equal to $D_1 = 0.4 \cdot 10^{-4} \pm 0.1 \cdot 10^{-4} \left(m^2 / h \right)$. The optimal values of k were: $k^{TR} = 2.817 \cdot 10^{-4} \pm 2 \cdot 10^{-5} \left(m / h \right)$

$k^{UTR} = 7.067 \cdot 10^{-5} \pm 1 \cdot 13^{-6} \left(m / h \right)$; k^{TR} was greater than k^{UTR} and means the greater capability of the pre-treatments to enhance water diffusivity in the grape skin relative to that in the untreated samples.

The same physical abrasion pre-treatment was evaluated by Di Matteo et al. (2002), to remove the cuticular waxy layer (the limiting factor for moisture loss) on plums. In this study, drying experiments were carried out in a convection oven at 60 °C, with an air speed of 0.5 m/s, to reduce the average moisture of plums to about 0.25% w/w. Before drying, samples of about 20 plums (average weight 61.6 g), were submitted to one of the following pre-treatments (TR): i) abrasion (Abr); ii) immersion in an aqueous solution of 2% (v/v) ethyl oleate and 2.5% (v/v) K_2CO_3 at 40 °C for 5 min (EtOl); iii) untreated samples as reference (UTR).

Results showed the great capability of both pre-treatments to enhance water diffusivity in the plum peel with respect to the untreated samples. Moreover, it was found that the physical treatment was more effective than the chemical one. Then data of moisture ratio were fitted using empirical models available in the literature, as reported in figure 59.

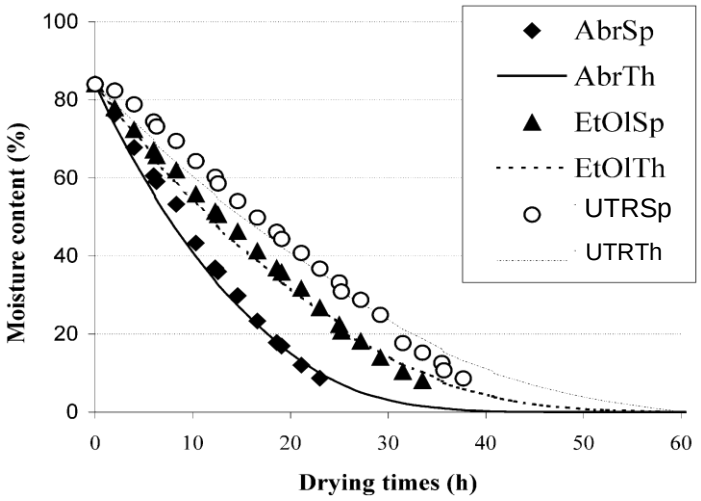

Fig. 59. *Experimental (Sp), and theoretical (Th) values of moisture changes (%) vs. drying times for plums, the peel of which was untreated (UTR) or pre-treated by dipping into ethyl oleate (EtOl) or by abrasion (Abr), (Di Matteo et al., 2002).*

Applying the same mathematical model used for grape, they found the optimum value of the diffusion coefficient in the pulp equal to: $D_1 = 2.648 \cdot 10^{-6} \pm 1 \cdot 10^{-9} \left(m^2 / h \right)$ and of transfer coefficient: $k^{TR} = 3.68961 \cdot 10^{-4} \pm 0.01 \cdot 10^{-4} \left(m / h \right)$ for chemically pretreated and $k^{UTR} = 6.78933 \cdot 10^{-4} \pm 0.006 \cdot 10^{-4} \left(m / h \right)$ for mechanically treated.

Esmaiili et al. (2007) studied the drying characteristics of pretreated grapes using a laboratory-scale tray dryer with the air temperature varied from 40 to 70°C and at air velocity of 1 ms^{-1}. Seedless grapes (Vitis vinifers L.) were subjected to the hot water (HW) and alkaline emulsion of ethyl oleate (EO) pretreatment. Variation of the moisture ratio with drying time showed at 50°C that the EO pretreatment shortened the drying time significantly compared to the HW pretreatment. As one might expected, an increase in the drying air temperature substantially increased the drying rate of the EO-pretreated grapes. The drying rate depend on both the pretreatment conditions and the operating conditions, as shown in figure 60.

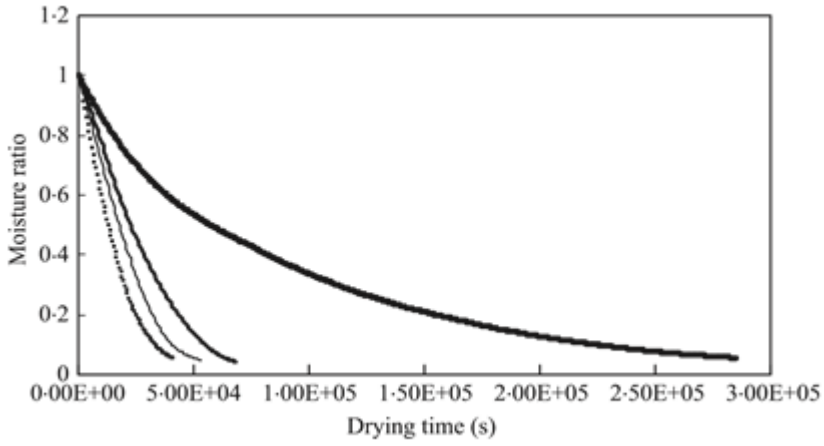

Fig. 60. *Variation of moisture ratio with drying time (s) under different conditions, 50°C (▬▬); ethyl oleate emulsion, 50°C (▬▬), 60°C (——), ethyl oleate emulsion, 70°C (---), (Esmaiili et al., 2007).*

They also determined the effective moisture diffusivities using an analytical-numerical solutions considering shrinkage. The seedless shrinkage was expressed by the following equation:

$$\frac{V}{V_0} = a + b \cdot \left(\frac{M}{M_0} \right) \qquad (85)$$

where V and V_0 are the volume and the initial volume of grape in m^3, and the constant a and b were calculated for the different pretreatments.

Figure 61 shows the variation of the effective moisture diffusivities with the moisture content for different temperatures. As can be seen at a given temperature and moisture content, the effective moisture diffusivity varies depending on the pretreatment method.

At 50°C the effective moisture diffusivity increases from 3.34 to 8.46 $*10^{-10}$ m^2/s using ethyl oleate pretreatment instead of hot water.

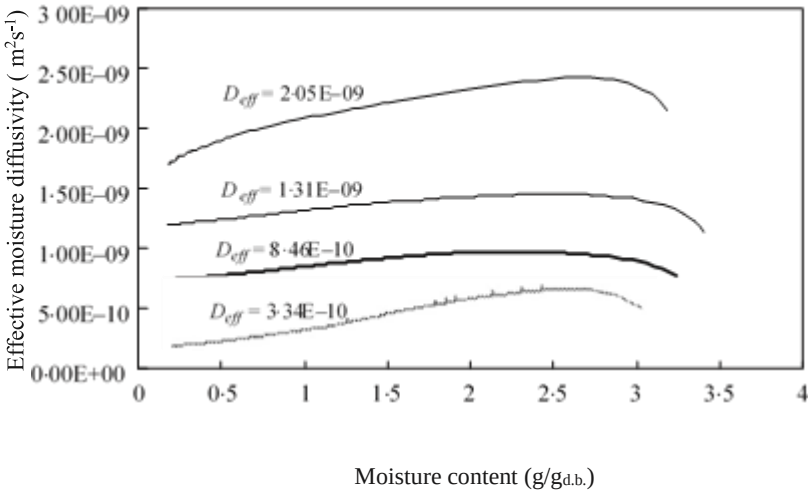

Fig. 61. *Variation of effective diffusivity (m^2s^{-1}) with moisture content ($g/g_{d.b.}$) of the ethyl oleate emulsion and hot water-pretreated grapes at different temperatures; hot water, 50°C (·····); ethyl oleate emulsion, 50°C (——); ethyl oleate emulsion, 60°C (·····); ethyl oleate emulsion, 70°C (——), (Esmaiili et al., 2007).*

Adiletta et al. (2016) analysed the effect of abrasive pretreatment of grape peel on quality parameters (color, total phenolic content and antioxidant activity, shrinkage and rehydration capacity) of raisins. Grape samples (cv. Red Globe) with an initial moisture content of 6.43±0.02 kg/kg$_{d.b.}$ and average diameter of 24.4±1.95 mm were used for experiments. In this study they compared three kinds of samples: untreated grape (UTR), abrades grape (TR-Abr) and dipped grape in chemical solution. Drying was carried out in a convective dryer at constant temperature 40, 50, 60 and 70 °C at air velocity of 2.3 m/s until water content plateau was reached (about 0.3 kg/kg$_{d.b.}$). They reported results in term of M_t/M_0 vs time (figure 62) and of volume shrinkage (V_t/V_0) calculated by means of a digital Vernier caliper (figure 63).

They found that peel abrasion combined with optimal drying temperature, which was 50°C, was not only effective in reducing the drying time, but also in improving the rehydration capability, preserving the antioxidant activity and reducing the shrinkage of grapes.

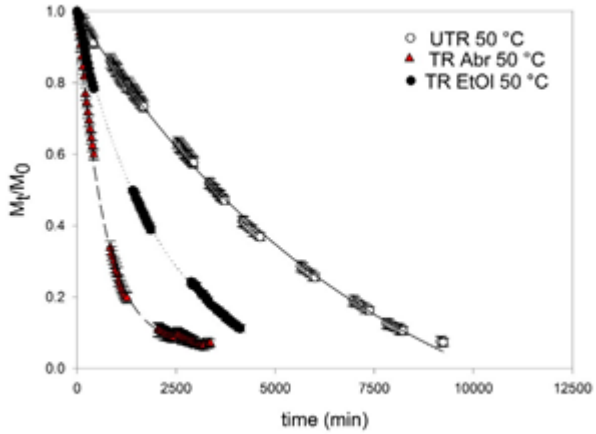

Fig. 62. *Experimental (symbols) and predicted (lines) drying curves of untreated (UTR) and pretreated (TR-ABR, TR-EtOl) samples at 50 °C, (Adiletta et al., 2016).*

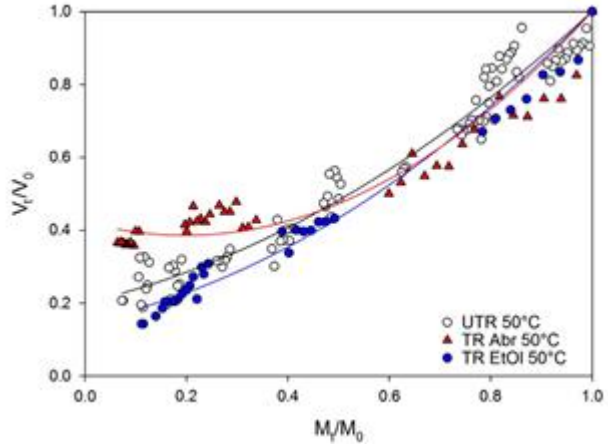

Fig. 63. *Experimental data (symbols) and prediction (curves) of volume shrinkage of grape during drying at 50 °C (Adiletta et al., 2016).*

4.2 Materials and methods

4.2.1 Sample preparation

Red grapes (*cv. Crimson)* with an initial moisture content of 4.08±0.02 kg/ kg_{db} and average diameter of 21.87±0.32 mm were used for the experiments. The grape were selected with uniform size and color and without damage.

In this study three kinds of sample were compared:

a. Untreated grape (UTR);
b. Abraded grape (TR-Abr);
c. Dipped grape in chemical solution (TR-EtOl).

The abrasion of the grape peel was carried out in a motorized rotating drum with diameter of 240 mm and length of 250 mm, made of plexiglass lined inside with sandpaper. The rotation speed of drum was 10 rpm, the pretreatment time was 15 min and the mass of grapes was 4 kg.

TR-EtOl samples were dipped in an aqueous solution of 2% vol ethyl oleate and 2.5% vol K_2CO_3 at 40 °C for 5 min.

Drying experiments on grapes were done in a convective dryier (see figure 19) at three temperatures: 50, 60 and 70 °C with an air velocity of 2.3 m/s. Drying tests were carried until the water content plateau was reached (about 0.25 $kg/kg_{d.b.}$). During drying at regular intervals the samples were weighted by means of a digital balance.

4.3 Results

4.3.1 Drying experiments

Drying kinetics were reported in terms of M_t/M_0 vs time in figure 64, where M_t is the moisture content (kg/kg_{db}) at a given drying time and M_0 the initial moisture value.

In the figure 64 a, b and c results for untreated (UTR), abraded grape (TR-Abr) and dipped grape in chemical solution (TR-EtOl) at the three temperatures are compared, respectively. For untreated grape, it is observed a reduction of total drying time from 194 h to about 35 h increasing the temperature from 50 to 70°C; while for both pretreated grapes the time reduction is from about 63 h to less than 37 h.

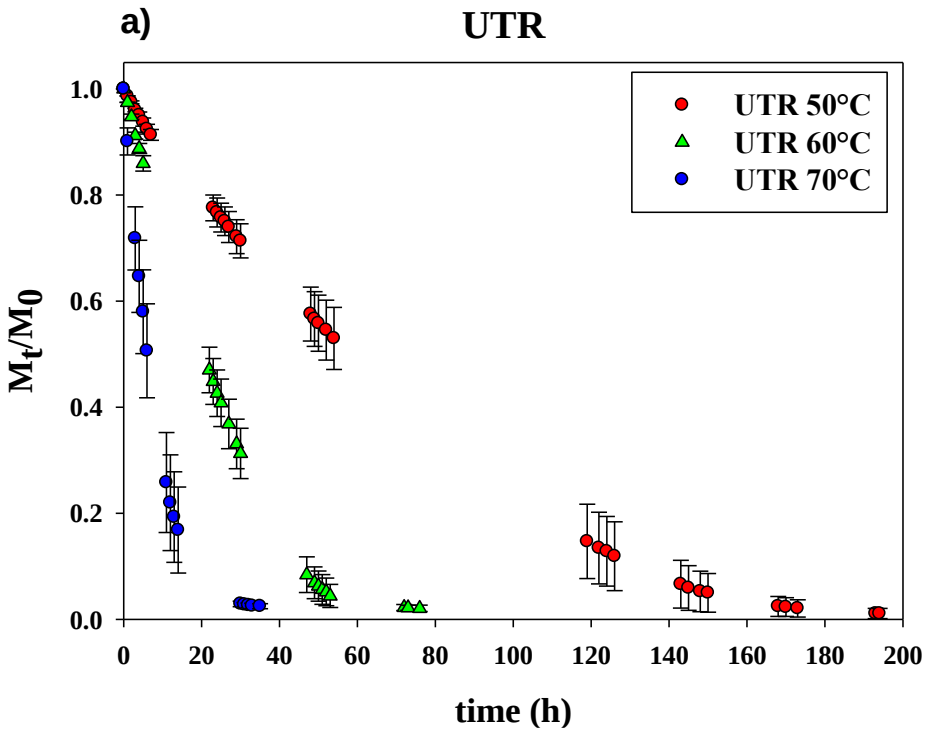
a)
UTR
UTR 50°C
UTR 60°C
UTR 70°C
M_t/M_0
time (h)

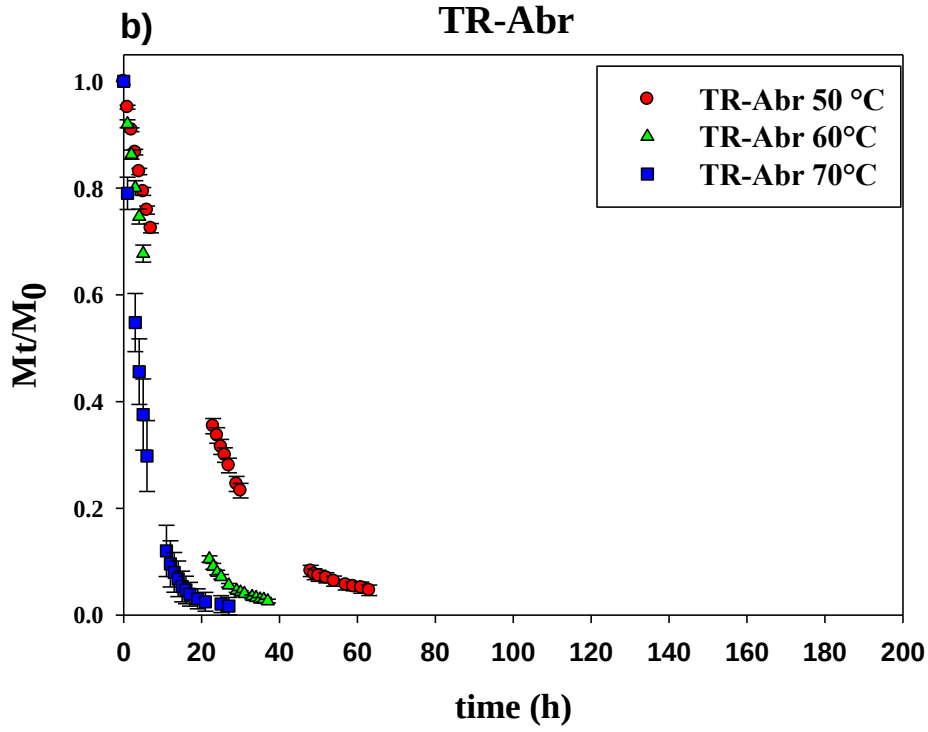
b)
TR-Abr
TR-Abr 50 °C
TR-Abr 60°C
TR-Abr 70°C
Mt/M0
time (h)

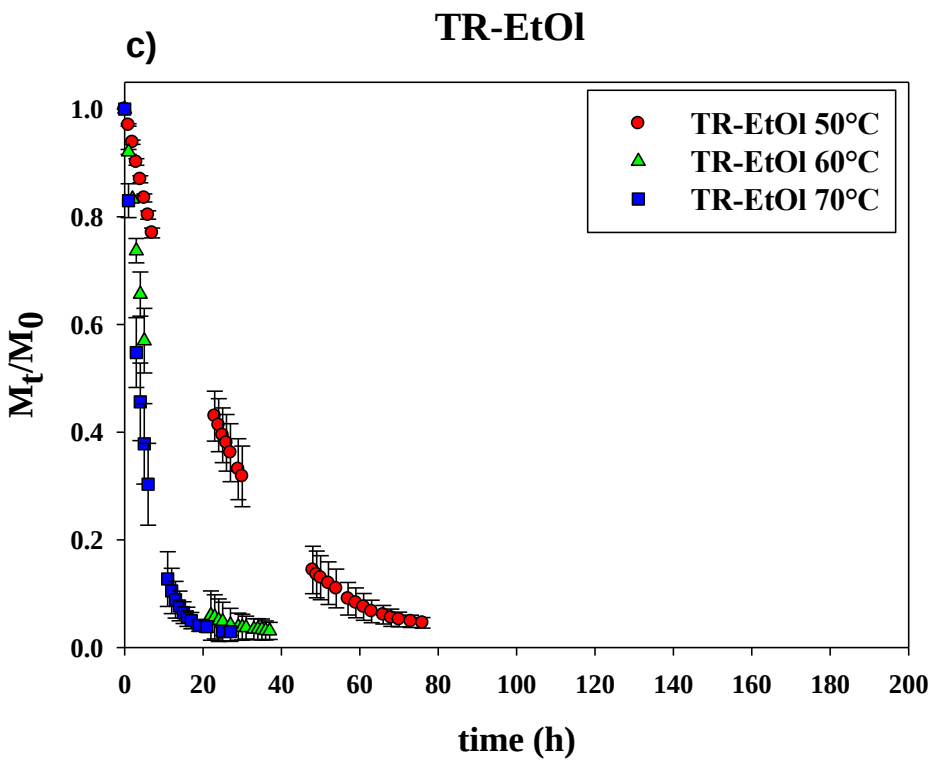

Fig. 64. *Experimental moisture ratio vs time of a) untreated UTR, b) pretreated TR-Abr, c) TR-EtOl grape at 50, 60 and 70 °C.*

4.3.2 Shrinkage measurements

At given drying times grape samples were removed from the oven and their dimensions were measured by means of a vernier caliper in all three orthogonal dimension (length, width and depth). The shrinkage of the samples was then expressed as the ratio between the sample average diameter (average of length, width and depth) at a given drying time (D_t) and average initial one (D_0) as reported in figure 65. It is shown that the dimension of the dried grape is lower than 50% of the fresh one in the case of untreated and ethyl oleate samples, while is higher than 50% for abraded ones.

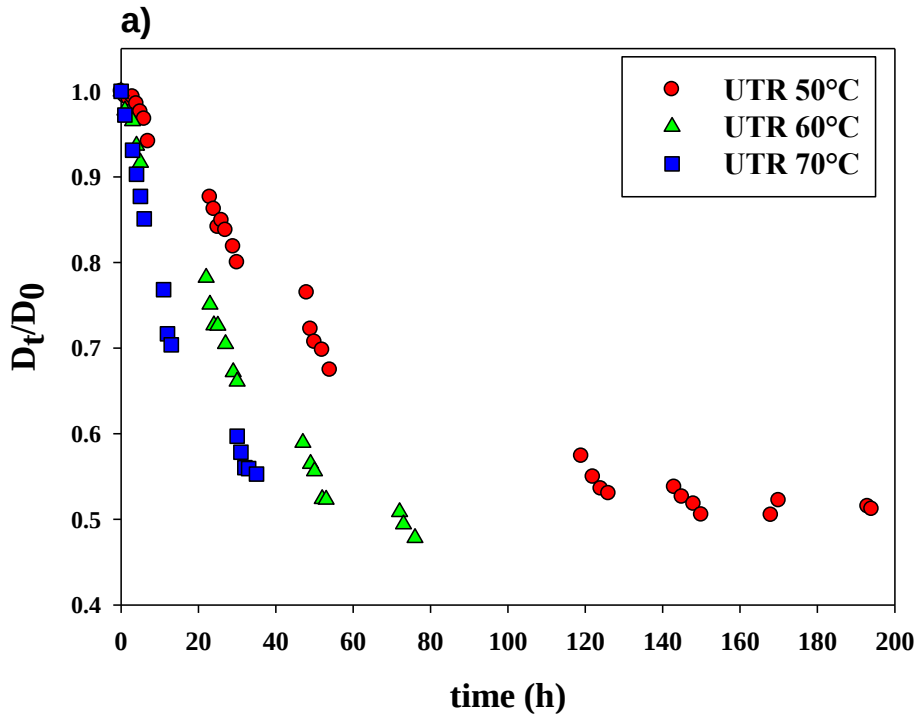
a)
UTR 50°C
UTR 60°C
UTR 70°C
D_t/D_0
time (h)

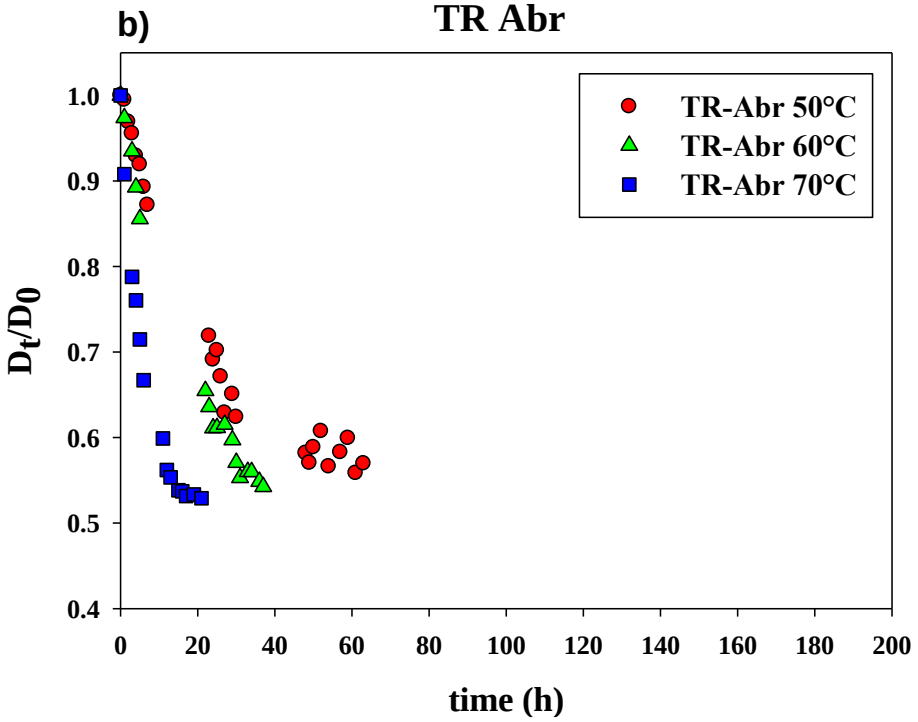
b)
TR Abr
TR-Abr 50°C
TR-Abr 60°C
TR-Abr 70°C
D_t/D_0
time (h)

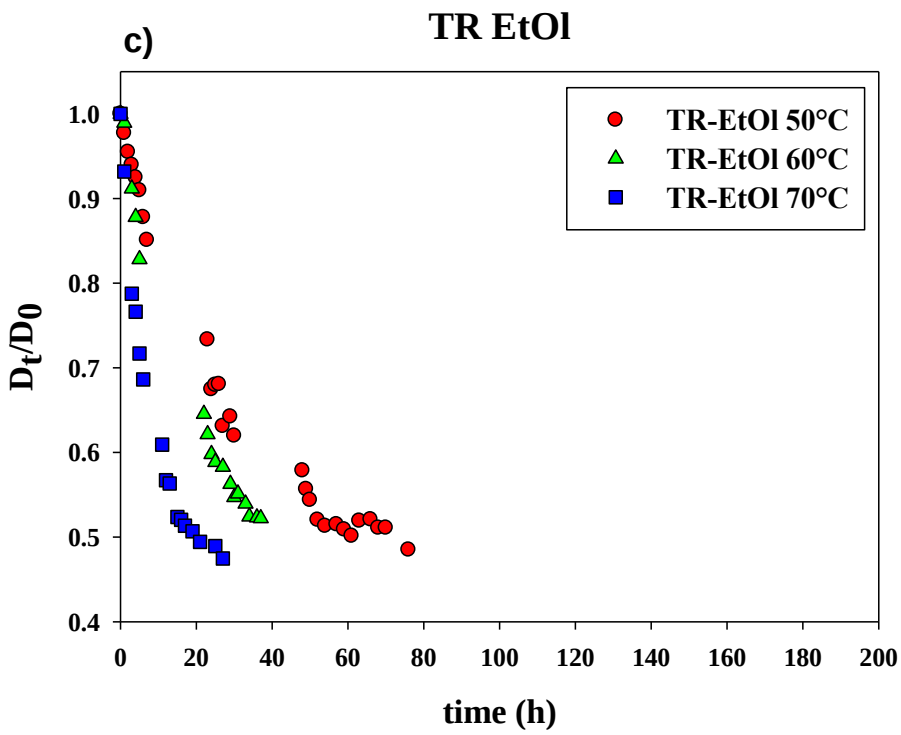

Fig. 65. *Experimental average diameter reduction D_t/D_0 vs time for a) UTR, b) TR-Abr, c) TR-EtOl at 50, 60 and 70°C.*

In figures 66 the variation of D_t/D_0 as a function of the relative moisture content (M_t/M_0) was represented for untreated (UTR), abraded grape (TR-Abr) and dipped grape in chemical solution (TR-EtOl) at the three temperatures evaluated. The variation of D_t/D_0 vs M_t/M_0 can be expressed as a linear law, equation (84), with constants and fitting parameters reported in table 15.

$$\frac{D_t}{D_0} = a + b \cdot \left(\frac{M}{M_0} \right) \qquad (86)$$

UTR	**50 °C**	**60 °C**	**70°C**
a	0.4770	0.5126	0.5951
b	0.5230	0.4874	0.4049
R^2	0.9728	0.9856	0.5195
TR-Abr	**50 °C**	**60 °C**	**70°C**
a	0.5459	0.5644	0.5195
b	0.4541	0.4356	0.4805
R^2	0.9891	0.9798	0.9953

TR-EtOl	50 °C	60 °C	70°C
a	0.4714	0.5504	0.5195
b	0.5286	0.4491	0.4805
R^2	0.9916	0.9613	0.9949

Table 15 *Fitting parameters*

Figures 66s show a decrease of grape diameter proportional to the water content decrease during drying.

At 50 °C the abrasive pretreatment produce less shrunk raisins; while for untreated and ethyl oleate the raisins have similar size reduction. At 60 and 70°C both ethyl oleate and abrasion produce less shrunk raisins with respect to the untreated grape.

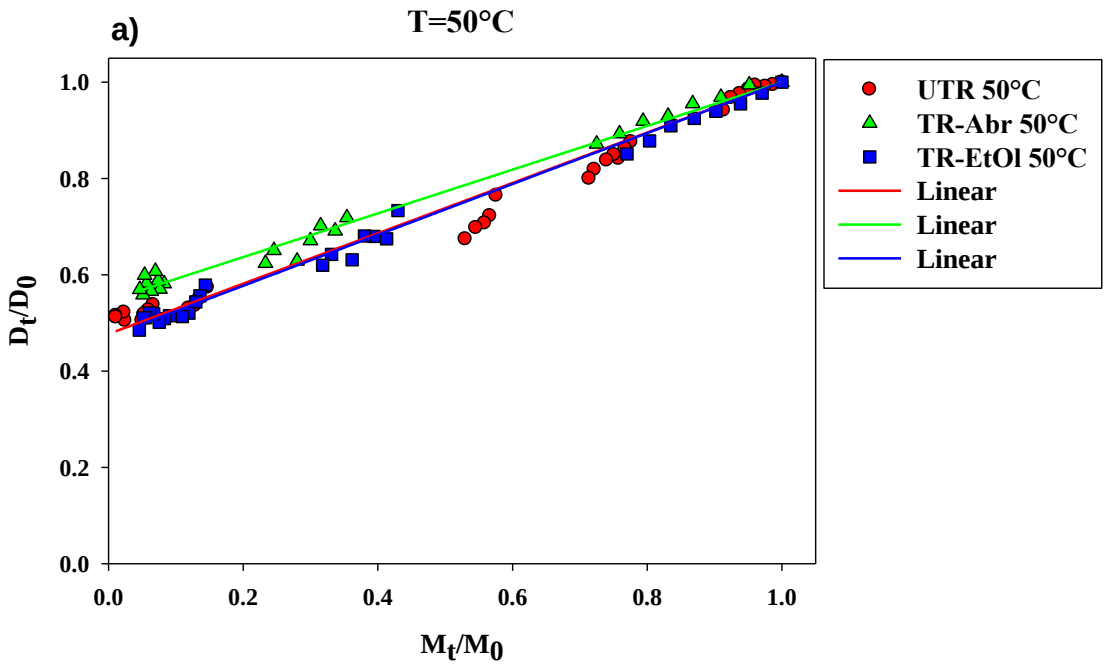

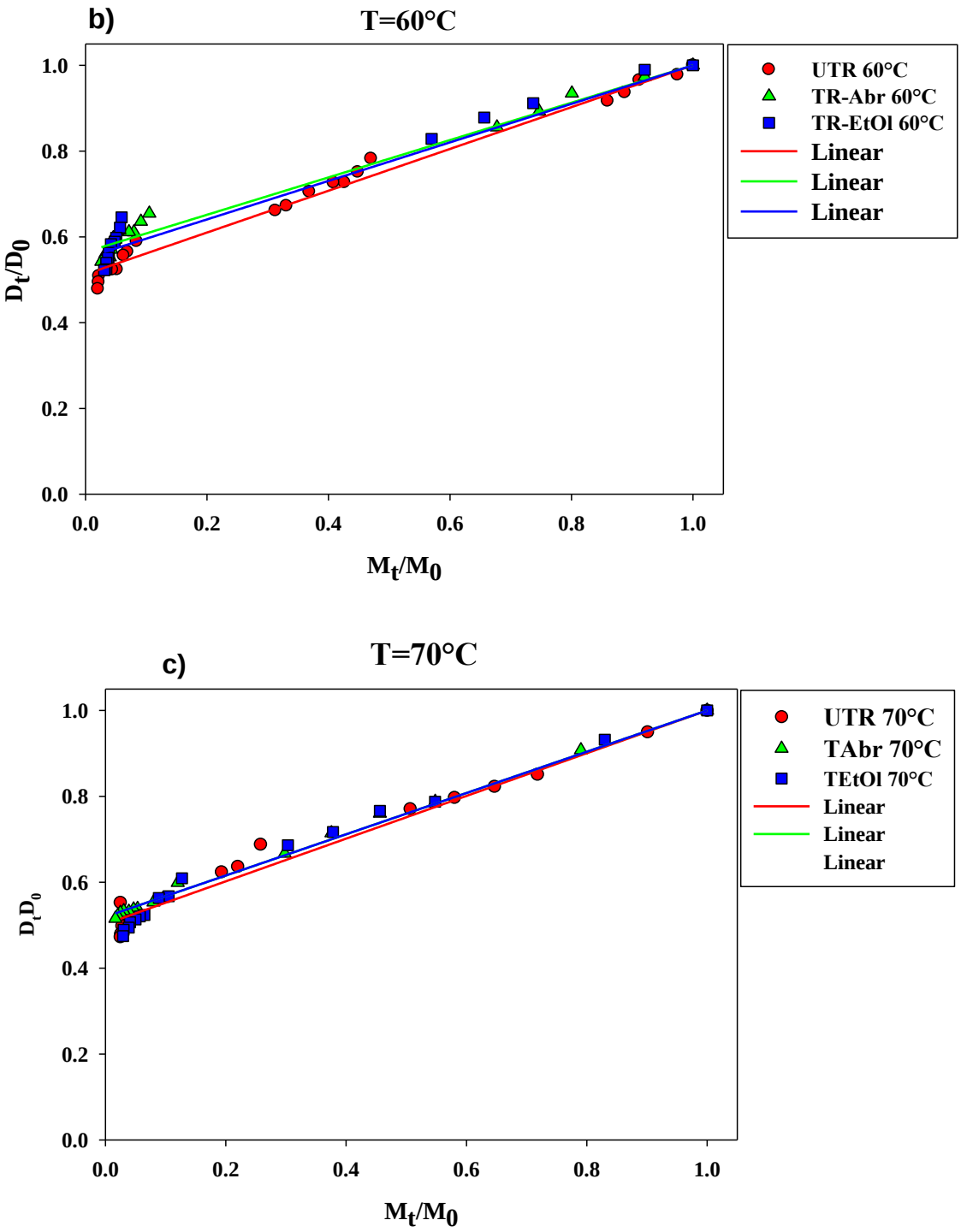

Fig. 66. *Experimental average diameter reduction D_t/D_0 vs M_t/M_0 for a) UTR, b) TR-Abr, c) TR-EtOl at 50, 60 and 70°C.*

4.4 SEM images

SEM analysis was used to estimate the peel structure of untreated, abraded and ethyl oleate grapes before drying (figure 67a-c).

Figure 67a shows the typical surface wax of untreated fresh grape. On the peel of the abraded grape the waxy layer was almost completely removed in a quite uniform way (figure 67b). As consequence of waxy solubilisation by ethyl oleate, a non uniform distribution of the waxy components on the grape surface resulted (figure 67c). After drying the surface of peel appears almost homogeneous for untreated (figure 67d) and abraded (figure 67e) raisins, while not homogeneous for ethyl oleate preteated raisins with the presence of micro-cracks (figure 67f). These results are in agreement with previous results of Vazquez et al. (1997), Riva et al. (1988), Saravacos et al. (1988). These researchers analyzing the effect of chemical pretreatments reported that micro-fissures in the grape peel were formed by using carbonate solution and ethyl oleate solution. Moreover, they concluded that the increased drying rate by chemical pretreatment was due to the formation of micropores on the surface of peel.

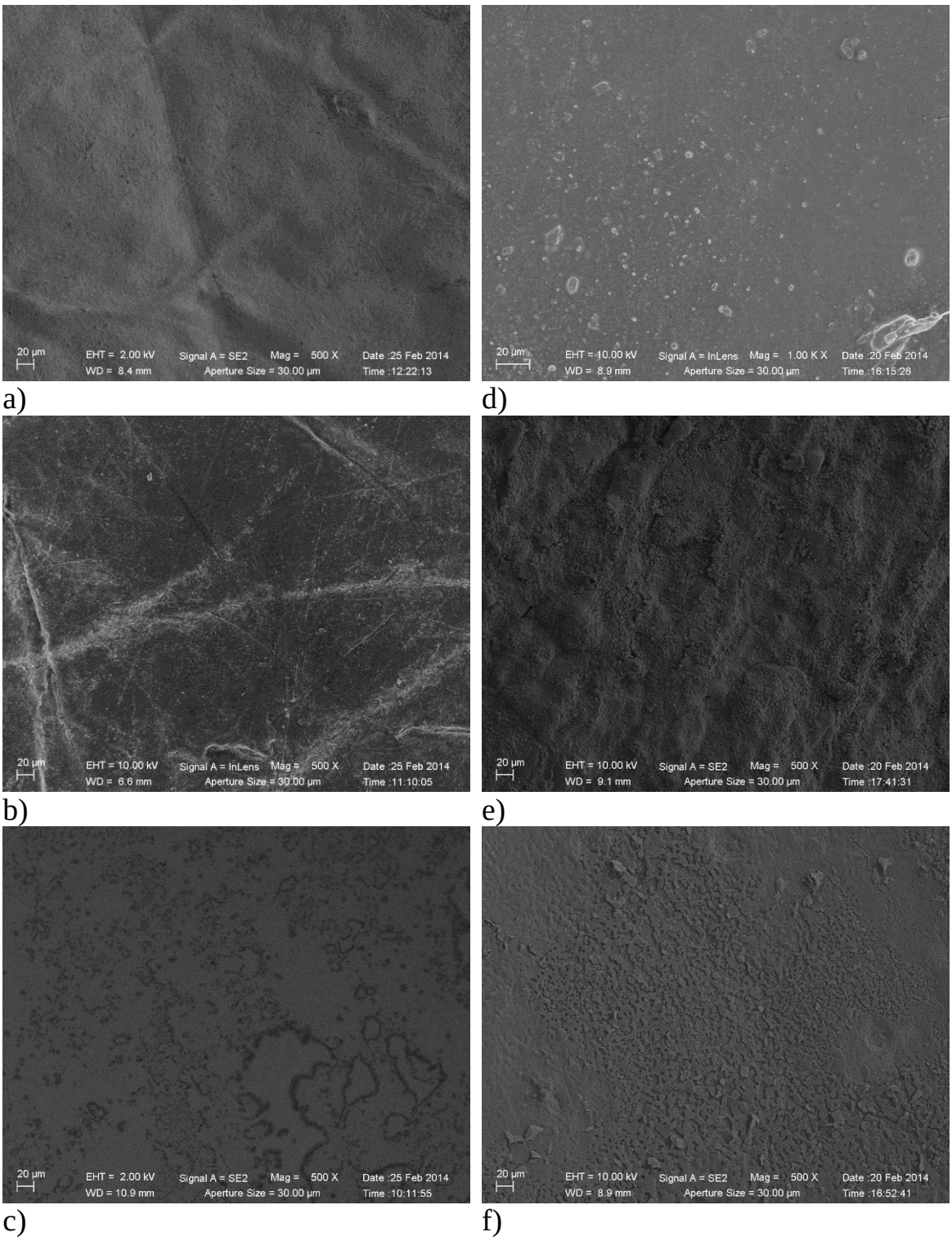

Fig. 67. *SEM images of peel for: (a) fresh untreated sample, (b) fresh abraded sample, (c) fresh sample dipped in ethyl oleate solution and for dried sample at 50 °C: (d) untreated, (e) pretreated by abrasion and (f) preteated by ethyl oleate.*

4.5 Modelling of grape drying

4.5.1 Model in cylindrical and spherical coordinate

Grape shape can be approximated to that of a cylinder or a sphere. So, first, the Fick's second law of diffusion for these two types of geometries was resolved applying the finite element method.

The equation that describes the mass diffusion phenomenon (i.e. water during drying) in cylindrical coordinates is:

$$\frac{\partial \mathrm{M}}{\partial \mathrm{t}} = \frac{1}{r}\left\{\frac{\partial}{\partial r}\left(\mathrm{r}D_{\mathrm{eff}}\frac{\partial \mathrm{M}}{\partial r}\right)+\frac{\partial}{\partial \mathrm{z}}\left(\mathrm{r}D_{\mathrm{eff}}\frac{\partial \mathrm{M}}{\partial \mathrm{z}}\right)\right\} \tag{87}$$

where D_{eff} is the diffusion coefficient (m^2/s) and M is the moisture content on a dry basis ($kg/kg_{d.b.}$).

The initial condition is:

$$\mathrm{M}\left(\mathrm{r},\mathrm{z},\mathrm{t}=0\right)=\mathrm{M}_0 \text{ for } 0<\mathrm{r}<\mathrm{R}_0,\ 0<\mathrm{z}<\mathrm{h} \tag{88}$$

The boundary conditions are:

$$\frac{\partial \mathrm{M}\left(\mathrm{r}=0,\mathrm{z},\mathrm{t}\right)}{\partial \mathrm{r}}=\frac{\partial \mathrm{M}\left(\mathrm{r},\mathrm{z}=0,\mathrm{t}\right)}{\partial \mathrm{z}}=0 \text{ for } \mathrm{t}>0 \tag{89}$$

At $r=R_0$, z=h and for t>0

$$-D_{\mathrm{eff}}\rho_{\mathrm{s}}\frac{\partial \mathrm{M}}{\partial r}=\mathrm{h}_{\mathrm{m}}\rho_{\mathrm{s}}\left(\bar{\mathrm{M}}_{\mathrm{sur}}-\bar{\mathrm{M}}_{\mathrm{e}}\right) \tag{90}$$

$$-D_{\mathrm{eff}}\rho_{\mathrm{s}}\frac{\partial \mathrm{M}}{\partial \mathrm{z}}=\mathrm{h}_{\mathrm{m}}\rho_{\mathrm{s}}\left(\bar{\mathrm{M}}_{\mathrm{sur}}-\bar{\mathrm{M}}_{\mathrm{e}}\right) \tag{90}$$

ρ_s is the solid density (kg/m^3) and it is kept constant; h_m is the moisture transfer coefficient (m/s); M_{sur} is the moisture at the surface of the cylinder and M_e is the equilibrium moisture content ($kg/kg_{d.b.}$) (i.e the moisture required to maintain equilibrium with the surrounding atmosphere).

Introducing the following dimensionless variables:

$$\bar{\mathrm{r}}=\frac{\mathrm{r}}{\mathrm{R}_0},\ \bar{\mathrm{z}}=\frac{\mathrm{z}}{\mathrm{R}_0} \text{ and } \bar{\mathrm{M}}=\frac{\mathrm{M}}{\mathrm{M}_0}\quad \bar{\mathrm{M}}_{\mathrm{e}}=\frac{\mathrm{M}_{\mathrm{e}}}{\mathrm{M}_0} \tag{91}$$

the equation (87) becomes:

$$\frac{\partial \bar{\mathrm{M}}}{\partial \tau}=\left(\frac{\partial^2 \bar{\mathrm{M}}}{\partial \bar{r}^2}\right)+\left(\frac{\partial^2 \bar{\mathrm{M}}}{\partial \bar{\mathrm{z}}^2}\right) \tag{92}$$

where τ is the dimensional time $\tau=\frac{\mathrm{t}\cdot D_{\mathrm{eff}}}{\mathrm{R}_1^2}$

Furthermore, the initial and boundary conditions become:

$$\bar{M}\left(\bar{r},\bar{z},\tau=0\right)=1 \text{ for } 0<\bar{r}<1,\ 0<\bar{z}<\frac{h}{R} \tag{93}$$

$$\frac{\partial\bar{M}\left(\bar{r}=0,\bar{z},\tau\right)}{\partial\bar{r}}=\frac{\partial\bar{M}\left(\bar{r},\bar{z}=0,\tau\right)}{\partial\bar{z}}=0 \text{ for } \tau>0 \tag{94}$$

At $\bar{r}$=1, $\bar{z}=\frac{z}{R}$, for τ>0

$$\frac{\partial\bar{M}}{\partial\bar{r}}=\text{-Sh}\left(\bar{M}_{sur}-\bar{M}_{e}\right) \tag{95}$$

$$\frac{\partial\bar{M}}{\partial\bar{z}}=\text{-Sh}\left(\bar{M}_{sur}-\bar{M}_{e}\right) \tag{96}$$

The convective mass transfer coefficient and the effective diffusion coefficient are correlated with the dimensionless Sherwood number:

$$\text{Sh}=\frac{h_m\cdot R_0}{D_{eff}} \tag{97}$$

where R_0 is the radius of the sample (m). It represents the ratio of the convective mass transfer to the rate of diffusive mass transport.

The equation in spherical coordinates is:

$$\frac{\partial M}{\partial t}=D_{eff}\left\{\frac{\partial^2 M}{\partial r^2}+\frac{2}{r}\frac{\partial M}{\partial r}\right\} \tag{98}$$

The initial condition is:

$$M\left(r,t=0\right)=M_0 \text{ for } 0<r<R_0,\ t=0 \tag{99}$$

The boundary conditions are:

$$\frac{\partial M\left(r=0,t\right)}{\partial r}=0 \text{ per } t>0 \tag{100}$$

at $r=R_0$, for $t>0$

$$-D_{eff}\rho_s\frac{\partial M}{\partial r}=h_m\rho_s\left(M_{sur}-M_e\right) \tag{101}$$

In dimensionless form the equation (98) becomes:

$$\frac{\partial\bar{M}}{\partial\tau}=\left\{\frac{\partial^2\bar{M}}{\partial\bar{r}^2}+\frac{2}{\bar{r}}\frac{\partial\bar{M}}{\partial\bar{r}}\right\} \tag{102}$$

The initial and boundary conditions in dimensionless form are:

$$\bar{M}\left(\bar{r},\bar{z},\tau=0\right)=1 \text{ for } 0<\bar{r}<1 \quad (103)$$

$$\frac{\partial\bar{M}\left(\bar{r}=0\right)}{\partial\bar{r}}=0 \text{ for } \tau>0 \quad (104)$$

At $\bar{r}$=1, for τ>0

$$\frac{\partial\bar{M}}{\partial\bar{r}}=\text{-Sh}\left(\bar{M}_{sur}-\bar{M}_{e}\right) \quad (105)$$

The finite element method is applied to solve the non-linear partial differential equations (Eq. 92 and 102) subjected to the initial and boundary conditions (Eq. 93-96 and 103-105). Simulations were run adopting 3710 cells and 5973 nodes for cylindrical geometry and 3426 cells and 5457 nodes for spherical geometry. The convergence criterion assumed at each node of the computational domain was $\left|\bar{M}^{k-1}-\bar{M}^{k}\right|\leq 10^{-8}$ (where k represents the k-th iteration).

The initial dimensions considered in the simulations, in agreement with size measurements are for cylinder: radius 14.20 mm and height 28.40 mm, for sphere radius 10.20 mm.

In figure 68 a and b, the domain considered in the simulations and the initial mesh are reported for cylindrical and spherical geometry, respectively.

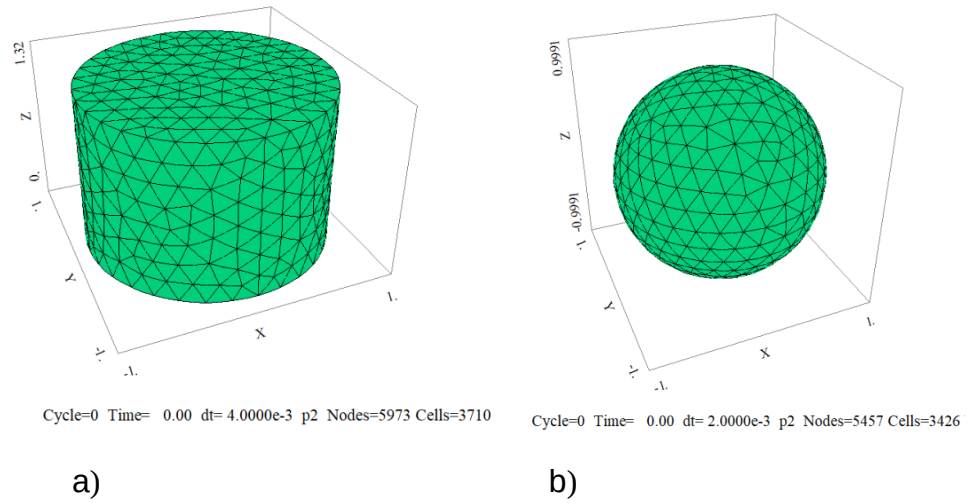

a) b)

Fig. 68. *Initial mesh for a) cylinder and b) for sphere.*

In order to determine the optimum value of the D_{eff}, the coefficient of determination of the fit (R^2), the reduced χ-square of the fit (χ^2) and the root mean square error of the fit $\left(RMSE\right)$ were used as objective functions.

4.5.2 Results of the model in cylindrical coordinate

Firstly, the effect of the model parameters, D_{eff} and h_m, on the predicted moisture ratio profile was evaluated.

As example, Figure 69 reports the results for the temperature of 50 °C for the Abraded sample. It is possible to see that by increasing D_{eff} from $1*10^{-8}$ to $1*10^{-11}$ m^2/s at constant h_m value the drying kinetics go slower, but the differences in rate are higher at D_{eff} >$1*10^{-9}$ m^2/s. Instead at fixed D_{eff}, increasing h_m from $1*10^{-8}$ to $1*10^{-5}$ m/s the rate of moisture ratio decrease is faster, but in the range $1*10^{-7}$ to $1*10^{-6}$ m/s small differences in the drying curves are observed.

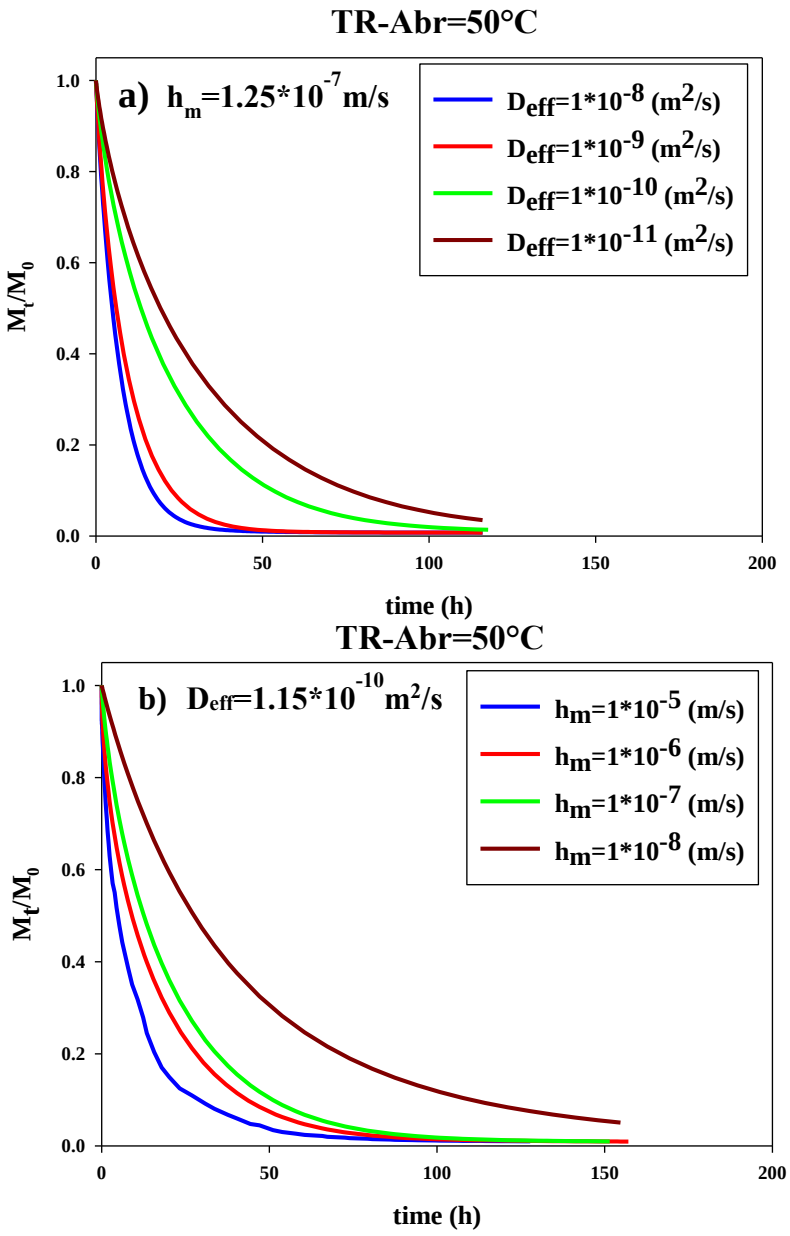

Fig. 69. *Moisture ratio during drying at fixed h_m and different value of D_{eff} (a); at fixed D_{eff} and different value of h_m (b) for TR-Abr=50°C.*

Results of the model in cylindrical coordinates (equations 92-96) are compared with experimental data in terms of moisture ratio in figure 70 (a-c) for the UTR (a), the TR-Abr (b) and TR-EtOl sample (c).

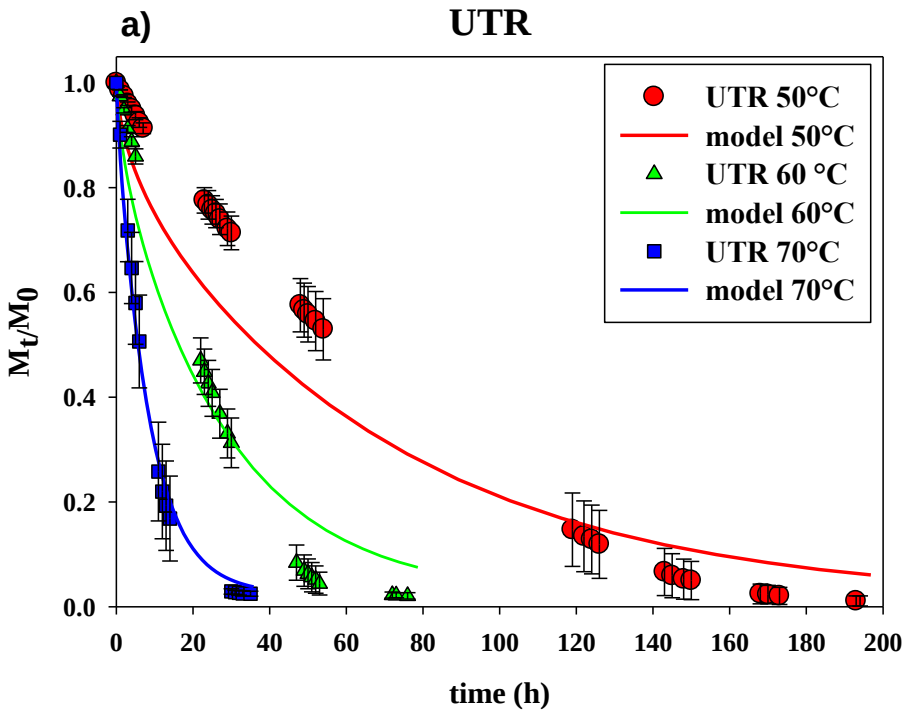

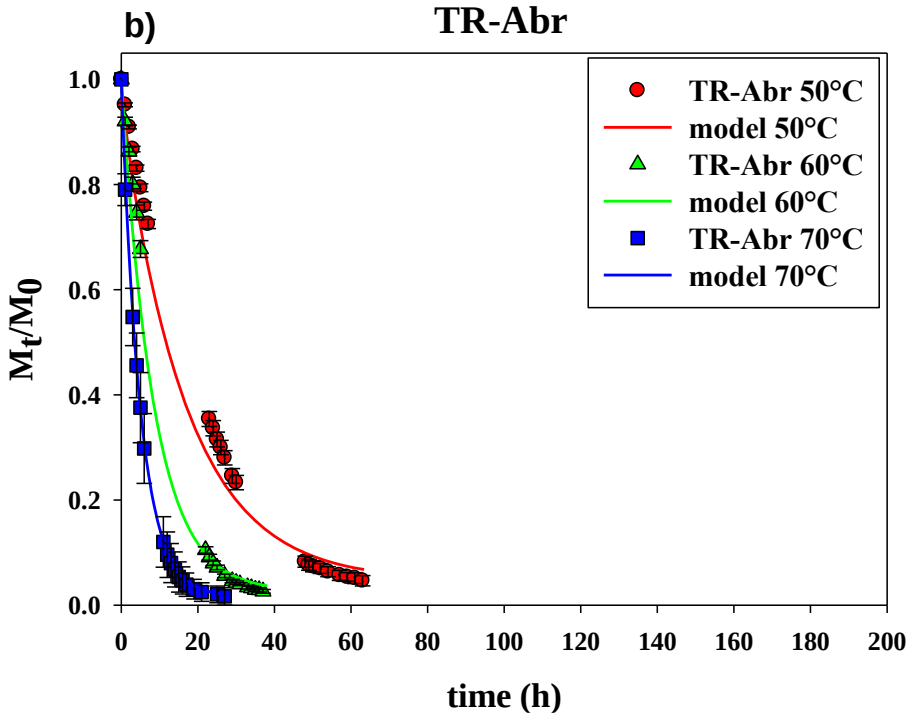

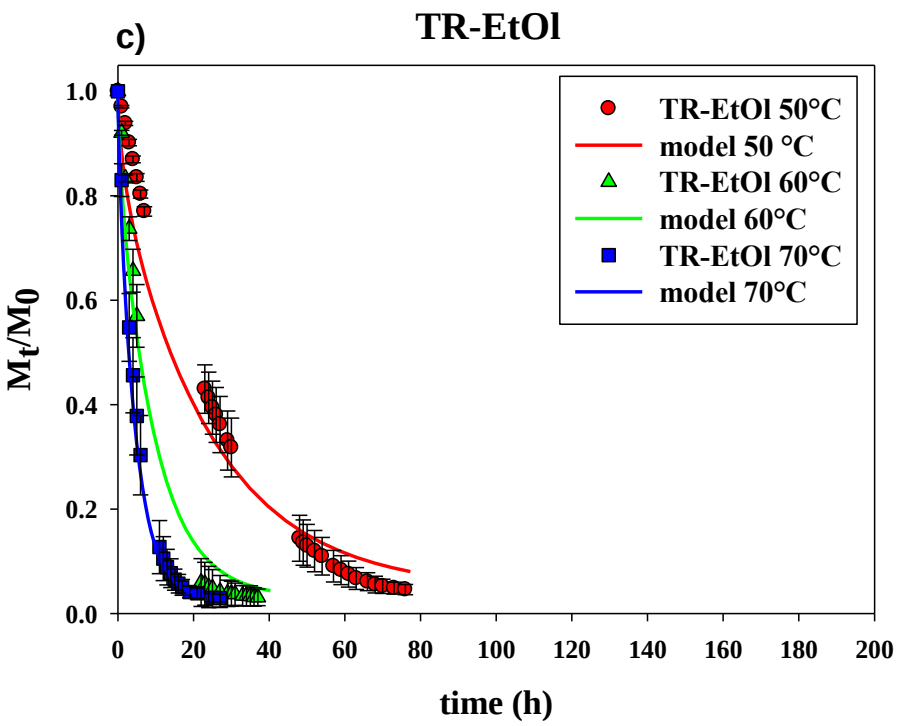

Fig. 70. *Experimental and predicted moisture ratio for cylindrical shape for a) untreated, b) pretreated TR-Abr, c) pretreated TR-EtOl at 50, 60 and 70°C.*

The results show that developed model in cylindrical coordinates is not able to well describe the experimental drying kinetics in the range of temperatures investigated, especially for the untreated samples. A better fitting is obtained for treated samples.

Table 16 reports the values of the D_{eff} and h_m estimated by the model and table 17 the corresponding values of fitting parameters. The values of the effective diffusion coefficient D_{eff} are in agreement with those reported in literature (Simal et al., 1998; Esmaiili et al., 2007 and Di Matteo et al., 2002).

	Temperature		
UTR	**50 °C**	**60 °C**	**70°C**
Sh	28.00	10.50	1.83
D_{eff} **(m²/s)**	3.38×10^{-10}	9.00×10^{-10}	5.17×10^{-9}
h_m **(m/s)**	8.80×10^{-7}	8.80×10^{-7}	8.80×10^{-7}
	Temperature		
TR Abr	**50 °C**	**60 °C**	**70°C**
Sh	0.260	0.064	0.0350
D_{eff} **(m²/s)**	1.1×10^{-8}	5.0×10^{-8}	9.0×10^{-8}

h_m (m/s)	3.0 x 10^{-7}	3.0 x 10^{-7}	3.0 x 10^{-7}
	Temperature		
TR EtOl	**50 °C**	**60 °C**	**70°C**
Sh	28.00	10.00	3.79
D_{eff} (m^2/s)	9.60 x 10^{-10}	2.69 x 10^{-9}	7.09 x 10^{-9}
h_m (m/s)	2.50 x 10^{-6}	2.50 x 10^{-6}	2.50 x 10^{-6}

Table 16 *Parameters estimated by the model in cylindrical coordinate.*

	Temperature		
UTR	**50 °C**	**60 °C**	**70°C**
R^2	0.979	0.985	0.994
χ-square	2.898 x 10^{-1}	1.644 x 10^{-1}	1.382 x 10^{-2}
RMSE	4.528 x 10^{-3}	4.110 x 10^{-3}	8.232 x 10^{-2}
	Temperature		
TR Abr	**50 °C**	**60 °C**	**70°C**
R^2	0.990	0.991	0.999
χ-square	6.887x10^{-2}	4.329 x10^{-2}	9.122 x 10^{-2}
RMSE	1.497 x10^{-3}	1.273 x10^{-3}	2.851 x 10^{-5}
	Temperature		
TR EtOl	**50 °C**	**60 °C**	**70°C**
R^2	0.990	0.990	0.994
χ-square	1.356 x 10^{-2}	5.764 x 10^{-2}	2.121 x 10^{-1}
RMSE	2.422 x 10^{-3}	1.601 x 10^{-3}	6.629 x 10^{-4}

Table 17 *Fitting parameters obtained by comparison with experimental data for cylindrical geometry.*

Results of the model in terms of D_{eff} and h_m show for the abrasion pretreatment a higher value of D_{eff}. Instead for the ethyl oleate pretreatment the effective diffusion coefficient is more similar to the untreated sample. This behavior can be explained by considering that in the case of abrasion pretreatment the moisture transfer occurs only through the pulp while for untreated samples through both pulp and peel. The effect of ethyl oleate pretreatment is to increase the moisture transfer coefficient by dissolving part of the wax on the surface peel.

4.5.3 Results of the model in spherical coordinates

Results of the model in spherical coordinates are compared with experimental moisture ratio in figure 71. Table 18 reports the values of the D_{eff} and h_m estimated by the model; table 19 reports the calculated value of fitting parameters.

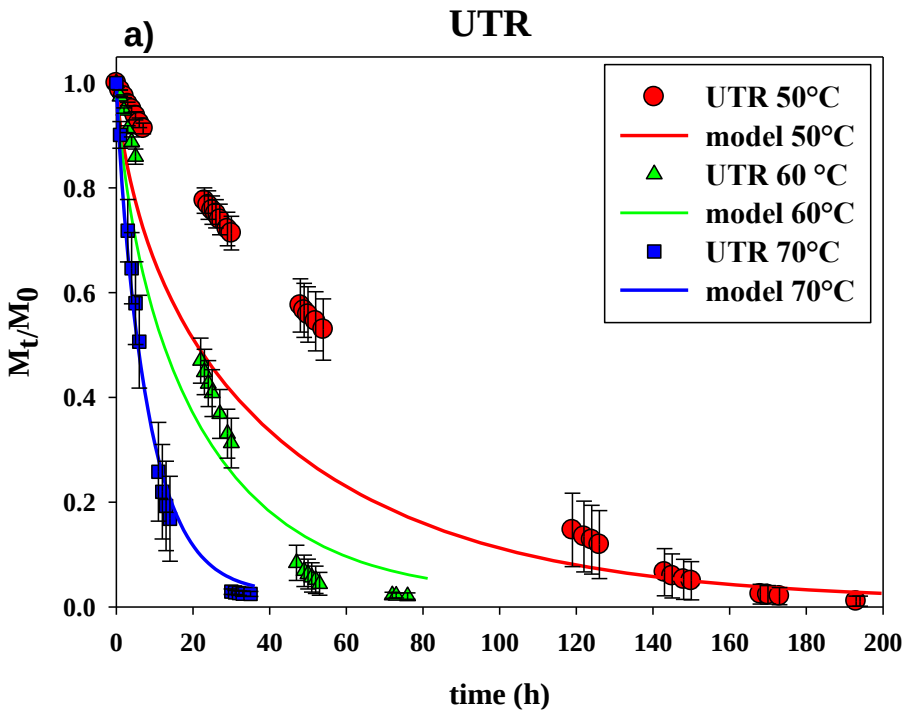

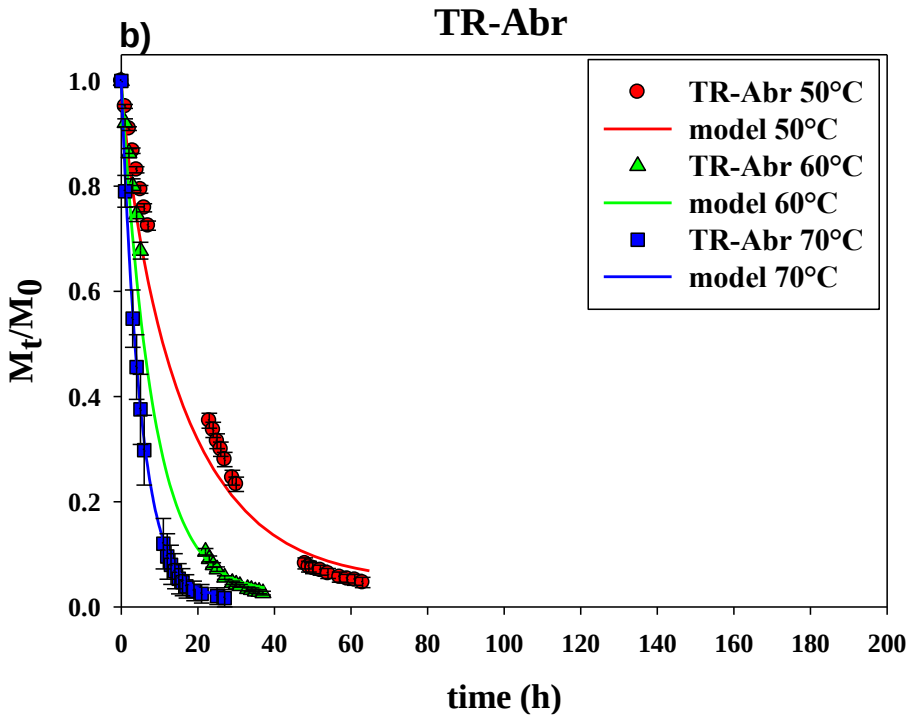

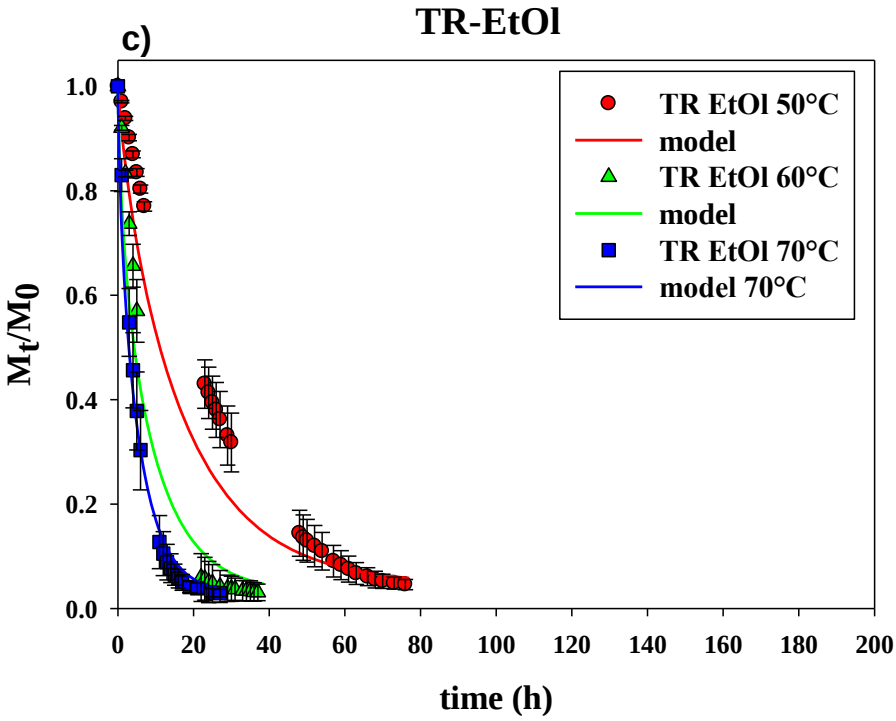

Fig. 71. *Experimental and predicted moisture ratio for spherical shape for a) untreated, b) pretreated TR-Abr, c) pretreated TR-EtOl at 50, 60 and 70°C.*

	Temperature		
UTR	**50 °C**	**60 °C**	**70°C**
Sh	28.00	12.00	3.00
D_{eff} **(m²/s)**	0.80×10^{-10}	1.80×10^{-10}	6.0×10^{-10}
h_m **(m/s)**	1.80×10^{-7}	1.80×10^{-7}	1.80×10^{-7}
	Temperature		
TR Abr	**50 °C**	**60 °C**	**70°C**
Sh	0.85	0.12	0.02
D_{eff} **(m²/s)**	1.13×10^{-8}	1.59×10^{-8}	6.75×10^{-8}
h_m **(m/s)**	1.25×10^{-7}	1.25×10^{-7}	1.25×10^{-7}
	Temperature		
TR EtOl	**50 °C**	**60 °C**	**70°C**
Sh	14.00	7.5	0.75
D_{eff} **(m²/s)**	1.38×10^{-10}	2.51×10^{-10}	2.52×10^{-9}
h_m **(m/s)**	1.75×10^{-7}	1.75×10^{-7}	1.75×10^{-7}

Table 18 *Parameters estimated by the model in spherical coordinate.*

	Temperature		
UTR	**50 °C**	**60 °C**	**70°C**
R^2	0.939	0.970	0.994
χ-square	1.280	1.696×10^{-1}	1.523×10^{-2}
RMSE	1.999×10^{-2}	4.239×10^{-3}	8.195×10^{-2}
	Temperature		
TR Abr	**50 °C**	**60 °C**	**70°C**
R^2	0.987	0.991	0.993
χ-square	9.065×10^{-2}	4.329×10^{-2}	2.748×10^{-3}
RMSE	1.971×10^{-3}	1.273×10^{-3}	8.586×10^{-5}
	Temperature		
TR EtOl	**50 °C**	**60 °C**	**70°C**
R^2	0.975	0.979	0.990
χ-square	2.304×10^{-1}	1.197×10^{-1}	2.150×10^{-2}
RMSE	4.115×10^{-3}	3.324×10^{-3}	6.719×10^{-4}

Table 19 *Fitting parameters obtained by comparison with kinetics data for spherical geometry.*

D_{eff} values estimated by the model for spherical geometry are similar to those for cylindrical one. The differences of $D_{eff\ values}$ between the samples were the same as observed for cylindrical geometry.

4.5.4 Results of the model with shrinkage

In order to take into account the effect of shrinkage, a law of variation of the sample size was adopted in the model of spherical geometry. The law of size reduction (i.e. D_t/D_0) for untreated and treated samples is expressed by an exponential decay law, equation (105), with correlation parameters and coefficient of determination (R^2) reported in table 20.

$$\frac{D_t}{D_0} = y_0 + a \cdot \exp(-b \cdot \tau) \qquad (105)$$

	Temperature		
UTR	**50 °C**	**60 °C**	**70 °C**
y_0	0.465	0.377	0.470
a	0.535	0.623	0.530
b	70.582	15.126	6.705
R^2	0.990	0.990	0.993
	Temperature		
TR-Abr	**50 °C**	**60 °C**	**70 °C**
y_0	0.544	0.371	0.508
a	0.456	0.629	0.492
b	5.211	9.015	16.789
R^2	0.988	0.994	0.996
	Temperature		
TR-EtOl	**50 °C**	**60 °C**	**70 °C**
y_0	0.4599	0.0320	0.4731
a	0.5342	0.0281	0.5209
b	12.9490	3.8202	54.2008
R^2	0.991	0.990	0.993

Table 20 *Model parameters and fitting parameters for model with shrinkage.*

Using these conditions, the size of sample is adjusted at each time step during the calculation of the mass governing equation and an adaptive grid was used for simulations. As an example, in Figure 72 the domain evolution is reported for the TR-EtOl al 50 °C.

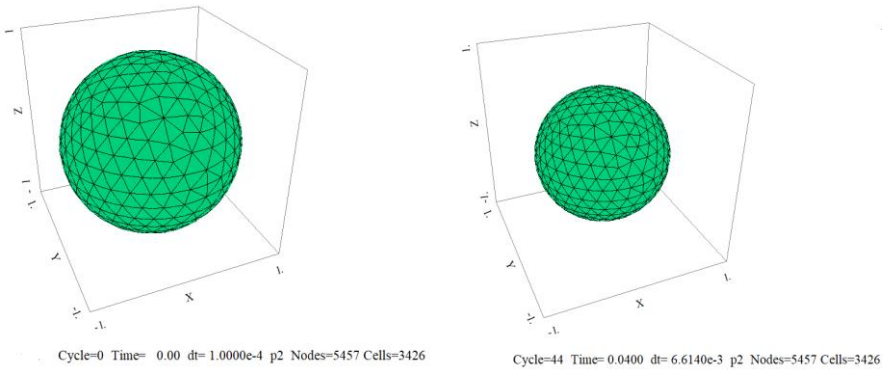

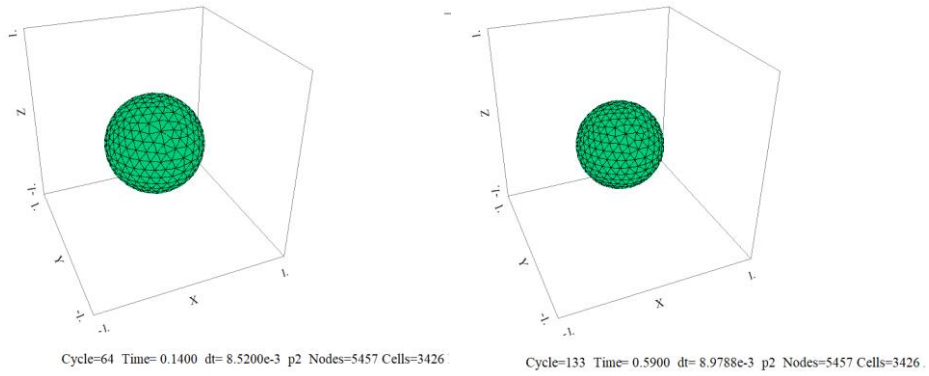

Fig. 72. *Evolution of the domain volume for spherical geometry during simulation, TR-EtOl, T=50°C.*

The comparison between results of model with shrinkage with experimental moisture ratio data is shown in figure 73. Table 21 reports the estimated values of the D_{eff} and h_m; table 22 reports the calculated values of statistical parameters.

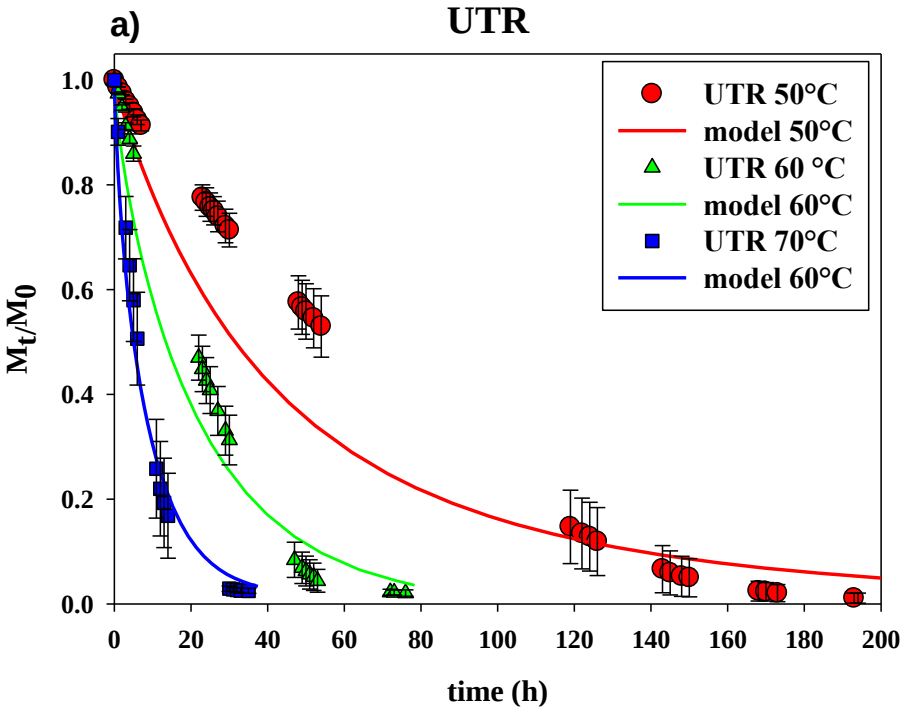

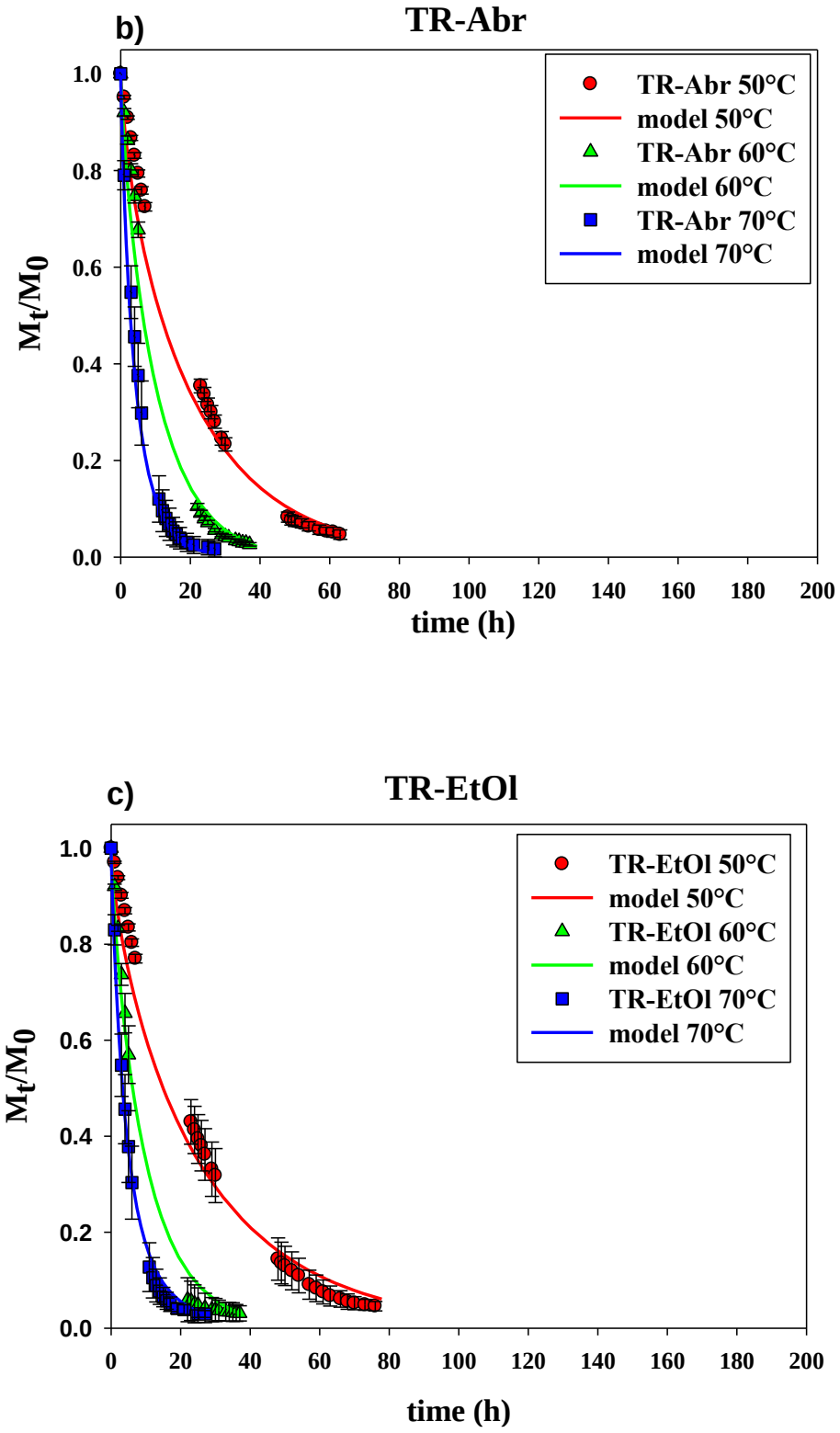

Fig. 73. *Experimental and predicted moisture for spherical shape with shrinkage for a) untreated, b) pretreated TR-Abr, c) pretreated TR-EtOl at 50, 60 and 70°C.*

	Temperature		
UTR	**50 °C**	**60 °C**	**70°C**
Sh	72.00	38.00	4.800
D_{eff} **(m²/s)**	1.48×10^{-11}	4.66×10^{-11}	4.13×10^{-10}
h_m **(m/s)**	1.80×10^{-7}	1.80×10^{-7}	1.80×10^{-7}
	Temperature		
TR Abr	**50 °C**	**60 °C**	**70°C**
Sh	18.50	14.00	7.00
$\underline{D}_{eff}$ **(m²/s)**	1.15×10^{-10}	1.52×10^{-10}	2.83×10^{-10}
h_m **(m/s)**	1.25×10^{-7}	1.25×10^{-7}	1.25×10^{-7}
	Temperature		
TR EtOl	**50 °C**	**60 °C**	**70°C**
Sh	42.91	25.81	21.39
D_{eff} **(m²/s)**	4.80×10^{-11}	6.83×10^{-11}	9.00×10^{-11}
h_m **(m/s)**	1.75×10^{-7}	1.75×10^{-7}	1.75×10^{-7}

Table 21 *Parameters estimated by the model in spherical coordinates considering shrinkage.*

	Temperature		
UTR	**50 °C**	**60 °C**	**70°C**
R^2	0.943	0.978	0.985
χ-square	4.307×10^{-1}	1.32×10^{-1}	5.69×10^{-1}
RMSE	6.730×10^{-3}	3.301×10^{-3}	6.990×10^{-3}
	Temperature		
TR Abr	**50 °C**	**60 °C**	**70°C**
R^2	0.993	0.992	0.993
χ-square	5.82×10^{-2}	4.90×10^{-2}	2.18×10^{-2}
RMSE	1.26×10^{-3}	1.44×10^{-3}	6.83×10^{-4}
	Temperature		
TR EtOl	**50 °C**	**60 °C**	**70°C**
R^2	0.994	0.995	0.996
χ-square	7.49×10^{-2}	2.27×10^{-2}	1.02×10^{-2}
RMSE	1.33×10^{-3}	6.32×10^{-4}	3.20×10^{-4}

Table 22 *Fitting parameters obtained by comparison with kinetics data for the model in spherical coordinate considering shrinkage.*

The values of the effective diffusion coefficient estimated by the model considering shrinkage range for UTR from $1.48*10^{-11}$ to $4.13*10^{-10}$ m^2/s in the range of temperature 50-70 °C, for TR-Abr from $1.15*10^{-10}$ to $2.83*10^{-10}$ m^2/s and for TR-EtOl from $4.80*10^{-11}$ to $9.00*10^{-11}$ m^2/s. These values are significantly lower than those estimated by the model without shrinkage, in particular for pretreated samples the decrease was of one order of magnitude for ethyl oleate pretreatment and two order of magnitude for abrasion.

Moreover, the model with shrinkage better describe the experimental M_t/M_0 data, as shown by the fitting parameters reported in table 22.

4.6 Conclusions

The effect of abrasive pretreatment and chemical pretreatment in alkaline ethyl oleate solution on drying rate of grapes was studied. For grapes obtained by abrasion method and with ethyl oleate solution shorter drying times (up to 1/3) than untreated samples were observed.

Furthermore, peel abrasion allows safer raisins production without the use of chemical additive.

SEM images showed the presence of micro-cracks on the peel surface of ethyl oleate pretreated raisins which are not evident for those untreated and pretreated with abrasion.

Then, the diffusion model developed including the effect of shrinkage better describe the drying process of grape. A very good agreement between experimental and theoretical data of moisture ratio during drying was found. The estimated values of the effective diffusion coefficient, ranging from $1.15*10^{-10}$ to $9.00*10^{-11}$ m^2/s in the range of temperatures 50-70°C, were in agreement with those reported in literature for grapes in similar drying conditions.

CHAPTER 5

Conclusions and future work

In this thesis, hot air drying was applied to fruits, such as pear and grape, which are characterized by high initial moisture levels and by cellular internal structure. The drying kinetics of the samples and their volume were measured during drying. Pear and grape samples were also characterized before and after drying by SEM and NMR analyses.

The distribution of transverse relaxation times for pear exhibited three components assigned to different compartments in pear tissue, namely cell walls, cytoplasm and extra-cellular space, and vacuole. However, most of water lost during drying was removed from the vacuolar compartment (77%), and the rate of water loss from vacuole slightly increased increasing the drying temperature. The net decrease of water in vacuole under drying suggested that this compartment may undergo shrinkage during drying. Due to the concomitant reduction of vacuolar water and, consequently, to the increase of sugars concentration it was observed a reduction of the self-diffusion coefficient.

Since from an industrial point of view the first goal is to achieve a precise control of the product moisture content at the end of the drying process, a mathematical model for pear drying was developed.

A diffusion model with Fickian moisture transfer coupled with an empirical law which considers the effect of shrinkage, was adopted to obtain a detailed prediction of moisture distribution during drying. A numerical solution technique, based on the finite element method , was used with an adaptive mesh.

The model results in terms of moisture ratio vs time match well with the experimental results. The model also well predicts the moisture profile along the pear thickness especially at first stages of drying (<15 h), when the sugar gradients inside the pear are smaller. The estimated value of the effective diffusion coefficient ranges from $0.84*10^{-10}$ to $3*10^{-10}$ m^2/s in the range of temperatures 45-55 °C. These results are in agreement with those reported in literature.

For grape, the effect of abrasive and chemical pretreatments on drying rate was studied. Both pretreatments determine shorter drying time (up to 1/3) than untreated samples, but peel abrasion allows safer raisins production with no use of chemical additives.

The diffusion model was developed both in spherical and cylindrical geometry. The one in spherical geometry better describes experimental results.

The values of the effective diffusion coefficient estimated by the model considering shrinkage range from $1.48*10^{-11}$ to $4.13*10^{-10}$ m^2/s for untreated grape sample in the range

of temperature 50-70 °C, from $1.15*10^{-10}$ to $2.83*10^{-10}$ m^2/s for abraded sample and from $4.80*10^{-11}$ to $9.00*10^{-11}$ m^2/s for chemical pretreated sample. These values are significantly lower than those estimated by the model without shrinkage, in particular for pretreated samples the decrease was of one order of magnitude for ethyl oleate pretreatment and two order of magnitude for abrasion.

According to this study, the shrinkage effect must not be neglected in moisture diffusivity determination for highly shrinking materials like fruit and vegetables; in fact the shrinkage implies diffusion path reduction. If the extension of shrinkage during the drying is controlled, quality of the dehydrated product can be improved. For this purpose a good knowledge of the shrinkage mechanism and the influence of process variables on shrinkage are needed.

Moreover, when porosity formation occurs during dying process, it should be included in the model to take into account that phenomenon. This porosity formation can change during the process conditions, and its inclusion in the models allows taking into account the influence of process conditions on shrinkage.

Since food are hierarchically structured, but at the fine scale are usually not modelled explicitly, detailed insight into the process at the microscale is lost. Multiscale modelling is a new area in food engineering, and the literature is relatively scarse. Multiscale models are essentially a hierarchy of sub-models which describe the material behaviour at different spatial scales in such way that the sub-models are interconnected.

A first step in multiscale modelling is often to visualize the structure of food at multiple scales and to construct a geometric model that can be used for further analyses. Methods as x-ray tomography and magnetic resonance imaging can provide 3-D images of foods that can be converted to solid models appropriate for numerical discretization of multiphysics models.

References

Abbaszadeh, A., Montevali, A., Ghobadian, B., Khoshtaghaza, M., A., Minaei, S., 2012. Effect of air velocity and effective moisture diffusivity for Russian Olive (Elaeagnusan gastifolial L.) in thin-layer drying. Iran J. Chem. Eng. Vol. 31, No 1.

Adiletta, G., Russo, P., Senadeera, W., Di Matteo, M, 2016. Drying characteristics and quality of grapes under physical pretreatment. Journal of Food Engineering, 172, 9-18.

Adiletta, G., Russo, P., Proietti, N., Capitani, D., Mannina, L., Crescitelli, A., Di Matteo M., 2015. Characterization of Pears During Drying by Conventional Technique and Portable non Invasive NMR. Chem. Eng. Trans. 44, 151-156.

Adiletta, G., Iannone, G., Russo, P., Patimo, G., De Pasquale, S., Di Matteo, M., 2014. Moisture migration by magnetic resonance imaging during eggplant drying: a preliminary study. Journal pf Food Science and Technology, 49, 2602-2609.

Akpinar, E., K., Toraman, S., 2013. Estimation of the moisture diffusivity and activation energy in thin layer drying of ginger slices. International Journal of Biological and Biomulecular, Agricultural and Biotechnological Engineering, vol 7, No 6.

Aprajeeta, J., Gopirajah, R., Anandharamakrishnan, C., 2015. Shrinkage and porosity effect on heat and mass transfer during potato drying. Journal of Food Engineering, 144, 119-128.

Bacelos, M., S., Almeida, P., I., F., 2011. Modelling of drying kinetic of potatoes taking into account shrinkage. Procedia Food Science 1, 713-721.

Brasiello, A., Iannone, G., Adiletta, G., De Pasquale, S., Russo, P., Di Matteo, M., 2017. Mathematical model for dehydration and shrinkage: Prediction of eggplant's MRI spatial profiles. Journal of Food Engineering, 203, 1-5.

Brasiello, A, Adiletta, G., Russo, P., Crescitelli, S., Albanese, D., Di Matteo, M, 2013. Mathematical modeling of eggplant drying: Shrinkage effect. Journal of Food Engineering, 114, 99-105.

Capitani, D., Sobolev, A.P., Delfini, M., Vista., S., Antiochia, R., Proietti, N., Bubici, S., Ferrante, G., Carradori, S., De Salvador, F.R., Mannina, L., (2014). NMR methodologies in the analysis of blueberries. Electrophoresis, 35, 1615-1626.

Capitani, D., Mannina, L., Proietti, N., Sobolev, A.P., Tommasini, A., Di Cocco, M.E., Capuani, G., De Salvador, F.R., Delfini, M., (2013). Metabolic profiling and outer pericarp water state in Zespri, CIGI, and Hayward Kiwifruits. JAFC., 61, 1727-1740.

Capitani, D., Mannina, L., Proietti, N., Sobolev, A.P., Tomassini, A., Miccheli, A., Di Cocco, M.E., Capuani, G., De Salvador, F.R., (2010). Monitoring of metabolic profiling and water status of Hayward kiwifruit by nuclear magnetic resonance. Talana, 82, 1826, 1838.

Casanova, F., Perlo, J., 2011. NMR in Inhomogeneous Field, in Single-Sided NMR (Eds: F. Casanova, J. Perlo, B. Blümich), Springer-Verlag, Berlin, p 11-56.

Ceylan, I., Aktas, M., Dogan, A., 2007. Mathematical modelling of drying characteristics of tropical fruits. Applied Thermal Engineering, 27, 1931-1936.

Chemkhi, S., Zagrouba, F., Bellagi, A. (2004). Mathematical model for drying of highly shrinkable media. Drying Technology, 22, 1023–1039.

Crank, J., 1975.The Mathematics of diffusion, second edition. Clarendon Press, Oxford.

Cinquanta, L., Di Matteo, M., Estia, M., 2002. Physical pre-treatment of plums (Prunus domestica). Part 2. Effect on the quality characteristics of different prune cultivars. Food Chem. 79, 233e238.

Datta, A. K. 2007a. Porous media approaches to studying simultaneous heat and mass transfer in food processes. I: Problem Formulations. Journal of food engineering, 80, 80-95.

Datta, A. K. 2007b. Porous media approaches to studying simultaneous heat and mass transfer in food processes. II: Property data and representative results. Journal of Food Engineering, 80, 96-110.

Devahastin, S., Niamnuy, C., 2010. Modelling quality of fruits and vegetables during drying: a review. Journal of Food Science and Technology , 45, 1755-1767.

Di Matteo, M., Cinquanta, L., Galiero, G., Crescitelli, S., 2002. Physical pre-treatment of plums (Prumus Domestica). Part 1 Modelling the kinetics of drying. Food Chemistry 79, 227-232.

Di Matteo, M., Cinquanta, L., Galiero, G., Crescitelli, S., 2000. Effect of a novel physical pretreatment process on the drying kinetics of seedless grape. Journal of Food Engineering, 46, 83-89.

Doymaz, I., Ismail., O., 2012. Experimental Characterization and modelling of drying of pear slices. Food Sci. Biotechnol. 21, 1377-1381.

Doymaz, I, 2005. Drying characteristics and kinetics of okra. J. Food Eng. 69, 275 e 279.

Doymaz, I., 2004. Effect of dipping treatment on air drying of plums. J. Food Eng. 64 (4), 465e470.

Doymaz, I, 2003. Convective air drying characteristics of a thin layer carrots. Journal of Food Engineering, 61, 359-654.

Duval, F., P., Cambert, M., Mariette, F., 2005. NMR study of tomato pericarp tissue by spin-spin relaxation and water self-diffusion. Applied Magnetic Resonance 28:29.

Esmaii, M., Sotudeh-Gharebagh, R., Mousavi, M. A. E., Rezazadeh, G., 2007. Influence of dipping on thin-layer drying characteristics of seedless grapes. Biosystems engineering 98, 411-421.

Fanta, S.W., Abera, M.K., Ho, Q.T., Verboven, P., Carmeliet, J., Nicolai, B.M., 2013. Microscale modeling of water transport in fruit tissue. J. Food Eng. 118, 229-237.

Farrar, T.C., Becker, E.D., 1971. Pulse and Fourier transform NMR, Academic Press, New York.

Guinè, R., P., F., Barroca, M., J., 2013. Estimation of the diffusivities and mass transfer coefficients for the drying of D. Joaquina pears. Worls Congress on Engineering, July 3-5 London.

Guinè, R., F., 2008. Pear drying: Experimental validation of a mathematical prediction model. Food and Bioproducts processing, 86, 248-256.

Guinè, R. P. F., Rodrigues, A. E., Figueiredo, M. M., 2007a. Modelling and simulation of pear drying. Applied Mathematics and Computation 192, 69-77.

Guiné, Raquel P. F., Castro José Almiro A. M., 2007b. Analysis of moisture content and density of pear during drying. Drying Technology: An International Journal, 21:3, 581-591.

Guinè, R. P. F., Ramos, M. A., Figueredo, M., 2007c. Shrinkage characteristics and Porosiy of Pear during Drying. Drying Technology: An International Journal, 24:11, 1525-1530.

Guiné, R., P., F., Ferreira D. M. S., Barroca M. J., Gonçalves, F. M., 2007d. Study of the drying kinetics of solar-dried pears. Biosystems engineerin, 98, 422-429

Guinè, R. P. F., 2006. Moisture diffusivity in pears: experimental determination and derivation of a mathematical prediction model. International Journal of Food Science and Technology, 41, 1177-1781.

Hassini, H., Azzouz, S., Peczalski, R., Belghith, A., 2007. Estimation of potato moisture diffusivity from convective kinetics with crrection for shrinkage. Journal of Food Engineering, 79, 47-56.

Henderson, S.M., 1974. Progress in developing the thin layer drying equation. Trans. ASAE 17, 1167e1168.

Henderon, S. M, Pabis, S., 1961. Grain drying theory I: temperature effect on drying coefficient. J. Agric Eng. Res 6, 169 -174.

Hernàndez, J., A., Pavòn, G., Garcìa, M., A., 2000. Analytical solution of mass transfer equation considering shrinkage for modelling food-drying kinetics. Journal of Food Engineering, 45, 1-10.

Hills BP, Nott KP *(*1999*)* NMR studies of water compartmentation in carrot parenchyma tissue during drying and freezing. *Appl Magn Reson* 17*:* 521–535.

Hills, B.P., Remigereau, B., 1997. NMR studies of water compartmentation in carrot parenchyma tissue during drying and freezying. Appl. Magn. Reson. 17, 521-535.

Karunasena, H. C. P., Gu, Y. T., Brown, R. J., Senadeera, W., 2015. Numerical investigation of plant tissue porosity and its influence on cellular level shrinkage during drying Biosystems Engineering, 132, 71-87.

Kashaninejad, M., Tabil, L.G., 2004. Drying characteristics of purslane (Portulaca oleraceae L.). Drying Technol. 22, 2183-2200.

Khan, M.I.H., Wellard, R.M., Nagy, S.A., Joarder, M.U.H., Karim, M.A., 2016. Investigation of bound and free water in plant based food material using NMR T_2 relaxometry. Innov. Food Sci. Emerg. 38, 252-261.

Kiranoudis, C., T., Tsami, E., Maroulis, Z., B., Marions-Kouris, D., 2007. Drying Technology: An International Journal, 15:5, 1399-1418.

Kiranoudis, C., T., Maroulis, Z., B., Marions-Kouris, D., 1995. Heat and mass transfer model building in drying with multiresponse data. International Journal of heat and mass transfer, 38, 463-480.

Krokida, M. K., & Maroulis, Z. B. (1997). Effect of drying method on shrinkage and porosity. Drying Technology, 15, 2441–2458.

Madiouli, J., Lecomte, D., Nganya, T., Chavez, S., Sghaier, J., & Sammouda, H. (2007). A method for determination of porosity change from shrinkage curves of deformable

Marigheto, N., Moates, G., K., Furfaro, M., E., Waldron, K., W., Hills, B., P., (2009). Characterisation of ripening and pressure-induced changes in tomato pericarp using NMR relaxtrometry. Appl. Magn. Reson. 36:35.

Maringheto, N., Venturi, L., Hills, B., 2008. Two-dimensional NMR relaxation studies of apple quality. Postharvest Biology and Technology 48, 331-340.

Mayor, L., Sereno, A., M., 2004. Modelling shrinkage during convective drying of food materials: a review. Journal of Food Engineering, 61, 373-386.

Mohammadi, A., Rafiea, S., Keyhani, A, Emam-Djomeh, Z., Jafary, A., 2008. Measuring moisture diffusivity and activation energy of kiwifruit (cv. Hayaward) during convective hot air drying. 10th International Congress on Mechanization and Energy in Agriculture, 14-17 October, Antalya-Turkie.

Moreira, R., Figueiredo, A., & Sereno, A. (2000). Shrinkage of apple disks during drying by warm air convection and freeze drying. Drying Technology, 18, 279–294**.**

Mulet, A., Garcia-Reverter, J., Bon, J., & Berna, A. (2000). Effect of shape on potato and cauliflower shrinkage during drying. Drying Technology, 18, 1201–1219.

Musse, M., Cambert, M., Mariette, F., 2010. NMR Study of Water Distribution inside Tomato Cells: Effects of Water Stress. Appl. Magn. Reson. 38 (4), 455–469.

Nguyen, Minh-Hue, 2007. Air-drying of banana: influence of experimental parameters, slab thickness, banana maturity and harvesting season. Journal of Food Engineering, 79, 200-207.

Nguyen, T., A., Verboven, P., Scheerlink, N., Vanderwalle, S., Nicolai, B., M., 2006. Estimation of effective diffusivity of pear tissue and cuticle by means of a numerical water diffusion model. Journal of Food Engineering, 72, 63-72.

Ochoa, M. R., Kesseler, A. G., Pirone, B. N., Marquez, C. A., & De Michelis, A. (2002). Volume and area shrinkage of whole sour cherry fruits (Prunus cerasus) during dehydration. Drying Technology, 20, 147–156.

Panarese, V., Laghi, L., Pisi, A., Tylewict, U., Dalla Rosa, M., Rocculi, P., 2012, Effect of osmotic dehydration on *Actinidia deliciosa* kiwifruit: a combined NMR and ultrastructural study. Food Chem., 132, 1706−1712.

Pangavhane, D.R., Sawhney, R.L., 2002. Review of research and development work on solar dryers for grape drying. Energy Convers. Manage. 43, 45e61.

Park, K.J., Bin, A., Brod, F.P.R., 2002. Drying of pear d'Anjou with and without osmotic dehydration. J. Food Eng. 56, 97-103.

Park, K. J., Vohnikova, Z., Brod, F. P. R., 2002. Evaluation of drying parameters and desorption isotherms of garden mint leaves (Mentha crispa L.). J. Food Eng. 51, 193 e 199.

Pavón-Melandez, G., Hernández, J. A., Salgado, M. A., García M. A., 2002. Dimensionless analysis of the simultaneous heat and mass transfer in food drying. Journal of Food Engineering, 55, 347-353.

Perlo, J., Casanova, F., Blümich, B., 2005. Profiles with microscopic resolution by single-sided NMR. J. Magn. Reson. 176, 64-70.

Raffo, A., Gianferri, R., Barbieri, R., Brosio, E., 2005. Ripening of banana fruit monitored by water relaxation and diffusion 1H-NMR measurements, Food Chem., 89 (1), 149-158.

Rastogi, N. K., Raghavarao, K. S. M. S., 2004. Mass Transfer during osmotic dehydration of pineapple: considering Fickian diffusion in cubical configuration. Leebensm. U.-Technol., 37, 43-47.

Rastogi, N. K., Niranjan, K., 1998. Enhanced mass transfer during osmotic dehydration of high pressure treated pineapple. Journal of Foos Science,volume 63, No. 3.

Rastogi, N. K., Raghavaro, Raghavaro, K. S. M. & Niranjan, K., 1996. Mass transfer during osmotic dehydration of banana: fickian diffusion in cylindrical coordinate. Journal of Food Engineering, 31, 423-432.

Riva, M., Peri, C., Lovino, R., 1986. Effects of pretreatments on kinetics of grapes drying. In: Le Maguer, M., Jelen, P. (Eds.), Food Engineering and Process Applications, Transport Phenomena, vol. 1. Elsevier Applied Science, London, pp. 461e472.

Ruiz-Lòpez, I., I., Garcìa-Alvarado, M., A., 007. Analytical solution for food-drying kinetics considering shrinkage and variable diffusivity. Journal of Food Engineering, 79, 208-216.

Russo, P., Adiletta, G., Di Matteo, M., 2013. The influence of drying air temperature on the physical properties of dried and rehydrated eggplant. Food and Bioproduct Processing, 91 (3), 249-256.

Sagar, V. R., Suresh, Kumar P., 2010. Recent advantages in drying and dehydration of fruits and vegetable: a review. Journal of Food Science and Technology-Mysore, 47 (1), 15-26.

Saravacos, G.D., Marousis, S.N., Raouzeos, G.S., 1988. Effect of ethyl oleate on the rate of air drying of foods. J. Food Eng. 7, 263e270.

Sebarez, Henry T., 2012. Computational modelling of the transport phenomena occurring during convective drying of prunes. Journal of Food Engineering 111, 279-288.

Silva, V., Costa, J., J., Figueiredo, A., R., Nunes, J., Nunes, C., Ribeiro, T., I., B., Pereira, Bruno, 2016. Study of three-stage intermittent drying of pears considering shrinkage and variable diffusion coefficient. Jurnal of Food Engineering, 180, 77-86.

Silva, V., Figueiredo A. R., Costa, J. J., Guiné, R. P. F., 2014. Experimental and mathematical study of the discontinuous drying kinetics of pears. Journal of Food Engineering, 134, 30-36.

Simal, A., Femenia, A., Garau, M. C., Rosselló, C., 2005. Use of exponential, page's and diffusional models to simulate the drying of kiwi fruit. Journal of Food Engineering, 66, 323-328.

Simal, A., Rosellò, C., Berna, A., Mulet, A. 1998. Drying of shrinking cylinder-shaped bodies. Journal of Food Engineering, 37, 423-435.

Simal, S., Deyà, E., Frau, M., Rosselló, C., 1997. Simple modelling of air drying curves of fresh and osmotically pre-dehydrated apple cubes. Journal of Food Engineering, 33, 139-150.

Singh, S.P., Jairaj, K.S., Srikant, K., 2012. Universal drying rate constant of seedless grapes: a review. Renew. Sust. Energy Rev. 16, 6295e6302.

Taheri-Garavant, A., Rafiee, S., Keyhani, A., 2011a. Effective moisture diffusivity and activation energy of tomatoe in thin layer dryer during hot air drying. International Transaction Journal of Engineering, Management & Applied Science & Technologies.

Taheri-Garavant, A., Rafiee, S., Keyhani, A., 2011b. Study on effective moisture diffusivity, activation energy and mathematical modelling of thin layer drying kinetics of bell pepper. Australian Journal of Crop Science, 5, 128-131.

Tu, S., Y., D., Choi, Y., J., McCarthy, K., L., (2007). Tomato quality evaluation by component force and NMR spin-spin relaxation time. Postharvest Biology and Technology, 44, 157-164.

Vagenas, G. K., Marinos-Kouris & Saravacos, G. D. (1990). An analysis of mass transfer in air-drying of foods. Journal of Food Engineering, 8, 323–342.

Vazquez, G., Chenlo, F., Moreira, R., Cruz, E., 1997. Grape drying in a pilot plant with a heat pump. Drying Technol. 15 (3e4), 899e920.

Veliè, D., Planiniè, M., Tomas, S., Biliè, S., 2004. Influence of air velocity on kinetics of convection of apple drying. Journal of Food Engineering, 64, 97-102.

Zogzas, N. P., Maroulis, Z. B. (1996). Effective moisture diffusivity estimation from drying data. A comparison between various methods of analysis. Drying Technology, 14 1543–1573.

Wang, H., Cao, G., Prior, R. I., 1997. Oxygen radial absorbing capacity of anthocyanis. J. Agric. Food Chem. 45, 304-309.

Yadollahinia, A., Jahangiri, M., 2009. Shrinkage of potatoes slices during drying. Journal of Food Engineering, 94, 52-58.

Yagcioglu, A., Degirmencioglu, A., Cagatay, F., 1999. Drying characteristics of laurel leaves under different drying conditions. In: Proceedings of the Seventh International Congress on Agricultural Mechanisation and Energy, May 26e27, Adana, Turkey. pp. 565-569.

Yan, Z. Y., Sousa-Gallagher, M. J., & Oliveira, F. A. R. (2008). Shrinkage and porosity of banana, pineapple and mango slices during air-drying. Journal of Food Engineering, 84, 430–440.

Yang, H., Sakai, N., & Watanabe, M. (2001). Drying model with non-isotropic shrinkage deformation undergoing simultaneous heat and mass transfer. Drying Technology, 19, 1441–1460.

Nomenclature

a	correlation parameter
A_0	amplitude of the echo at the shortest time τ_1 (s)
A_t	amplitude of the echo at time t (s)
b	correlation parameter
c	correlation parameter
cp	specific heath (kJ/kg K)
D	self-diffusion coefficient of water (m^2/s)
D_0	pre-exponential factor (m^2/s)
D_{eff}	effective diffusion coefficient of water in food (m^2/s)
E_a	activation energy (kJ/mol)
G	gradient field (T/m)
^1H	proton
h	temperature transfer coefficient (W/m K)
h_m	moisture transfer coefficient (m/s)
I	integral of NMR profile (arbitrary unit)
k	thermal conductivity (W/m K)
L	thickness of the sample along the z-axis (m)
M	moisture content ($kg/kg_{d.b.}$)
M_R	moisture ratio (M_t/M_0)
M_z	longitudinal magnetization (arbitrary units)
N	number of components of the decay (-)
q	heat flux (W/m^2)
r	radius (m)
R	gas constant (kJ/mol K)
R	rate of T_1/T_{1fresh} shortening with time (h^{-1})
RMSE	root mean square error (-)
R_1,R_2,R_3	half length of sample along the x-, y-, z-axis (m)
R^2	coefficient of determination (-)
Sh	Sherwood number (-)
S_r	rate of thickness reduction with the drying time (h^{-1})
S_v	shrinkage
t	times (s)
T	temperature (K)
T_1	longitudinal or spin-lattice relaxation time (s)
T_2	transverse or spin-spin relaxation time (s)
V	volume (m^3)
V_F	final (dry) volume (m^3)
W	weight of one component of the decay (%)
y_0	correlation parameter in Eq.
Y	transverse magnetization (arbitrary units)

Greek letters

α	thermal diffusivity (m^2/s)
β	shrinkage coefficient
γ	gyromagnetic ratio ($s^{-1}radT^{-1}$)
Δ	diffusion time (s)
ρ_s	food density (kg/m^3)

λ	latent heat evaporation (kJ/kg)
τ	dimensionless time (-)
τ_1	shortest echo time (s)
χ^2	chi-square or objective function (-)

Subscript

0	initial condition (t=0)
air	air
a	peak A
b	peak B
c	peak C
d.b.	on dry basis
e	equilibrium
fresh	raw, not dried
i	i^{th} component
sur	surface
t	actual
VC	vernier caliper

Subscript

‾	dimensionless variable (-)